School of Science and Engineering

ME40005 Honours Project

Building a lightweight robotic arm for a mini-Mars rover with the use of 3D printing

Jack Simpson

2504896

Project Supervisor - Dr Jan Bernd Vorstius

Academic Year 2024/25

Word Count – 14,542

ACKNOWLEDGMENTS

Dr Jan Bernd Vorstius – Project Supervisor, providing amazing overall feedback, providing many useful tools, testing equipment, and giving incredible experienced-based knowledge

Svetlana Zolotovskaya – secondary supervisor, amazing feedback from project

Robert Keatch – Head of Mechanical & Electronic engineering, helping with overall structure and providing useful feedback.

David Turbyne – Technical help

Cameron Anderson – Printing Help

Gary Smith – Workshop help

Dave Simpson – Help with proof reading and providing feedback as well as unwavering support.

Denise Simpson – Providing moral and emotional support helping in time of need.

Matthew Simpson – Providing technology-based help and overall support.

Alahtul (Mikel) Kibria – For providing so much support and care during academic tenure.

Imran Kibria – For also providing fantastic support and witnessing the final presentation of the prototype.

Ben Sloan – Providing sensor equipment.

Finnbar Home – Flatmate who provided both technical and emotional support.

Kyle Tait – Flatmate who provided both technical and emotional support.

Lewis Simmonds – Flatmate who provided both technical and emotional support.

Lucca Camargo – Flatmate who provided both technical and emotional support.

Class of 2025 – To all my friends in the class who I share this burden with and getting through this together!

ABSTRACT

This project details the design, modelling, fabrication, and testing of a lightweight robotic arm intended for mounting onto a mini-Mars rover. Aims were set to develop a compact, structurally sound, dexterous robotic arm, capable of performing sample acquisition while working within mass, power, and mechanical limitations typical of interplanetary robotic systems. The main objectives being the ability to lift 1kg and have a mass under 5kg. A comprehensive design methodology was followed, including component selection, CAD modelling with use of Onshape, and forward kinematic simulations performed in MATLAB using Denavit-Hartenberg parameters. Finite Element Analysis (FEA) was conducted using ANSYS Workbench to validate structural performance under simulated load conditions.

The arm underwent additive manufacturing using PETG and ABS materials, with part-specific infill strategies and orientation chosen to optimise strength-to-weight ratio. A combination of Prusa MK3, MK4, XL printers, with select components manufactured in the Stratasys F170 in Heathfield labs. Assembly involved friction fit and bolted connections, with additional refinements made post print to improve tolerance and fit. Autonomous capabilities were partially integrated using an ultrasonic sensor connected to an Arduino mega 2560 microcontroller, enabling basic proximity detection for gripping tasks.

Testing showed that the arm successfully lifted the required mass of 1Kg alongside a final mass of 2.25Kg, falling within the parameters. Any limitations were a result to the opening closing mechanism of the gripper. Key findings informed improvements to the design, material changes, tolerance between components, and code refinements. While Martian environmental simulation was not feasible, the project successfully demonstrated a cost-effective and scalable approach to rover robotic arms using widely accessible tools and materials. Future work includes implementation of inverse kinematics, full autonomy, increased lifting capacity, and greater environmental resilience.

Contents

ACKNOWLEDGMENTS

ABSTRACT i

CHAPTER 1 - INTRODUCTION 1

1.1 AIM & OBJECTIVES 1

CHAPTER 2 - LITERATURE REVIEW 2

2.1 ROBOTIC ARM DESIGN CONSIDERATIONS 2

2.2 ANALYSIS OF CURRENT NASA MARS ROVER PLATFORMS...................................... 2

2.3 EUROPEAN CONTRIBUTIONS TO MARS EXPLORATION...................................... 4

2.4 MICROCONTROLLER AND COMPUTATIONAL 6

2.5 ROBOTIC ARM MOUNTING CONSIDERATIONS...................................... 6

2.6 MECHANICAL AND OPERATIONAL FEATURES OF PERSEVERANCE'S ROBOTIC ARM...................................... 6

2.7 CONTROL AND KINEMATIC MODELLING...................................... 7

2.8 AUTONOMOUS NAVIGATION SYSTEMS 8

2.9 EDUCATIONAL ROBOTIC INSIGHTS 8

2.10 THE EFFECTS OF MARTIAN GRAVITY ON ROBOTIC ARM DESIGN 8

2.11 AUTONOMOUS ROBOTIC MOVEMENT...................................... 9

2.12 3D PRINTING FOR LIGHTWEIGHT ROBOTIC ARM FABRICATION 10

2.13 LOW COST AND MODULAR ARM DESIGN USING 3D PRINTING..... 11

CHAPTER 3 - DESIGN METHODOLOGY 12

3.1 INITIAL CONCEPT...................................... 12

3.1 INITIAL CONCEPT...................................... 12

3.1.1 Arm Placement...................................... 12

3.1.2 Component considerations...................................... 13

3.1.3 Power transfer...................................... 14

3.2 SOFTWARE SELECTION 15

3.3 MATERIAL AND PRINTER SELECTION...................................... 16

3.4 HARDWARE 16

3.4.1 Microcontroller...................................... 17

3.4.1 Tools & Sensors...................................... 18

CHAPTER 4 – RESULTS 19

4.1 DESIGN AND MANUFACTURING...................................... 19

4.1.1 Base...................................... 20

4.1.2 Bearing mount and bush...................................... 20

4.1.3 Bearing...................................... 21

4.1.4 Mounting block..21
4.1.5 Arm support..22
4.1.6 Upper and lower arm..23
4.1.7 Structural arms (arms 2 and 3)..24
4.1.8 Gripper head..24
4.1.9 Final Assembly..25
4.1.10 Printing..27
4.1.11 Construction..29
4.2 SIMULATION RESULTS..32
4.3 CIRCUITRY AND CODING..33
4.4 TESTING..34
4.4.1 Carrying capacity..34
4.4.2 Autonomy..35
4.5 MODIFICATION..35
CHAPTER 5 – DISCUSSION..37
5.1 PRESENTATION OF IDEAS..37
5.2 CRITICAL ANALYSIS..37
5.2.1 LIMITATIONS..37
5.2.2 FUTURE WORK..37
CHAPTER 6 – CONCLUSION..39
References..40
APPENDICES..43
APPENDIX A – ADDITIONAL 3D MODELS..43
APPENDIX B – EXPLODED DIAGRAMS..47
APPENDIX C – WEIGHT REDUCTION..48
APPENDIX D – MATLAB COMPARISON..49
APPENDIX E - CAD DRAWINGS..50
APPENDIX F – MASS OF ROBOTIC ARM..62
APPENDIX G - MATLAB CODE..63
APPENDIX H – FEA..69
APPENDIX I- ARDUINO CODE..72
TIME-MANAGEMENT CHART..74
RISK ASSESSMENT..75

Figure 1 - Perseverance Rover [8] 3
Figure 2 - Rocky 7 [10] 4
Figure 3 - Factors impacting surface mission productivity [11] 4
Figure 4 - Rosalind Franklin [12] 5
Figure 5 - Earth Return Orbiter (ERO) [12] 5
Figure 6 - A simplified model of the robotic arm [18] 7
Figure 7 - 3D Robotic Arm Model 10
Figure 8 - Robotic hand prototype assembled [27] 11
Figure 9 - Arduino Mega 2560 17
Figure 10- MBED NXP LPC1768 17
Figure 11 - HC-SR04 Ultrasonic Sensor 18
Figure 12 - Annotated robotic arm sketch 19
Figure 13 - Base of robotic arm 20
Figure 14 – A) Bearing Mount, B) Bearing Bush 21
Figure 15 – Plan view of bearing assembly 21
Figure 16 - Mounting block 22
Figure 17 - Lower section assembly 22
Figure 18 - Arm support 23
Figure 19 – A)Arm 1, B) Slider arm 23
Figure 20 - Arm 2 (support-pivot) & arm 3 (joiner arm-slider/pivot-gripper head) 24
Figure 21- Gripper head & locking plate 24
Figure 22 - Gripper "finger" and gear arm 25
Figure 23 - Full robotic arm assembly 26
Figure 24 - Slider Arm printed 28
Figure 25 - Multiple components on Prusa print bed 28
Figure 26 - Lower base with bearing installed 29
Figure 27- A) Lower arm assembly, B) Lower arm assembly attached to base 30
Figure 28 - First prototype of robotic arm 31
Figure 29 – A) Robotic arm holding 1Kg at full extension, B) Calibrated mass 32
Figure 30 - Circuitry of robotic arm 33
Figure 31- Physical circuit with 3/5 headers connected 34

Table 1 - Estimates of Martian lithospheric parameters [21] 9
Table 2 - Bill of Materials 26

CHAPTER 1 - INTRODUCTION

One of the defining traits of human civilisation is the indomitable spirit and desire to explore the uncharted. From early exploration of the continents to hopefully mapping star systems in the near future, humans have continually pushed past their limits of exploration. This drive has led to unimaginable achievements. From launching the first manned mission to the moon; still one of the greatest feats to have ever been done, to launching small drones and landing them on asteroids flying through the cosmos at unimaginable speeds and, ultimately to landing multiple rovers on another planet. Since 1997, 5 rovers have successfully been landed on the surface of the Red Planet, providing invaluable research and discoveries in both interplanetary travel and breakthroughs into the possibility of life on Mars, due to the discovery of liquid water on the surface [1].

Space exploration plays a crucial role in understanding extra-terrestrial environments, with robotic systems performing tasks humans cannot yet perform. This includes such things as terrain analysis, sample collection, and data collection, all of which is done by a robotic arm mounted to the main body of the platform. With the first being the rover, Sojourner. These robotic arms need to provide precise manipulation and handling of objects while in hazardous environments. It is also essential that robotic arms are both lightweight, which require the use of advanced materials such as low-mass graphite epoxy and titanium [2]. All this is to make sure that overall launch costs are low as well as reducing power consumption, since heavier arms require stronger motors, drawing more power.

1.1 AIM & OBJECTIVES

The aim for this project was to build a rover that could withstand the foreign environment of Mars using simulations. A robotic arm would be mounted to the rover that could take a sample, either by drilling or surface pickup, based on sensor data and determining best course of action in an autonomous manner. An additional goal was to reduce the weight through informed selection of materials. Lighter materials such as 3D printing materials and high strength plastics were the first choice.

- Design a robotic arm with optimal balance between weight and structural strength.
- Select appropriate actuation mechanisms that minimise power consumption.
- Develop a tool tip capable of grabbing geographical samples.
- Perform basic simulations and FEA analysis to ensure overall operability and structural integrity.
- To construct a real-world prototype.

With these aims in mind, there are two main objectives that must be met in order for the robotic arm project to be a success:

- Have the capability of lifting 1Kg of mass under full extension.
- Remain under 5Kg of overall mass.

CHAPTER 2 - LITERATURE REVIEW

Since the Sojourner mission in 1997, laying the groundwork for all future rovers, Mars rover technology has undergone some major advancements in both autonomy and mechanical complexity. Rovers such as the twin rovers, Spirit & Opportunity and Curiosity, as well as the newest, most advanced rover, Perseverance have successfully conducted long-distance traverses, geological sampling, and highly resolution image capture across different Martian environments. This is all due to the subsystems implemented within the rover that allow it to operate independently due to the high latency communications between Earth and Mars. This is a particular issue, since signals can only travel at the speed of light and it takes light between 3 and 22 minutes, with an average of 12.5 minutes [3]. In particular, the Mars 2020 rover's vision compute element, made use of stereo vision systems, and "thinking-while-driving" capabilities made a shift towards more autonomous surface operations that maximise scientific output [4].

2.1 ROBOTIC ARM DESIGN CONSIDERATIONS

Robotic arms mounted on the Mars rovers have become a crucial tool for interacting with the environment, with constant improvements being made after every rover iteration, performing tasks such as core sampling, and sample deployment. Over the years, design considerations have moved towards achieving high performance with lower payloads, as well as improved thermal resistance, and reliability. Such as the Mars surveyor 2001 robotic arm utilized a 4 DOF backhoe design, similar to that on excavators on Earth, integrating scooping, scraping, and deployment mechanisms, while remaining extremely light at 5KG in total weight [2]. In other projects, as shown by Czaplicki [5], researchers have emphasized the importance of intuitive control systems and inverse kinematics to allow for precise movements in confined locations remotely. Dexterity, precision, mobility, energy efficiency are crucial in conceptualising robotic arm designs to overcome constrains of a miniaturised platform.

One Study showed a robotic arm with 5 DoF controlled using an Arduino Mega 2560 and MATLAB, which also incorporated forward and inverse kinematic modelling. This aligns closely with the goals of this project in developing a lightweight robotic arm. [6]

In a similar study, a researcher implemented a 6 DoF robotic arm for a Mars rover using aluminium 6061, applying FEA to validate the structural resilience and integrating prismatic and revolute joints for improved dexterity and control [7].

2.2 ANALYSIS OF CURRENT NASA MARS ROVER PLATFORMS

When understanding what is required from a Mars rover, the best place to learn would be NASA's own creations, from Sojourner all the way to the newest rover, Perseverance. However, this project should be compared with the two most recent rovers (Curiosity and Perseverance) as they are proven designs with successful deployments. By considering the design, functionality, what went wrong and how it was improved, and examining the past knowledge and information I have shaped the development of this rover with an understanding of the challenges that go into designing such a machine.

Ensuring the chassis has a strong exterior is crucial to protecting the sensitive electronics and equipment, as in-situ repairs are impossible, as well as increasing the lifespan of the rover. On the Perseverance rover this is called the “Warm Electronics Box” or WEB for short, circled in Figure 1 [8]. The body is large enough to accommodate different drill types and samples. By prototyping with acrylic then moving on to aluminium and even steel in more vulnerable places, a WEB can be constructed that is both lightweight and durable and, with the requirement to hold a robotic arm means it must also be balanced and stable.

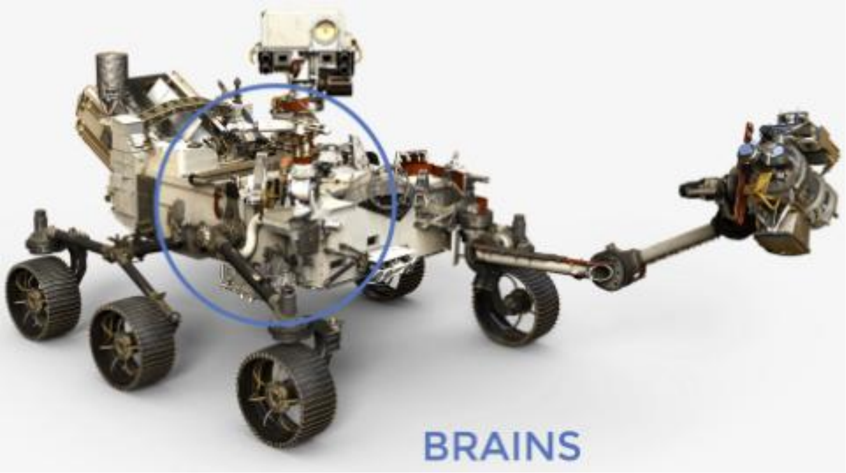

Figure 1 - Perseverance Rover [8]

The design and function of Perseverance’s robotic arm were optimised to support geological sampling and caching operations that target a diverse range of terrain types. These samples are carefully selected and sealed for potential return to Earth, forming a critical part of the Mars sample return program [9].

One of the standout examples of a next generation Mars rover prototype is the Rocky 7, shown in Figure 2, developed at the Jet Propulsion Laboratory. Unlike its predecessor, Rocky 7 incorporated significant design innovations focused on increasing overall autonomy and mobility, while reducing system complexity. By shifting from four corner steering to two corner steering, similar to that of car steering configuration, it reduced the number of degrees of freedom required for navigation. The savings were then used to enhance scientific capabilities by integrating a compact manipulator arm for sample collection and sensor alignment. This design shift enabled Rocky 7 to explore terrain with greater efficiency, supported by a flexible, modular software architecture that allowed for real time control and data gathering. These optimisations reflect the need for future rovers to operate reduced computational and mechanical overhead, particularly under constraints of mass and power for miniaturised platforms [10].

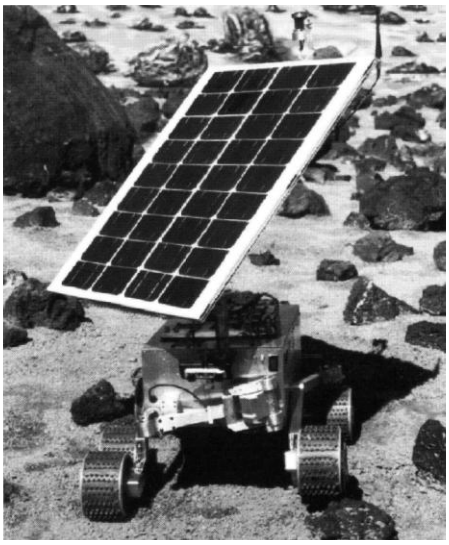

Figure 2 - Rocky 7 [10]

In parallel, operational productivity has emerged as a critical performance metric in recent rover missions, especially with the Mars Science Laboratory (MSL) and the Curiosity rover. The complexity of daily planning, constrained uplinks, and a reliance on Earth-based decision making often led to underutilised rover resources. Studies by NASA's Jet Propulsion Laboratory identified key restrictions such as conservative terrain estimation for autonomous driving and rigid task sequence validation process. To mitigate these, there is now a shift towards "self-reliant rover" models where the rover autonomously interprets goals rather than waiting for detailed step-by-step instructions. This mode of operation not only increases responsiveness to unpredictable Martian conditions but also allows ground teams to focus on mission goals rather than micromanaging each task, improving scientific outcomes over multiple Martian years. A visual model showcasing these workflow stages, ranging from intent formation to activity execution and refinement, is shown in Figure 3, highlighting how limited state knowledge and delayed downlinks complicate the planning cycle [11].

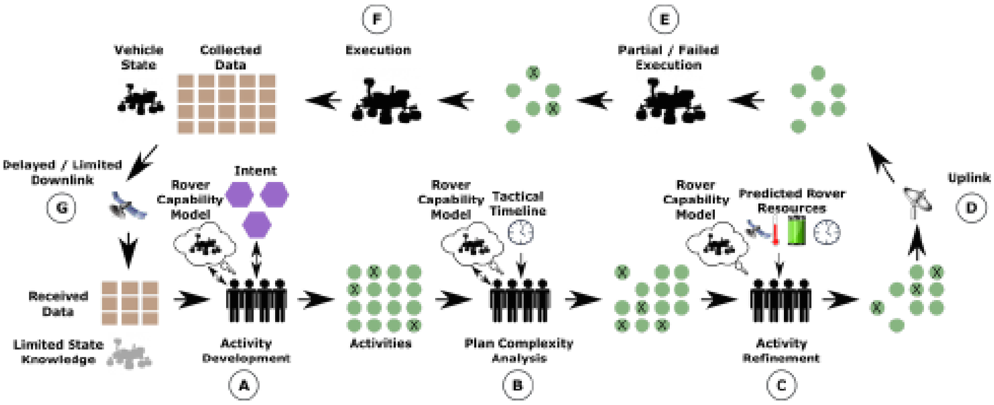

Figure 3 - Factors impacting surface mission productivity [11]

2.3 EUROPEAN CONTRIBUTIONS TO MARS EXPLORATION

Europe's involvement in Mars exploration has been significantly advanced through Airbus's contributions, one such program being the ExoMars program. The ExoMars rover, named Rosalind Franklin, represents Europe's first rover mission to the Red Planet. Built by Airbus in Stevenage, UK, the rover is designed to search for evidence of past, or even present life on Mars, to gain better understanding of the history of the water that was discovered on Mars. Equipped with an autonomous navigation system, it can travel across the Martian terrain more efficiently than systems reliant on Earth-based control. Its drill is also capable of collecting samples from a depth of up to two meters below the surface, and its 3D panoramic camera provides detailed visual data on surface textures and atmospheric conditions [12].

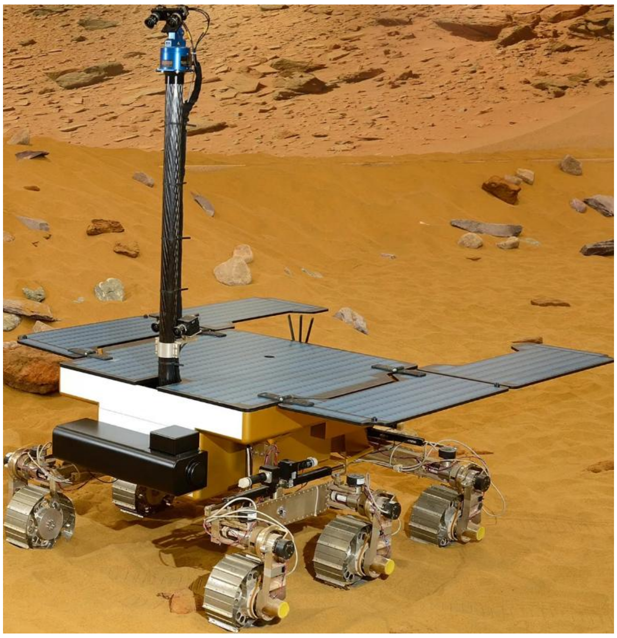

Figure 4 - Rosalind Franklin [12]

In addition to the rover, Airbus is proving to be a vital asset in the Mars sample return mission through the development of the Earth Return Orbiter (ERO). This spacecraft is tasked with retrieving samples collected one Mars and returning them to Earth's surface. The ERO will also function as a communication relay with surface missions, rendezvous with the samples sent to space, and safely return them to Earth. Notably, ERO will utilise fully autonomous docking capabilities developed by Airbus through decades of research in optical space navigation [12].

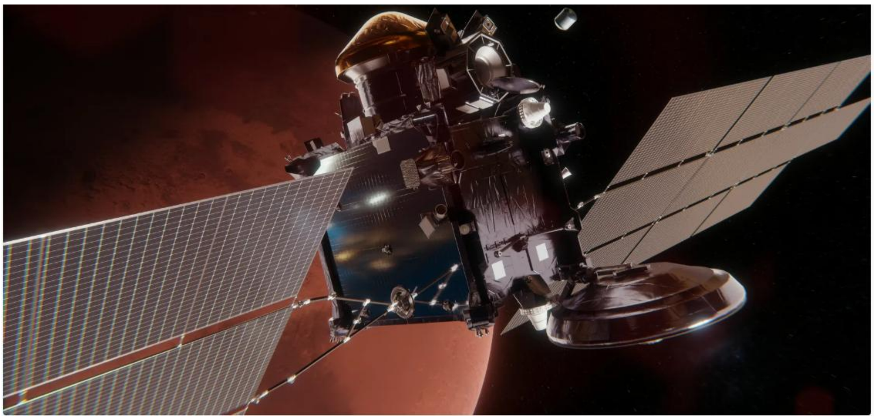

Figure 5 - Earth Return Orbiter (ERO) [12]

ESA's broader exploration roadmap includes not only the Rosalind Franklin rover and ERO, but also long-term commitments to robotic and eventually human exploration.

ESA's Partnership with Roscosmos for the ExoMars project, alongside collaborations with NASA, demonstrates Europe's integral role in global Mars exploration. The mission aims to combine deep drilling with surface mobility, enabling subsurface sample analysis and real-time data transmission from the surface of Mars, capabilities that align closely with future requirements of miniaturising rover platforms [13].

2.4 MICROCONTROLLER AND COMPUTATIONAL

In contrast to the simplified single-board control systems typically seen in small-scale terrestrial robotics, Mars rover platforms typically utilised more robust and distributed architectures. The Mars Science Laboratory (MSL) and Mars 2020 Perseverance rover were both equipped with dual Rover Compute Elements (RCEs) to support parallel processing, redundancy, and autonomy-driven tasks [14]. These systems manage onboard hazard detection, visual odometry, motion planning, and system health monitoring in real-time. While such architecture is not feasible for small-scale prototypes due to cost and availability, The Arduino Mega 2560 is more than capable for the project objectives.

2.5 ROBOTIC ARM MOUNTING CONSIDERATIONS

A major design consideration for the mini-Mars rover was the provision of a robotic arm that can take and store samples on board. This meant one of two possible mounting points, each with their own advantages and disadvantages. The first option was mounting the arm to the top portion of the frame as this allows for the most stable positioning and 360° access around the rover. However, a limitation of this was that it must first reach over the rover body before being able to sample the soil, resulting in a heavier arm due to the additional length [2]. The second option was to mount the rover arm at the very front of the body, like that of Curiosity and Perseverance [15]. This would give the reverse of the previous solution, that being it would make the rover more unstable by shifting weight to the front and giving it a longer reach. One other possibility for a robotic arm was a gantry that resided inside the shell of the rover. The rover would then drives over the sample required, lower down and retrieve the sample. Whilst reducing the range of the robotic arm it creates a super simplistic 3D mapping system, as only the X and Z plane need to be considered with Y being only once the others reach the requirements. It would also result in an easier system for changing the heads of the drill (as the mast arm would need to have an "all-in-one" style head, creating more mass up front).

2.6 MECHANICAL AND OPERATIONAL FEATURES OF PERSEVERANCE'S ROBOTIC ARM

I examined the Perseverance arm, which was created and manufactured by Motiv Space Systems in partnership with Nasa's Jet Propulsion Lab (JPL). The arm is front mounted and has a length of 2 metres with 5 joint's offering 5 degrees of freedom, all finely tuned to allow for a payload capacity of 45Kg. The arm is retrofitted with forensic instruments and coring material to create sample caches that will hopefully be returned to Earth. [16] NASA placing the arm at the front of the rover suggests that it may be the better of the two previous options, as not only would allow for greater reach, but it also allows for the camera mast to be mounted to the top, allowing for a larger field of view.

Perseverance takes samples using multiple different drill heads and coring tools where they deposit rocks and regolith into a titanium tube to then dump onto the surface for future retrieval. They can also fill these tubes with atmospheric samples. Each sample is always duplicated to create a “witness tube.” All of the witness tubes kept inside the “belly” of the rover could then be passed to a sample retrieval lander [17].

2.7 CONTROL AND KINEMATIC MODELLING

When building the robotic arm, research into robotic arms control systems was crucial. Useful insights were drawn from the studies of Szczęsny and Rećko [18], whose work focused on creating a control system for a robotic arm with 6 Degrees of Freedom (DOF) for a Mars rover replica, where a simplified model can be shown in Figure 6. First, the joint angles of the arm needed to be determined as to understand how it would move. They applied techniques such as Denavit-Hartenberg parameters to model the arm’s range of motion. Next, the joint angles were determined to make specific positions, making it easier to control the arm. All of this combined with an algorithm called SLERP (Spherical Linear Interpolation), which referred to the constant-speed motion along a unit radius, for smooth rotational movement, combining both straight line and rotational motion [18]. While the SLERP algorithm was not explicitly implemented, the Denavit-Hartenberg parameters were used to calculate the forward kinematics of the robotic arm for this project. After multiple tests using simulations such as environmental conditions, remote and automated testing, gave useful insights on how to improve upon the designs, something that was implemented into the design of the robotic arm. Looking into both mathematical and simulation testing gave further insight on how the robotic arm would react in certain circumstances.

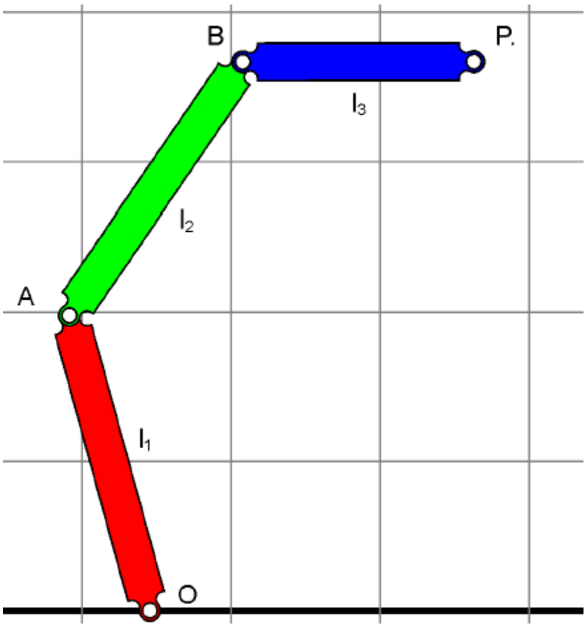

Figure 6 - A simplified model of the robotic arm [18]

Ideally, the robotic arm design would ideally have 6 degrees of freedom to allow for collection of samples all around the rover, although 4 DOF would suffice. However, and more importantly, range and weight were more of a focus, since the evolution of robotic arms using modern design techniques has resulted in increased range of movement and reduced weight while consuming less power. These are all advancements which are crucial to Mars missions [19].

The Denavit-Hartenberg convention is one of the most widely used methods for modelling the geometry of serial-link manipulators. In this framework, each joint is described by 4 parameters: Joint angle (), link length (), link twist (), and link offset (). These parameters define the relative position and orientation between joining links in the robotic arm. With use of 4x4 transformation matrices based on the parameters, it is possible to determine the final position and orientation of the end effector, usually the tool tip of the arm, with respect to the base.

This methodology is particularly valuable for miniaturised robotic arms where mass, space, and control simplicity are critical constraints. A lightweight robotic arm such as the one design in this project Denavit-Hartenberg forward kinematics for motion simulation and trajectory prediction, but also for ensuring all planned movements stay within a set boundary as well as torque limits. This is usually done in software such as MATLAB to provide visuals on the overall positioning of the robotic arm.

2.8 AUTONOMOUS NAVIGATION SYSTEMS

The Mars rover's navigation system must enable it to traverse harsh terrain in lower gravity and higher radiations levels than those found on Earth, all whilst being over 225 million kilometres away. Therefore, the rover must have some form of autonomy alongside the remote operation, since large antennas are not a viable option, due to both the cost of the antenna and its power consumption. The system uses a stereo camera to create a 3D map of the terrain which enables the rover to identify any deep craters and determine safe paths [14]. Navigation algorithms plan the distance from the goal by breaking the route into shorter segments, these images are then used to update the 3D map. This system has been tested over numerous rover platforms and a simulator, showing significant improvements in daily traverse distance [4].

2.9 EDUCATIONAL ROBOTIC INSIGHTS

When considering robotic arms, educational versions can give insight into how the one on Curiosity functions. They still share mechanical and kinematic characteristics with the ones on the different Mars rovers, but are made of cheaper materials and have more ease of use and modularity. Many experiments that have been conducted highlight important details that can be included in all of robotics, such as user accessible interfaces and real-time feedback of sensors, such as potentiometers or force sensors. Using similar programs such as MATLAB for the simulations or simple microcontrollers such as the Arduino UNO can give valuable insight to building a robotic arm [20].

Designing a Mars rover has multiple different aspects to consider, such as mobility, arm precision, or how effective it is at executing tasks in the harsh Martian landscape. Multiple studies into operational productivity show that a large amount of human effort is put into planning, co-ordinating and sequencing different actions performed by the rover. This limits how many tasks an overall robotic system can perform every day. By improving autonomous actions, such as hazard detection or science, or providing operators with a combination of helper scripts and task sequencing interfaces can help overall productivity [11].

2.10 THE EFFECTS OF MARTIAN GRAVITY ON ROBOTIC ARM DESIGN

Understanding the gravitational characteristics of Mars is essential for designing robotic arm systems that can operate on the surface of Mars. The planet's gravitational field is roughly a third of what is experienced on Earth, approximately 0.38G. This directly affects structural loading and has implications for component selection, weight distribution, and joint torque requirements.

One foundational study linked to the relationship of gravity and topography of various Martian regions, estimated the elastic thickness (Te) of the Martian lithosphere (the solid outer layer of a planet) using tracking data, the findings show that Te varies significantly from 70Km in the Tharsis, 29Km within Elysium, to as little as 14.5Km all within the southern hemisphere. These factors indicate that the lithosphere has thickened over time due to planetary cooling. For robotic systems, these spatial variability changes in the overall crustal rigidity highlights the importance of designing robotic arms that can maintain operational stability over diverse terrain [21]. A table of these values is shown in Table 1. These are taken from a study that showcases multiple variables such as the elastic thickness and temperature the layer, density of the layer, the age in Giga-annums (Ga). The data highlights the different properties at the different lithospheric regions.

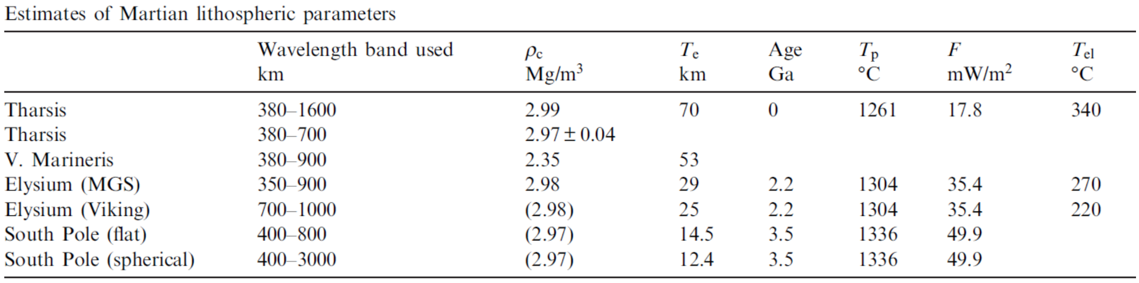
Estimates of Martian lithospheric parameters

	Wavelength band used km	ρ_c Mg/m^3	T_e km	Age Ga	T_p °C	F mW/m^2	T_{el} °C
Tharsis	380–1600	2.99	70	0	1261	17.8	340
Tharsis	380–700	2.97 ± 0.04					
V. Marineris	380–900	2.35	53				
Elysium (MGS)	350–900	2.98	29	2.2	1304	35.4	270
Elysium (Viking)	700–1000	(2.98)	25	2.2	1304	35.4	220
South Pole (flat)	400–800	(2.97)	14.5	3.5	1336	49.9	
South Pole (spherical)	400–3000	(2.97)	12.4	3.5	1336	49.9	

Table 1 - Estimates of Martian lithospheric parameters [21]

A later study combined both surface and subsurface load models and identified that the densities of major Martian volcanoes, such as Olympus Mons, exceed 3200kg/m³. These high-density regions, alongside subsurface mass deficits, such as mantle plumes, cause localised variations in gravitational forces and surface support. For the mini-Mars' rover, these variations mean that seemingly stable terrain might show uneven resistance or support. As a result, careful planning must be given to the arms centre of mass, range of movement, and any acting torques to prevent destabilisation during sample collection [22].

For designing the robotic arm, gravitational and lithospheric data offer essential information that guide overall design methodologies. This data ensures that joint tolerances, servo selection, and arm stability are of the highest quality. While Mars' lower gravity reduces the overall loads experienced by the arm, the smaller scale and more fragile materials mean minor imbalances or terrain-induced shifts can significantly affect overall stability, both dynamically and statically.

2.11 AUTONOMOUS ROBOTIC MOVEMENT

Autonomy in robotic systems, particularly in manipulator-based applications, is defined as the ability for a robot to sense its environment, with the use of control systems, plan a response, and execute actions independently based on the inputs. While full autonomy remains challenging in dynamic environments, it has been successfully implemented in systems operating under structured and repetitive conditions.

Autonomous and semi-autonomous systems have widespread development in surgical robotics, where precision and repeatability are of utmost importance. These systems leverage a combination of sensor data, motion planning algorithms, and task databases to perform complex operations such as suturing, tissue retraction, and tool guidance, while the operator maintains supervisory control [23].

Similar frameworks have been developed in field robotics. The DARPA Autonomous Robotic Manipulation (ARM) program demonstrated significant progress in enabling robotic arms to complete manipulation and grasping tasks with minimal operator input. In this program, identical robotic platforms were tested across a series of standardised manipulation tasks using software and code developed by different research teams. Tasks such as grasping with tools or interacting with mechanical devices were completed autonomously or with only high levels of instructions by operators. These trials highlighted the importance of perpetual feedback and standardisation in achieving reliability, autonomy, and control across numerous different tasks [24].

More recent advances have focused on the implantation of shared control systems with robotic interfaces. A study showed that a semi-autonomous robotic arm using a hybrid gaze and brain machine interface (BMI). This system allowed users to use the hybrid gaze to move the end-effector through gaze tracking, while adjusting movement speed via a motor. Unlike traditional shared control systems that switch between operator and autonomous control, this system continuously blended both inputs. The result was a smoother experience and improved efficiency in task completion. Including obstacle avoidance and object manipulation [25].

2.12 3D PRINTING FOR LIGHTWEIGHT ROBOTIC ARM FABRICATION

Additive manufacturing, more commonly known as 3D printing, has become a revolutionary method for producing lightweight and custom components both large and small scale that is available for everyone. A recent study presents the design of a 6 DOF robotic arm fabricated using fused deposition modelling (FDM) of which can be shown in Figure 7, highlighting its ability to print 54 distinct parts at a total cost of €350 [26]. Design strategies included integrated hollow channels and modular joint elements to reduce overall material without sacrificing mechanical function. The kinematic model was developed using Denavit-Hartenberg parameters.

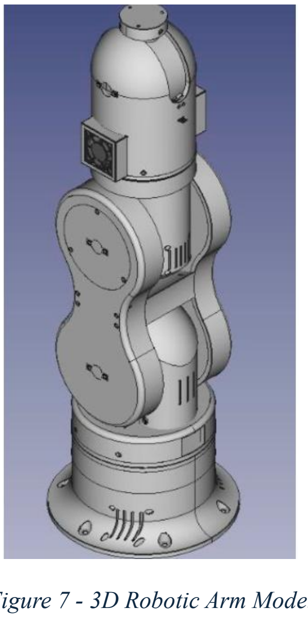

Figure 7 - 3D Robotic Arm Model

Furthermore, the arm used NEMA 17 stepper motors for actuation, highlighting those low-cost motors is more than enough to provide the required torque and resolution for complex multi-joint systems when combined with lightweight construction. Similar design strategies will be implemented to consider a similar model for a Mars mission.

2.13 LOW COST AND MODULAR ARM DESIGN USING 3D PRINTING

Low cost, modular robotic arms developed through 3D printing offer valuable insights to the mini-Mars rover arm project. One study showed the development of a wearable prosthetic arm featuring modular segments actuated by micro servos [27]. While intended for biomedical purposes, the arms design objectives(lightweight construction, ease of assembly, and adaptability) closely align with the requirements of robotic rover arms.

The components were fabricated using PLA filament and structured as replaceable modules to allow for fast iteration and repair, with the finished prototype shown in Figure 8. Gripping force test demonstrated that the fingers could apply up to 1.67N of force, capable of lifting small rocks and soil samples, if it were implemented onto a rover body. The microcontroller used was an Arduino nano, with user input received via flexor sensors. The use of open-source electronics with lightweight hardware supports quick and easy prototyping under strict mass and power limitations.

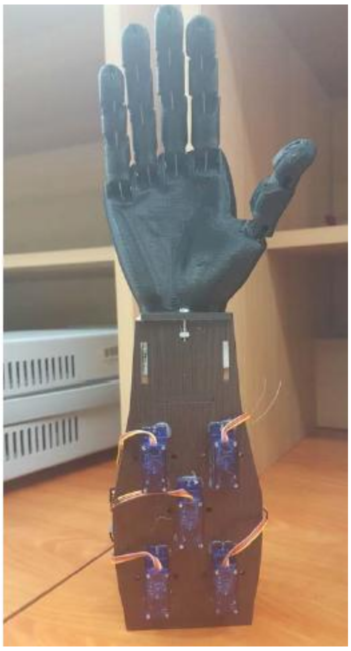

Figure 8 - Robotic hand prototype assembled [27]

The design emphasis on layered modularity allowed for individual segments to be replaced without reconfiguring the entire arm. Incredibly useful in space applications, where systems must be reliable and tolerant to partial failures without human interaction [27].

CHAPTER 3 - DESIGN METHODOLOGY

This chapter describes the first prototype design of the lightweight robotic arm. The chapter starts with the initial design phases of the robotic arm, how the robotic arm was intended to look and move, how it was assembled with a bill of materials (BOM), as well as exploded views of the assembly. The following section describes the manufacturing process of the robotic arm, how the parts were created as well as material selection for each individual component. The struggles that came with it and how those problems had were solved through redesigns and creative thinking. The last section details the finalised design and coding of the movement.

3.1 INITIAL CONCEPT

This chapter describes the first prototype design of the lightweight robotic arm. The chapter starts with the initial design phases of the robotic arm, how the robotic arm was intended to look and move, how it was assembled with a bill of materials (BOM), as well as exploded views of the assembly. The following section describes the manufacturing process of the robotic arm, how the parts were created as well as material selection for each individual component. It also discusses the struggles that came with it and how those problems were solved through iterative design and creative thinking. The last section details the finalised design and coding of the movement.

3.1 INITIAL CONCEPT

The initial concept involved deciding between a gantry system and a robotic arm. Initially, the gantry approach was favoured due to its design simplicity and linear manoeuvrability. The gantry would remain fixed within the rover's chassis and operated by positioning a gripper head in the x and y plane, then lowering along the z axis, this would then deposit the material inside of the rover body. Another primary benefit was its compactness; this internal integration also offered more chassis real estate for other kinds of instrumentation. However, limitations included dependency on the rover's ability to directly traverse over the sample and restricted reach for elevated or sunken sample areas, leaving multiple limitations to the gantry system as a whole. As a result, a multi-joint robotic arm was selected as the final design due to its improved versatility and functionality, as not only were there be more challenges to test, but the advantages of the robotic arm also outweighed the negatives, in comparison to the gantry system.

3.1.1 Arm Placement

The design goals required a high payload capacity and material efficiency, using 3D printed filaments to fabricate components, ensuring that the structural integrity of the robotic arm was not compromised by adjusting infill percentages depending on the component's function. The only limiting factor was hardware, such as servos and sensors, whose weight could not be changed. Initial design efforts focused on arm placement, as seen on NASA's Curiosity and Perseverance rovers. It could either have been mounted at the front, which offered extended reach, or mounted to the top of the rover. Mounting on the top gives 360° coverage making it usable in any orientation, meaning the rover did not have to position itself. Distribution of weight and balance was also far better due to the mass of the arm being over the centre of mass of the entire rover. For those reasons, the decision was made to mount the robotic arm to the top of the rover body.

3.1.2 Component considerations

For the top-mounted design, the robotic arm was conceptionally built from the base up and had to be considered first. Looking into the dimensions of the rover as well as the design brief, it was clear that the base had to be both wide enough to provide support as well as being lightweight. To achieve this, infill was kept low alongside potential cutouts for weight reduction. Before any technical aspects of the baseplate were considered, the overall shape needed to be formed to give a solid foundation. Between the structural integrity of a triangle, to the perfect fitment of a square. A circular base was decided for its even load distribution as well as the compatibility for bearings, having better fitment and provide an overall cleaner look. The base was designed with 4 extruded points to be given “feet” for testing purposes and act as mounting points for the rover.

The next few parts to be considered were the bearing mount and bearing bushing. These required a cutout in the base, with depth being half of the overall base thickness, if possible, to allow for the bearing to be lower down and therefore lower its centre of gravity, thus preventing it from tipping over. The bearing mount was mounted to the base with fasteners for a secure connection. This was a specific diameter that was then narrowed down to allow for a ball bearing assembly to be put over the top of it. The bushing was a simple cylindrical piece that was slid over the top of the bearing assembly, with countersunk screw holes to allow for a flush finish that did not interfere with the rotational movement.

Finally, the initial design of a mounting plate was considered.

At first the robotic arm was going to be a single arm that would extend out to a desired length that would function as a lower arm i.e. the bicep/triceps of the robotic arm with a forearm attached to it to provide extra length and pivotal point. However, due to potential loading problems and overall consideration of structural integrity, it was advised against going down that design path. Instead, two parallel arms were used, which increased overall weight although weight reduction methods were implemented, such as cutouts and reduced overall material to counterbalance this. Due to these new design considerations, the baseplate had two cutouts for arm supports either side, as well as cutouts for a servo and mounting holes for the bushing. Finally, with most of the lower base imagined, dimensioning was done to ensure a properly fitted ball bearing.

With the lower design having a strong foundational concept, the arm supports needed to be considered as they served as the secondary “foundational base.” Crude sketches were made up highlighting different designs for the supports that fit cutouts on the mounting block itself. The design also had to consider the direct mounting of a servo, offering proper alignment, strength, and placement on the mounting block. After careful consideration, the servo was mounted in an angular position, with smoothed edges in the direction of the arm itself to not only distribute loads, but to be able to know constant servo spindle positioning. The supports also required more infill due to the entire weight of the arm, as well as the samples carried acting on the servo.

The angular placement also distributed the load over a greater cross-sectional area with the arm itself designed appropriately. As previously stated, the robotic arm required two parallel arms to keep structural integrity, therefore, a curved design was considered to reduce overall tensions in the arm, as parabolic structures are self-supported, which reduced both the amount of material needed and the overall weight. Inspired by other robotic arm designs, the arm included pivot points to control its extension, with structural arms stretching out from different key points of the arm, allowing for structural integrity and smooth control.

Design of the upper arm was done through a similar iterative design process. This was initially achieved by making a direct copy of the lower arm; however, this created mounting and stability issues, as it proved to be too front-heavy. This evolved to eventually include an additional piece near the mounting point of the arm to allow for one of the structural arms to hold onto, refining the movement.

Finally, the gripper head needed to be designed with both large and small samples in mind, as there was a requirement to handle a large range of rock sizes. The other part that had to be considered was the clamping mechanism and grip strength, as this had to meet the required 1kg of holding power. Initial sketches were made of 2 angled beams that would be mounted to a gear to allow for the open/close mechanism which was then attached to a servo. However, this made it prone to breaking, especially if too much torque was applied, and could cause it to fail under shearing. Compound gear trains were also considered to increase the torque of the gripper head; however, this led to a bulky head, making it front heavy. The final design consisted of two separate sections that were slotted into each other, 1 piece being the gear assembly and the other the gripper itself.

The gripper had teeth cutouts to get better grip of the object as well as an elliptical cutout for larger rocks to fit into, offering a firmer grip and allowing all sets of teeth to bite into. With the gripping section planned out, integrating the actual arm was considered next. This section needed to have space for both a servo as well as the gearheads that would control the open and closing movement. A simple rectangular piece with a rounded top was created with a cutout for a crosspiece to be inserted into, which could be attached to a servo to create a wrist-like rotation. This servo was mounted onto a simple bracket which was then mounted into some form of gripper head that was attached to the arm itself. Numerous design iterations were, again, developed for this piece. However, a final design having an almost a T-like shape, where a structural arm was attached to the top with the robotic arm at the larger diameter mounting hole, and a fastener or support rod through the front most hole was eventually settled on.

3.1.3 Power transfer

A gear box was considered to drive the arms of the robotic arm and arm supports were initialized with planetary gears to provide a substantial torque increase. However, this increased the weight by a large margin, so alternative methods were explored, with the best being the use of high torque servos that had built in compound gear trains with the use of metal gears and higher design tolerances.

Another consideration for the initial design of the robotic arm was the development of a custom printed circuit board (PCB) as part of the signal routing and operation of electronics. A dedicated PCB would have allowed for the linkage of all control wiring, sensor connections, and power distribution into a single compact platform, improving reliability and reducing complex wiring.

3.2 SOFTWARE SELECTION

When designing the robotic arm, the use of 3D CAD software was quickly decided upon. 2 CAD software packages were considered; SolidWorks and Onshape. Both are solid CAD software with exceptional user interface and simplicity of use. However, Onshape is a cloud-based CAD software, making all parts accessible on any device, without hardware limitations, which allowed remote work, which made it an optimal choice for this project. Drawings were also made up with Onshape's built-in templates shown in the appendix E.

When it came to running simulations, such as forward kinematics, MATLAB was chosen as the platform of choice due to its wide use in the engineering industry and its suitability for matrix-based computation. It was used to model and simulate the forward kinematics of the robotic arm using Denavit-Hartenberg parameters, which defines the spatial relationships between consecutive joints. Each joint was described by its joint angle, link length, offset, and twist, allowing for accurate mapping of the arm's kinematic structure. A custom MATLAB script was developed to take operator inputs and compute the collective transformation matrix from the base to the end-effector. The resulting output included Cartesian position (x,y,z), in both separate planes and 3D visual plots of the orientation of the gripper, providing a non-destructive means of testing (NDT) the movement limits and spatial constraints before assembly.

To assess the structural integrity of the robotic arm of any loads acting on the components, ANSYS workbench was selected for the Finite Element Analysis (FEA) platform. This software was chosen due to its use in class, giving familiarity over other FEA software, along with its broad selection of simulation tools and its ability to make complex geometries under realistic boundary and loading conditions. Specifically, the static structure module within Workbench was used to simulate the stress/strain, distribution, and total deformation across the robotic arm. ANSYS is also a dependable, industry standard software for structural analysis, with accurate solvers, and compatible with standard CAD files such as STEP or 3MF, which can be exported from Onshape. The ability to apply precise boundary conditions, such as fixed supports at mounting points, and defined loads at the tool head, allowed for in depth testing for maximum loads, and even worst-case scenarios. Additionally, mesh refinement tools, such as methods, face meshing, and others, were used to increase solution resolution in critical stress regions, such as the joints and maximum load bearing points, such as the end of the robotic arm.

With respect to 3D printing and using Prusa printers, it was obvious that the Prusa Slicer offered the best features and was selected due to the direct compatibility with the Mk3, Mk4, and XL printers. The software provided a user-friendly interface while offering both basic and advanced control over slicing parameters, making it extremely useful for beginners and experienced users alike. It also had advanced control over slicing parameters such as layer height, infill density, print orientation, automatic bed arrangement, and support structure generation. These capabilities were essential in tailoring print settings in order to meet the structural and weight limitation requirements of the robotic arm components. It was also chosen over other options such as Cura or Simplify3D, due to its seamless integration with the chosen hardware, ensuring consistent G-code generation which could be optimised for the selected printer firmware. It also had pre-configured material profiles, such as PETG, ABS, PLA, to name a few, reliable first layer adhesion, and extrusion temperatures without the need for manual calibration. Furthermore, the ability to implement variable infill and adaptive layer height allowed for part-specific optimisation which could be used to increase strength is certain areas of the print.

For the design of the robotic arm's control circuit, Cirkit designer was selected as the preferred software tool. The platform was chosen due to its accessibility. Being both free to use and browser-based, which eliminated the need for dedicated installations and allowed for work across multiple different devices. The software featured an intuitive interface and a wide range of components in the built-in library, which included key components used in the project, such as the Arduino mega, high torque servos, and sensors. These features made it well-suited for accurately modelling the electronics of the system. In addition to its functional capabilities, it also offered a visually clear and professional looking modelled components, making it visually appealing and easy to plan and present wiring configurations.

Similar to the selection of the 3D printing software, the coding software was also an obvious choice, that being the Arduino IDE coding software. With its straightforward interface, extensive customer support and large library to make use of, such as the servo.h library, made it an excellent choice for coding with use of the Arduino mega 2560 microcontroller. The IDE allowed for efficient code development, real time serial monitoring (if it were integrated in the future), and quick uploads via USB connection, directly to the onboard memory, only requiring power afterwards. The use of Arduino IDE ensured a consistent and reliable workflow from initial testing to final prototype.

3.3 MATERIAL AND PRINTER SELECTION

After the designing and modelling phase of the robotic arm it came down to manufacturing and fabrication. This involved the use of Prusa MK3 & MK4 3D printers, with priority parts being printed on the Prusa MK4 as it was superior in every technical aspect. All components were printed with either PETG or ABS, depending on what properties were most desired for each component. For prints that took over 8 hours or more, the use of the University of Dundee Heathfield Labs' Stratasys F170 printer was used due to the safety features implemented into them, the printer also made use of soluble filament making more complex components easier to print with supports that were easier to remove, all prints from this were done in ABS. If given the space and the time, certain parts were printed together to allow for increased productivity.

The materials chosen for the fabrication of the robotic arm components were PETG (polyethylene Terephthalate Glycol) and ABS (Acrylonitrile Butadiene Styrene), both of which offered a favourable balance between mechanical strength, thermal stability, and ease of printability for a lightweight robotic arm. PETG was the primary material for the structural components, when applicable. This is due to the high impact resistance, dimensional stability, and minimal warping during printing, which are crucial for maintaining tolerances in mechanically loaded assemblies [28].

3.4 HARDWARE

This subsection broke down the design methodologies in hardware selection.

3.4.1 Microcontroller

The primary microcontroller selected for this project was the Arduino Mega 2560, chosen primarily for its availability and number of digital inputs and output. Other options that were considered included the Arduino Uno and the MBED NXP LPC1768. While the Uno would have been enough for the fundamentals of the robotic arm (including servo control libraries and basic sensor feedback), there were none available to use for the project or in a working condition to be used, if one were available, it would have been used in place of the Mega due to the more favourable size for mounting purposes.

The Arduino mega, shown in Figure 9, provided numerous advantages in terms of scalability however, due to its size. Its 54 digital I/O pins (15 of which are PWM capable) and 16 analogue inputs, which allowed for flexibility for servo allocation, sensors, and potential feedback modules such as encoders or Inertial Measurement Unit (IMUs) [29].

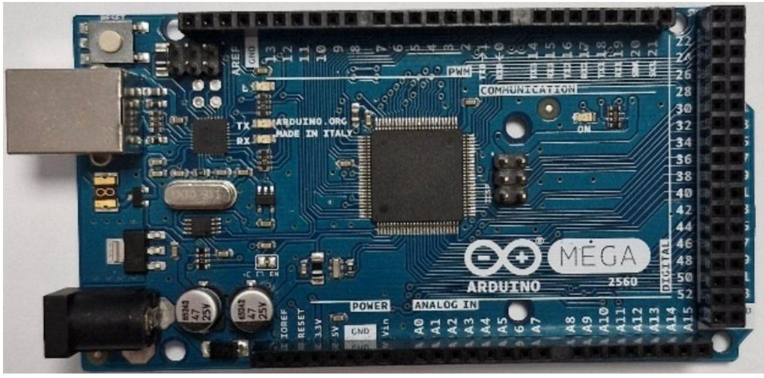

Figure 9 - Arduino Mega 2560

The MBED NXP LPC1768, shown in Figure 10, was also considered due to usage in class in previous modules, however for this exact same reason it was why it wasn't chosen, as the MBED wasn't user friendly in terms of its usability, alongside more familiarity with Arduino and its capabilities made the MBED undesirable overall.

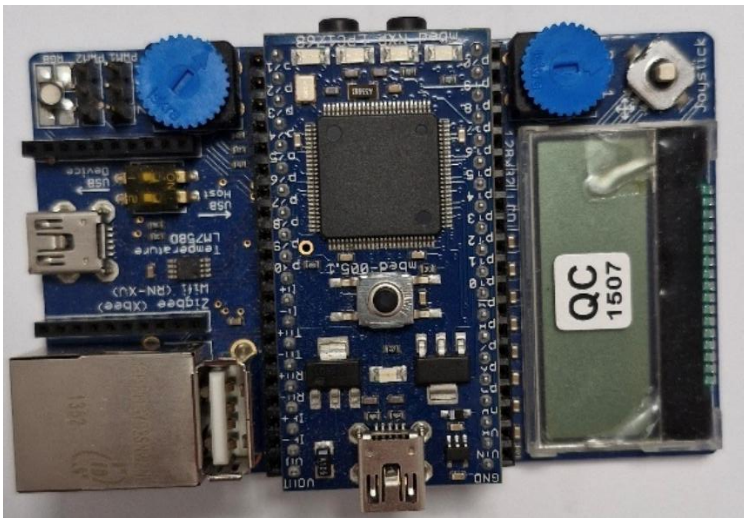

Figure 10- MBED NXP LPC1768

3.4.1 Tools & Sensors

A range of basic workshop tools were used for the construction of the robotic arm, such tools including hand files, hacksaws, wrenches and screwdrivers, etc. Larger equipment was also required such as pillar drills, in case of amendments to certain components that did not require reprinting. These tools were essential for ensuring precise fitment between components, particularly where tolerances from 3D printing require manual adjustments.

During the construction phase, general workshop safety procedures and good working practices were followed. Parts were secured with a vice during cutting or drilling, protective eyewear were worn during operation of said tools, and sharp edges from metal fasteners were de-burred to prevent handling risks. When working with PETG or ABS, fasteners were tightened incrementally to avoid deformation, and alignment was checked during assembly to ensure level parts, when applicable, for loads to be evenly distributed, especially across structural components.

For the sensors, a HC-SR04 ultrasonic sensors, shown in Figure 11, compatible with the Arduino device, were mounted on the robotic arm, with offsets considered if mounted higher or lower than the gripper tip. The sensor connected to the digital input/output pins of the Arduino and was used to measure the proximity through time-of-flight calculations based on the ultrasonic echo response. According to published data-sheets specifications, the HC-SR04 is capable of measuring distances between 20-4000mm with an accuracy of ±3mm under stable environmental conditions [30]. Its mounting position was based on a clear, forward-facing view while remaining mechanically separate from the moving components, such as wrists and the fingers, reducing the odds of interference and false activation.

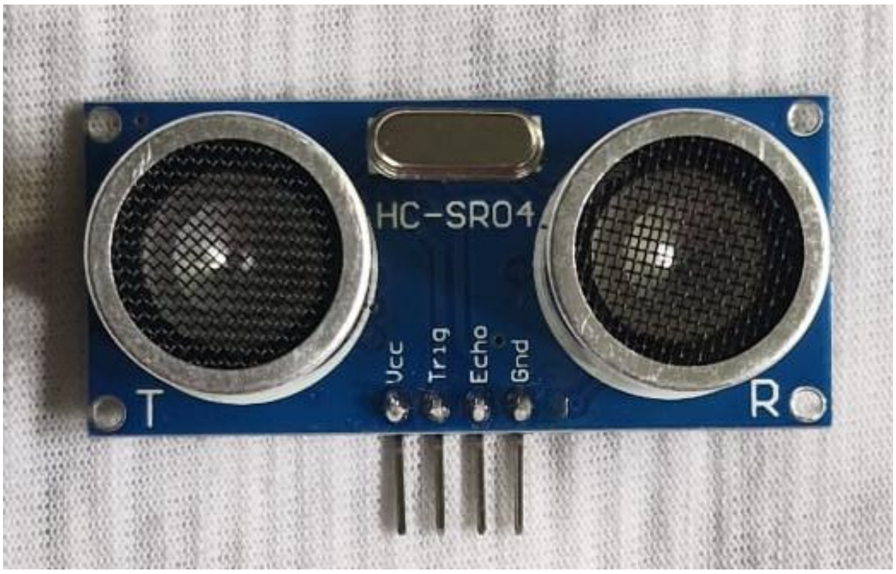

Figure 11 - HC-SR04 Ultrasonic Sensor

CHAPTER 4 – RESULTS

This chapter outlines the key outcomes derived from the design, simulation, manufacturing, and testing phases of the project. It begins with a breakdown of the construction stages for each major component of the robotic arm, detailing the design rationale and iterative refinements made during development. This is followed by a discussion of the simulation of the results, including MATLAB-based forward kinematics and ANSYS FEA outputs used to validate the mechanical and operational performance of the system.

The control system was built with a breadboard circuit and programmed using the Arduino IDE, where custom code was written to manage servo position, sensor integration, and partial autonomous movement. Experimental testing of the physical prototype was then presented, focusing on carrying capacity and autonomous functionality. Finally, modifications made in response to design limitations or operational inefficiencies are summarised. The combination of simulations and empirical results offers a comprehensive evaluation of the arm's effectiveness within the constraints of a lightweight mini-Mars rover platform.

4.1 DESIGN AND MANUFACTURING

This section provides a detailed breakdown of the design and manufacturing process of the robotic arm. It outlines the modelling stages of each major component, including the base, arms and supports, bearing assembly, and gripper assembly. The process began with early sketches involved through CAD modelling and iterative refinement to address structural and functional requirements. As shown in Figure 12, an annotated sketch of the full robotic arm with each component labelled to serve as visual reference for the parts described in the following subsections.

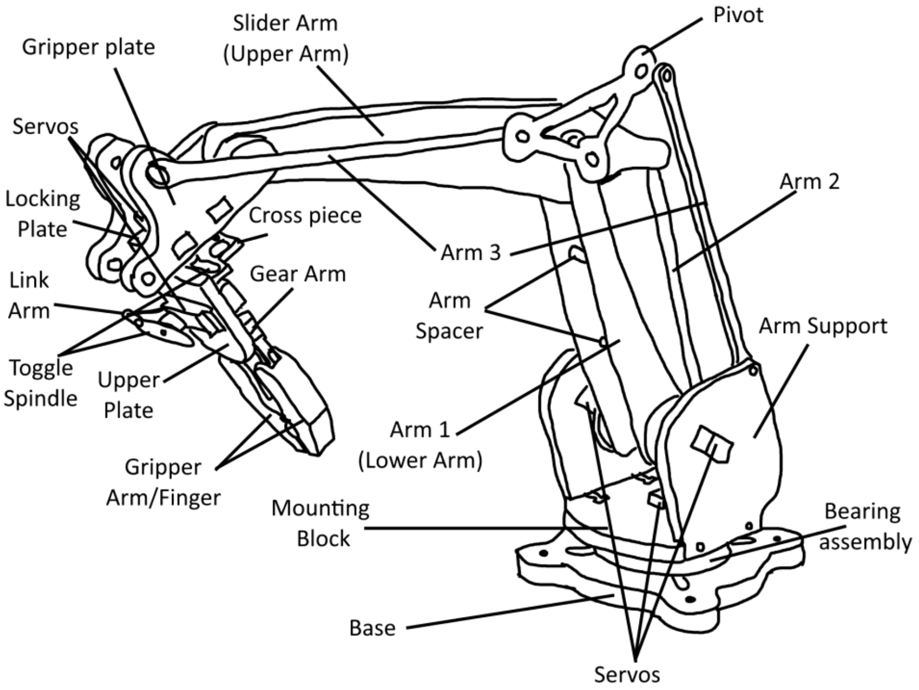

Figure 12 - Annotated robotic arm sketch

4.1.1 Base

With the overall size of the rover body being 292mmx432mm (WxD) The overall base was designed at 200mm diameter to allow for some clearance at the edges with a 48mm diameter circle also added to create the aforementioned mounting points. the circular pattern tool was used to create an even placement, and the fillet tool was used to smooth out any sharp corners created by the extrusions. The slots and mounting holes were cut into the material using the hole tool to create M8 drilled holes to allow for some clearance for fasteners to mount it to the rover. Finally, the shallow cutout for the bearing mount was cut out to a depth of 9mm. The final design of the base shown in Figure 13.

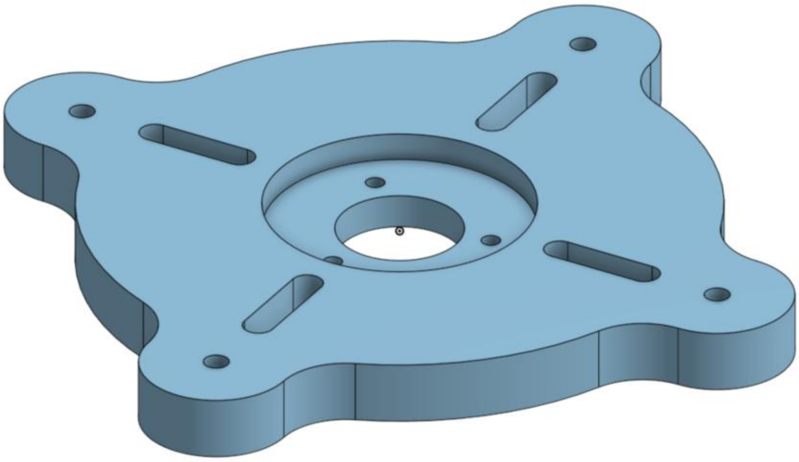

Figure 13 - Base of robotic arm

4.1.2 Bearing mount and bush

The bearing mount and bearing bush were created in similar ways, to save time on creating stacking multiple extruding circles, the bearing mount made use of the revolve tool. The process began with a half cross section of the part. The overall height of the profile was 24mm, with the intended radius being 40mm. A vertical notch for the bearing was included at 10mm of height from the base (starting at the end of the 40mm radius) with a depth of 5mm, with an upper segment of 14mm. All of this was revolved around the vertical plane to create a stepped cylindrical shape. Afterwards a 40mm cutout was made at a depth of 15mm was created for the mounting point of a servo spindle, with four M4 mounting holes cutout, followed by a 16mm through-all cutout created to allow a servo screw to be passed through. Finally, 6mm drilled holes equally spaced in an equilateral triangle shape were cutout for the mount of the base. Moving onto the bushing, it simply had 2 circles of diameters 88mm and 128mm extruded to a height of 26mm with countersunk holes drilled through all with the holes being offset as to not interfere with the servo mounted to the mounting block, both shown in Figure 14.

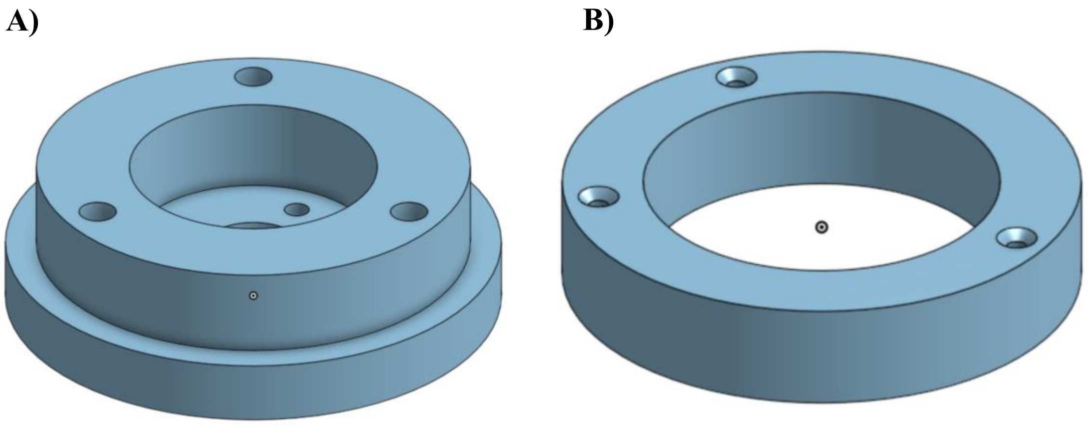

Figure 14 – A) Bearing Mount, B) Bearing Bush

4.1.3 Bearing

The bearing was created in a similar way to the bearing mount, where a cross-sectional piece was drawn and revolved around the vertical plane. A rectangle with dimensions 9mmx14mm (WxH) was created 35mm away from the origin, with a 5mm diameter circle placed in the centre which be used to create the channel in which the balls would reside, with the plan view shown in Figure 15. Once revolved it created 2 rings that were spaced 3mm apart, enough space to ensure the ball bearings did not fall out once installed. With these careful dimensions both inner and outer diameter matched the bearing mount and bearing bush respectively, creating a tight friction fit.

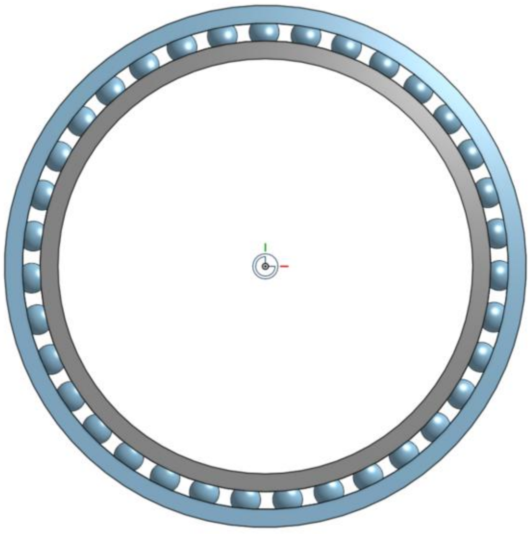

Figure 15 – Plan view of bearing assembly

4.1.4 Mounting block

The mounting block of the robotic arm started on the top plane and built upwards. First, the overall shape was designed. A circle with the diameter of 184mm was drawn from the origin followed by a line that created a flat edge. This was dimensioned to 75mm from the centre of the plate, as this created the ideal gap between the arm supports. The line was then mirrored and the excess circle trimmed, then extruded by 16mm. Afterwards, the cutout for the arm supports and the fasteners were created using rectangular sketches on the surface of block. The cutout was 10mm deep and 92mm wide with the fastener cutouts being 15mm deep with a larger cutout at the end to allow space for washer and bolt to attach the arm support. Finally, a cutout was created that had the dimensions of a standard servo as well as mounting holes that match the bearing bushing, shown in Figure 16.

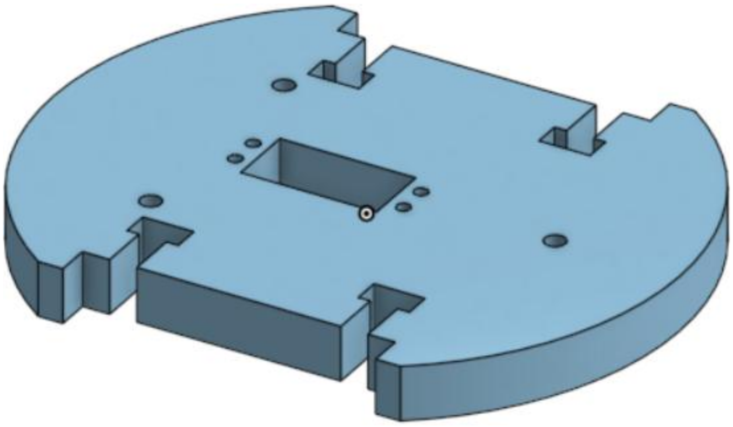

Figure 16 - Mounting block

Simple parts such as spindles, bearing cover, placeholder feet, and a servo model were created and placed into an assembly to visualise the lower section of the robotic arm before moving to the upper section, as shown in Figure 17, to ensure proper fitment and no interference between fasteners, with an exploded view in appendix B. With everything functioning as intended the upper section was worked on.

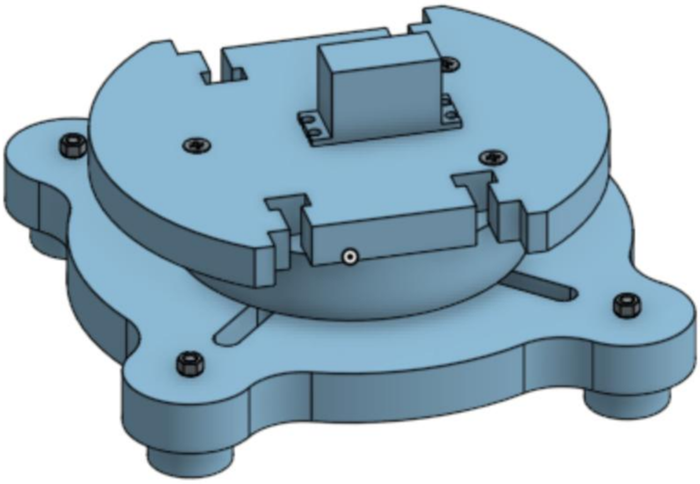

Figure 17 - Lower section assembly

4.1.5 Arm support

With the previously designed components, the arm supports were modelled next, shown in Figure 18. Unlike the other components, this was designed on the front plane. The total height of the part was roughly 170mm and a base width of 92mm, matching the slot on the mounting block, and a rounded front formed using a 45.75mm radius circle. For material reduction and structural strengthening angular features were implemented at the edges of the support. The servo slot was also angled at 35° for the aforementioned increased structural support and placement of spindle. M6 holes were also placed based on precise geometrical references for the structural arms as well as the joiner arms that supported the upper arm.

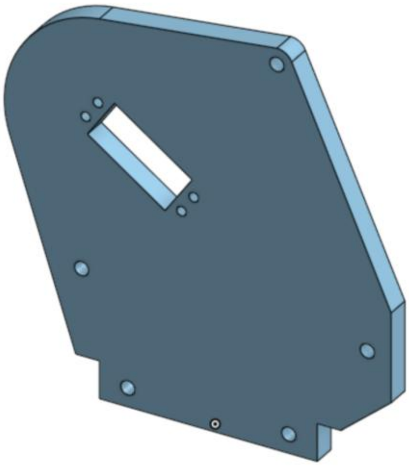

Figure 18 - Arm support

4.1.6 Upper and lower arm

The next stage in the modelling process was to move onto the robotic arm itself. The robotic arm consisted of four components made from two parts, both shown in Figure 19, the first part was the lower arm with a tip-to-tip length of 346mm, created with the use of circular drawings and tangent arcs of radius' 1700mm and 1000mm, which created the smooth curvature of the overall arm. It included a 16mm diameter hole for a shaft to pass through, M10 connecting hole, and two M6 holes for arm spacers to ensure proper distance and that structural integrity was maintained. A taper was created using 2 circles, a large one by the shaft hole of 35mm radius and a smaller one at the mounting hole of radius 15mm, which were connected with the tangent arcs and trimmed. A similar pattern was applied to the upper section, namely the slider arm, with circular features forming the frame, with radii of 9mm, 20mm, and 6mm from bottom to top, again connected together with the use of tangent arcs. Both of these arms were extruded to a thickness of 6mm, a good balance between structural strength and lightweight, low usage of materials.

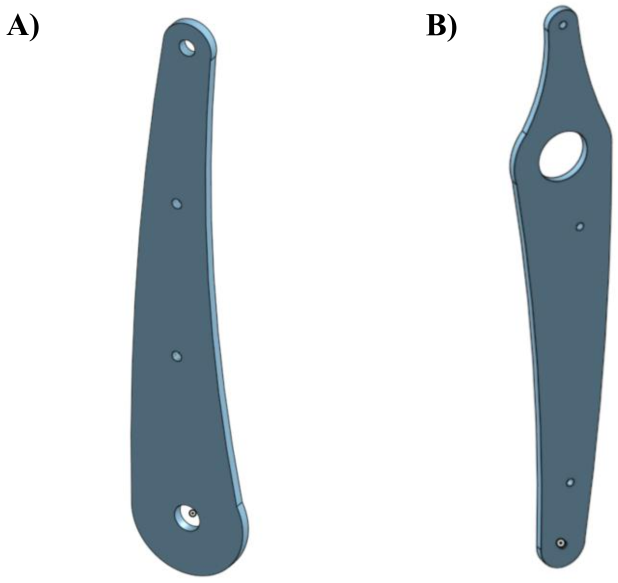

Figure 19 – A)Arm 1, B) Slider arm

4.1.7 Structural arms (arms 2 and 3)

Next to be designed were the structural arms, both shown in Figure 20, that kept the gripper head upright, the slider arm supported relative to the movement of the arm, and keeping the pivot point supported. This made use of two arms of similar design, with the only difference being the length of the arm depending on the location it was mounted. Both arms had a 10mm at either end, extruded out to 6mm thickness, with rounded edges created using the fillet tool, with one having a length of 296mm and the other 320mm.

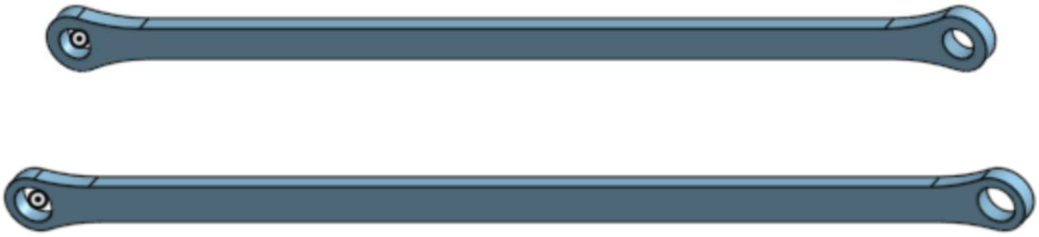

Figure 20 - Arm 2 (support-pivot) & arm 3 (joiner arm-slider/pivot-gripper head)

4.1.8 Gripper head

The gripper head was made up of a locking plate and two gripper plates, both shown in Figure 21. The gripper plate consisted mainly of three circular features with two rectangular cutouts for the locking plate to slot into. The radii of the frame were 18mm and 12mm on the sides, and 16mm for the top part, where one of the structural arms mounted, with two M8 holes and an 18mm diameter hole cut out for the mounting point, the slot cutouts were 16x10mm, and once sketched, extruded out to 14mm. The locking plate was simply a cuboid structure with a servo cut-out and shunts to lock into the cutouts prior mentioned.

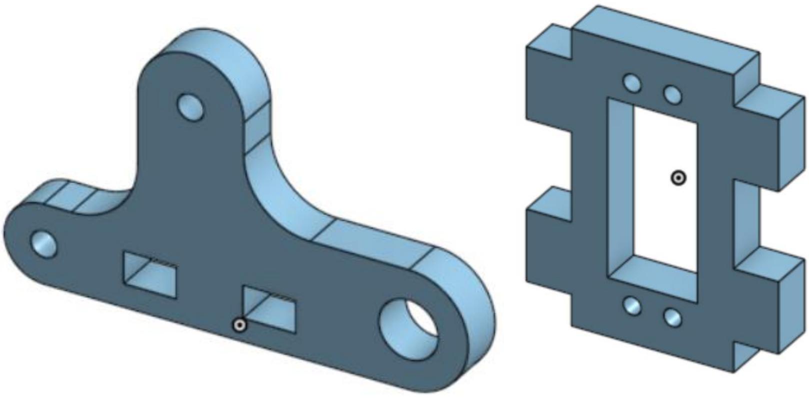

Figure 21- Gripper head & locking plate

The final creation of the main components was the gripper tool tip, shown in Figure 22. The gripper tooltip consisted of 2 components which slotted into each other to ensure a secure and rigid design. The gear arms made use of the toolbox in Onshape to place a 12-tooth spur gear onto the workspace. Six of the teeth were then removed to create the surface for the arm as well as limiting to how far it can open, a module of 3, and pitch angle of 14.5° were then set, alongside a shaft diameter of 8mm, where a custom printed bolt was slotted through to allow for smooth rotation. One of the arms had a protruding arm that came from the gear which would control the opening and closing through a link arm attached to a spindle. The length of this piece, from shaft centre to tool tip, was 75mm, with the arm reaching out around 65mm. The arm has 2 M6 hole cutouts for fasteners to secure the gripper to the gear arm. The gripper itself has the serrations and circular cutout for the larger samples, as per the design conditions. However, during the modelling process rib structures were placed in an effort to remove material from the gripper to reduce the overall material content whilst maintaining structural integrity. This was deemed successful based on the Onshape predictions, shown in appendix C, with a mass reduction of 17%. The cutout for the gear arm had a depth of 20.5mm, ensuring the entire arm was located within the gripper tool.

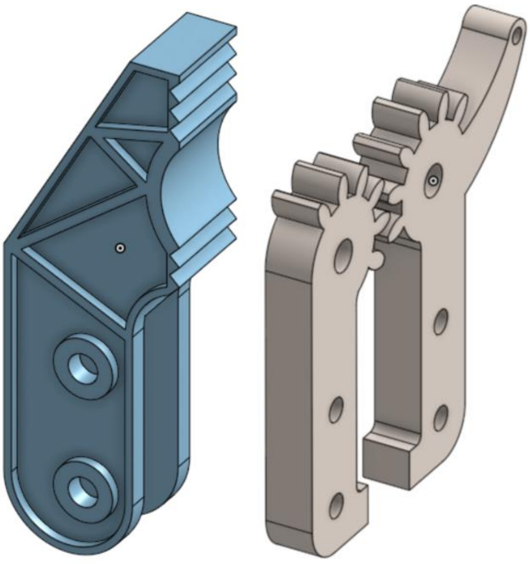

Figure 22 - Gripper "finger" and gear arm

Smaller components and servo models were then created that would bring the completion of the robotic arm assembly, such as a 16mm diameter shaft, 12mm diameter arm spacers 30mm long, 3-point pivot component with three 36mm diameter circles were connected together with M10 holes for mounting. 70mm diameter circular spacer with a width of 7.3mm, a link arm 45mm long with two mounting holes were also created, all shown in appendix A.

4.1.9 Final Assembly

Once all components were modelled, it was combined with the lower assembly to create the full assembly of the robotic arm using fastened mates, revolute mates and even some cylindrical mates. The arm supports were fastened to the slots of the mounting block followed by servos fastened to the support cutouts. Spindles were then revolute mated to the splines of the servo to allow for the simulated rotation. The spacers were then fastened to the spindles to create a place for the shaft to be mated to; in construction, this was friction fit to allow for ease replacement of components during testing and modification. The joiner arms and lower arms were then mounted to that shaft, with the arm spacers combing two arm 1s. The shorter of the two structural arms were then revolute mated to the arm support and to the pivot point. One of the two longer structural arms were then mated to the slider arm rear and another form the pivot to the gripper head. A combination of revolute and fastened mates Were then used to combine the gripper plates to the locking plates, the spindles to servos, cross piece to upper and lower plates, gear arm to upper plate and finally gear arm to gripper fingers. The final product shown in Figure 23, and a bill of materials also shown in Table 2.

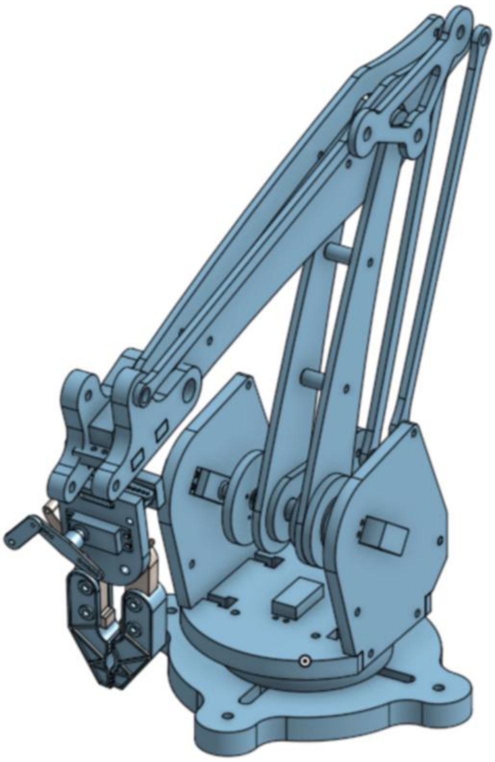

Figure 23 - Full robotic arm assembly

Item	Quantity	Item	Quantity
Base	1	Locking plate	1
Bearing mount	1	Toggle spindle	2
Bearing outer	1	Cross piece	1
Bearing inner	1	Upper plate	1
Ball bearing	35	Link arm	1
Bearing bush	1	Gear arm	2
Mounting block	1	Gripper arm	2
Arm support	2	M3 x6mm	13
Servo spindle	3	M4 Hex nut	25
Spacer	2	M4 washer	25
Shaft	1	M4 x16mm	25
Arm 1	2	M4 x30	4
Arm 2	1	M5 Washers	5
Arm 3	2	Countersunk M5 x50mm	7
Slider arm	2	M5 hex Nuts	16
Arm spacer	2	M6 x40mm hex head	3
Joiner arm	2	M8 x40mm	3
Pivot	1	M8 Hex nut	2
Gripper head	2	M10 x70mm	1
		M10 Hexnuts	4

Table 2 - Bill of Materials

Forward kinematics of the robotic arm was carried out on MATLAB with the use of Denavit-Hartenberg parameters. First, the robotic arm was broken down into its links and joints, giving the robotic arm 4 joints and 7 links. The 4 joints are the servo base, the shaft of the arm, the point where the lower arm and the slider arm connect, and finally the "wrist" of the robotic arm, at the gripper head. The links include the origin to base, the base to the shaft, the shaft to the arm connector, the arm connector to the gripper head, the gripper stem, and the tool itself (open and closed) which serves as the end effector. For each of the joints and links, a 4x4 transformation matrix was created to describe the translation between adjacent coordinate frames. These matrices were then multiplied in sequence to compute the position and orientation of the gripper fingers relative to the base of the robotic arm itself. This approach allowed for joint angles to be input and further translated into a 3D coordinate system highlighting the end effector position, forming the basis for motion control.

FEA analysis was conducted on ANSY workbench using static structural testing. The model of the robotic arm was exported from Onshape to a STEP file that could be used as the geometry of the FEA testing. Once applying the appropriate material to each component, A basic mesh was applied to the geometry of the model. Boundary conditions for the model were then set, such as the fixed position to the mounting points of the base and a force of the 1Kg requirement between the gripper fingers to simulate grabbing a surface sample.

4.1.10 Printing

Similar to that of the design phase, the lower section of the robotic arm was printed first. Both the base and the mounting block were printed on the Strayas because they both took over 10 hours to print. The structural infill of these materials was set to similar values because they bore the vertical load (compressive forces) of the robotic arm, so it was higher than most other components, with a selected value of 30% infill. The Ball bearing was made on the MK4 as it was crucial that tolerances were kept as close as possible, as any discrepancies would have caused the bearing to not function as intended. Since these components were going to be under constant wear, an infill of 100% was chosen. For the bushing, bearing mount, and bearing cover, all were non-structural parts whose only purposes was to combine the base and mounting plate via the bearing. Due to the low forces acting on them as well as no frictional and direct movements, an infill of 15% was selected with the bearing cover printed with other parts due to the size of the piece. While assembling the lower section the arm segments and supports were undergoing their prints, once again increasing overall productivity through time reduction.

For the larger supporting components, arm supports and joiner arms, they were printed on the Prusa MK4 with PETG due to them supporting a large portion of the robotic arm during operation, making use of the high strength PETG provides, as well as the printing quality. The smaller components, spacers, shaft, and servo spindles were printed on the Prusa MK3, as they required less time to print and had greater tolerances in terms of dimensions. Material selection for these components were either ABS or PETG, depending on availability at the time of printing. Although PETG would be chosen if it were available.

Most of the arm components, such as the upper and lower arm were printed on the Prusa XL due to length and for the material selection, all of the arm components themselves were made of PETG apart from the structural arms that maintain pivoting, which were made of acrylic due to time constraints as well as printer availability at the time. One such print of the slider arm is shown in Figure 24.

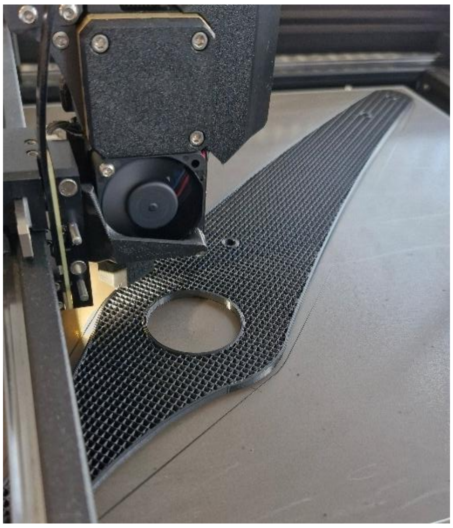

Figure 24 - Slider Arm printed

Printing for the arm segments took the most time out of all the components, and experienced the most printing failures, taking several days before a usable print was achieved. Some other reprints were the bearing bush to create a tighter fit around the bearing as well as the shaft and, for a similar reason the spacer and the lower arms to allow for rotation.

Some components were printed in batches, with multiple different components printed at the same time. One example was printing 2 servo spindles, a cover plate, and shaft at the same time to create multiple components at once. Although this took longer, it did reduce the number of printers allowing larger components to be printed which, if timed correctly would enable everything to finish at the same time. One instance of this is shown in Figure 25, where multiple components were spread across the printing bed to produce multiple components at once.

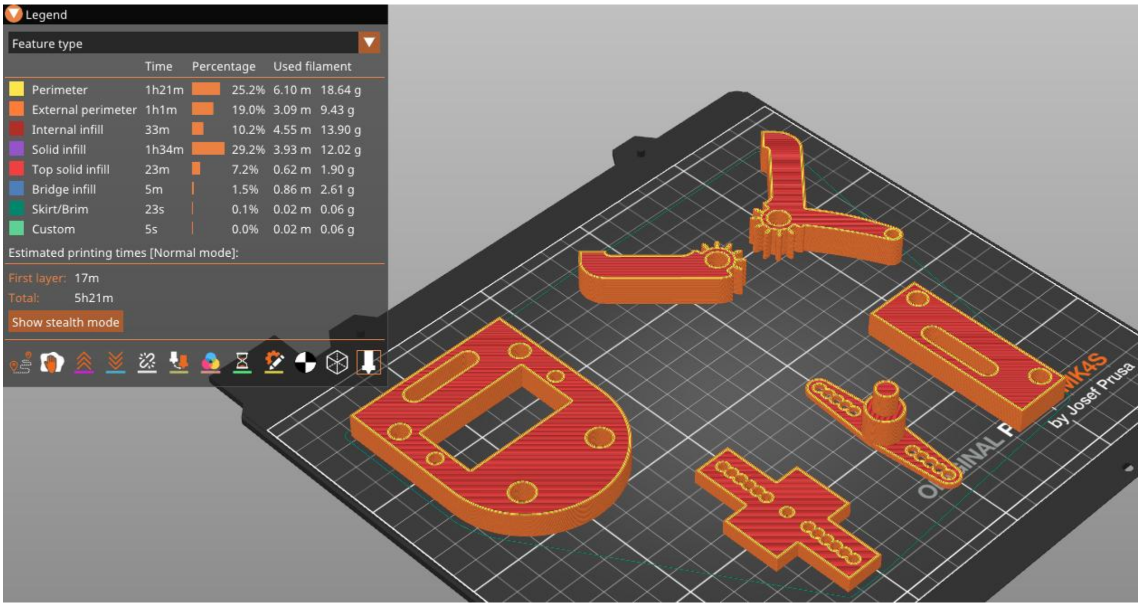

Legend

Feature type

		Time	Percentage		Used filament	
🟨	Perimeter	1h21m	25.2%		6.10 m	18.64 g
🟧	External perimeter	1h1m	19.0%		3.09 m	9.43 g
🟥	Internal infill	33m	10.2%		4.55 m	13.90 g
🟪	Solid infill	1h34m	29.2%		3.93 m	12.02 g
🟥	Top solid infill	23m	7.2%		0.62 m	1.90 g
🟦	Bridge infill	5m	1.5%		0.86 m	2.61 g
🟩	Skirt/Brim	23s	0.1%		0.02 m	0.06 g
🟩	Custom	5s	0.0%		0.02 m	0.06 g

Estimated printing times [Normal mode]:

First layer: 17m

Total: 5h21m

Figure 25 - Multiple components on Prusa print bed

4.1.11 Construction

Once printed the components were assembled in the Heathfield workshop which offered easy access to high quality tools and all the fasteners needed. Safe storage space for the robotic arm was also provided, allowing for quick resumption of the construction of the project.

As before, the construction was done from the base up. The bearing mount was secured into the cutout of the base with the use of M6 hex head bolts that were cut to size with the use of a hack saw, using a file to create the chamfer for easier installation and remove burr. The thread bit into the plastic easily due to the drill and tapped section in Onshape giving a slightly smaller diameter, allowing it to grip hard to the material. This was then followed by the mounting of the bearing bush to the mounting block. Originally, countersunk M6 screws were to be used, however during the construction purchase, the only suitable screws available were countersunk M5x50 screws. Therefore a washer and nut had to be used to ensure adequate fastening.

The bearing assembly had some challenges when combining the printed parts into an assembly. The technique was used to allow for proper loading of the balls into the shroud, where the casing was placed upright, similar to a wheel, followed by placing the balls in the groove of the outer casing. The inner shroud was then placed over the top of those balls and pressure applied to keep everything together. One-by-one the remaining balls were forced into the casing, keeping constant pressure on the inner shroud to keep the balls inside the groove. This gave a completed ball bearing assembly which was pressed down onto the bearing mount, shown in Figure 26.

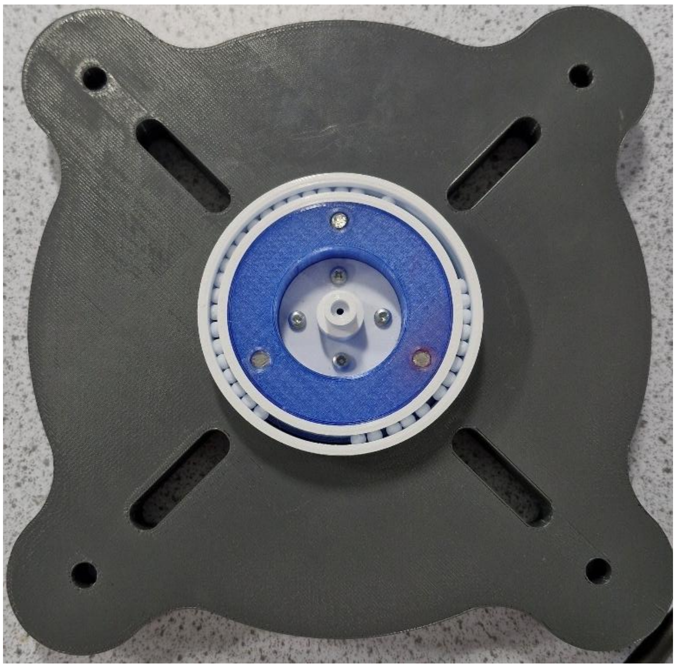

Figure 26 - Lower base with bearing installed

With the bearing fitting tightly onto the bearing mount, one of the spindles was then attached to the mount with M4 screws and secured tightly with washers and hex nuts, as it needed to be secured due to the servo causing the rotation. The bearing bush-mounting block combination was then be pressed on top of the bearing assembly to ensure it fitted properly and rotated smoothly. Once checked for fitment, the servo was then installed, but due to some printing tolerances the slot had to be filed back to ensure a proper fitment. Once the modification was made, the servo was secured with four M4 screws, washers and hex nuts, with all following servos undergoing the same installation method.

Assembling the lower arm section was moved onto starting with the 40kg/cm servos being mounted to the arm supports, the spindles were fixed on top of the servos, with the spacers being attached prior with M4 screws. The lower arms were pressed onto the shaft first, then the joiner arms, finally pressing the shaft into the spacers for a secure fit. The assembly was then installed with the use of m5 screws, washers and nuts. Each screw was fed through the arm support hole with a washer being fed onto it, followed by a hex nut, with the use of needle-nose pliers for precision placement and to hold the nut in place to tighten the screw. This created a very strong grip, something that is crucial as this assembly holds most of the mass of the robotic arm. However this construction provides a challenge because if it is needed to be removed for maintenance, the unscrewing process to be repeated 4 times as shown in Figure 27.

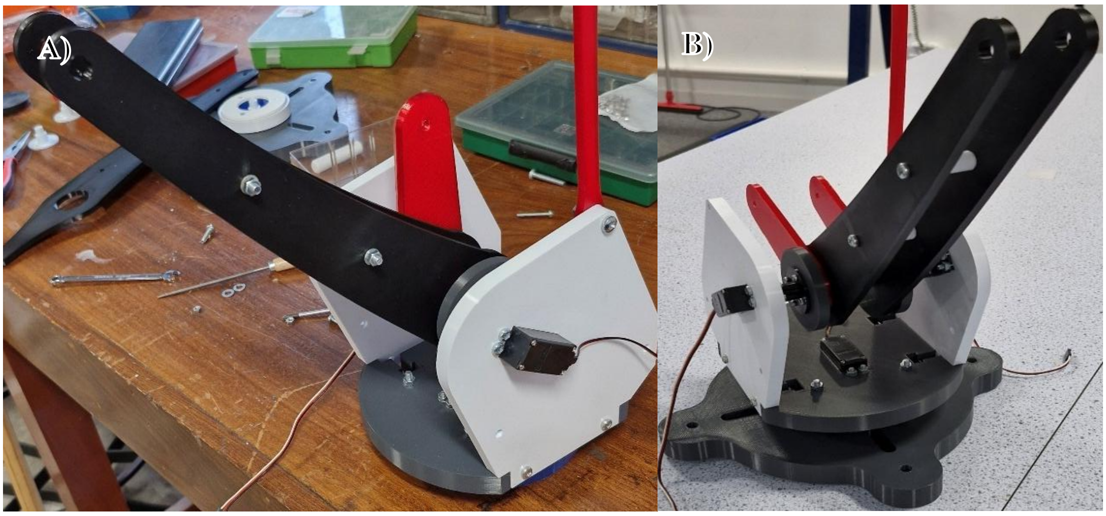

Figure 27- A) Lower arm assembly, B) Lower arm assembly attached to base

Before moving onto the upper arm section some smaller additions had to be made. 300mm threaded M6 rods were bought and cut to around 150mm which were threaded through one of the arm-supports and through one joiner arm This is where one of the structural arms, arm 3 in figure 10, was placed onto. The reverse was then done on the opposing side connecting the two arm supports together. Another task, as shown in Figure 27 A & B, involved arm 2 being bolted on using M6 shoulder screws and nuts. Shoulder screws were used as a bearing/fastener combo, allowing for smooth rotation without the hex nut coming undone.

Once key structural components were on, the slider arm and pivot was added next, with the use of an M10 bolt. This was fed through the pivot, through the lower arm and the two slider arm segments were then slotted in between the two lower arm segments. The bolt was then passed through the second lower arm segment and bolted securely. Once attached the rear structural arm was fastened to the slider arm to control the forward and backwards movement, the final structural arm fastened to the pivot point and the gripper head ready to be mounted to the slider arm and structural arm for usage.

The gripper head was assembled primarily using friction-fit components and a 3D printed bolt to minimise the overall weight, as excessive mass at the end-effector had the greatest negative impact on overall performance. Upon securing the servos to the locking plate and upper plate, the cross piece was inserted into the upper plate and fastened to a servo spindle, which itself was connected to the servo on the locking plate. This configuration formed the gripper stem of the assembly. For the gripping segments of the overall gripper assembly, a custom M8 shoulder bolt was 3D printed and then manually threaded using an M8 threading die, with a thread length of 6mm. This bolt was passed through the gear arm and upper plate, then secured with a nylon nut. This allowed for smooth rotational movement with significantly less torque required, particularly compared with a standard ANSI M8 shoulder bolt, which highlighted excessive friction causing the gripper to bind during operation. Finally, the gripper fingers were slotted into position and bolted onto the gear arms, while the locking plate was securely seated into the gripper plates to form the gripper head structure. This was attached to the assembled body, as shown in Figure 28.

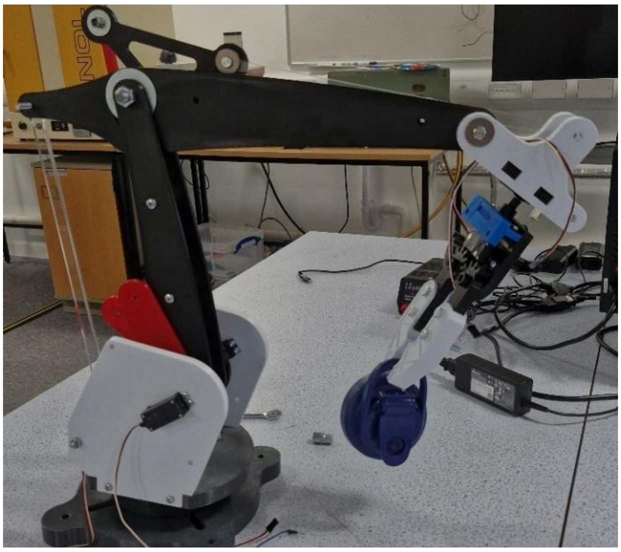

Figure 28 - First prototype of robotic arm

After careful modifications the robotic arm was capable of lifting the goal weight of 1kg at full extension, without any failures or issues. This is shown in Figure 29A, where the robotic arm had a mass of 1Kg hanging freely from a strap, the mass being weighed before use as shown Figure 29B. The final weight of the robotic arm also came down to 2.25kg, 55% lower than the set objective of 5kg, satisfying the requirement of it being a lightweight robotic arm. An image of this is shown in appendix F.

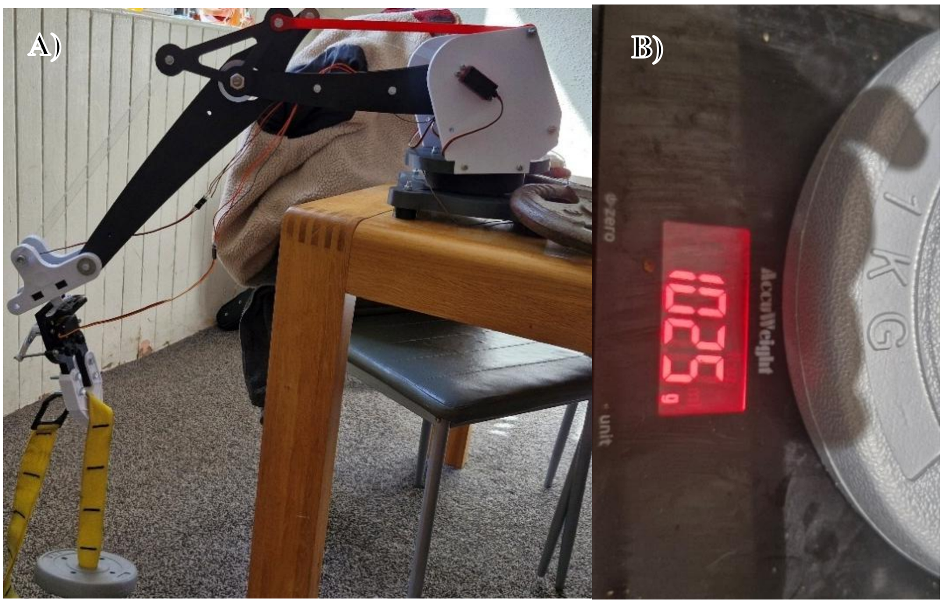

Figure 29 – A) Robotic arm holding 1Kg at full extension, B) Calibrated mass

4.2 SIMULATION RESULTS

The simulation of the forward kinematics, using MATLAB, was run to validate the accuracy of the robotic arm, using the custom function call, Robo_arm([0,80,-30,0],[0,0],1), a simplistic, proof of concept code. This input defined joint angles for the base, shoulder, elbow, and wrist respectively, while the final two parameters are gripper width, and distance from the tip to the actual gripping location (how far it opens and where it will be grabbing). As shown in Appendix D, the simulation generated a 2D and 3D visualisation of the arm's posture under the join conditions. A corresponding pose was replicated in the 3D model of the arm to compare the predicted and end effector position with the physical model. Despite the minor mechanical restrictions in the real assembly, particularly around the joiner arm section, there was a close alignment between the simulated and replicated end effector locations. This confirmed that the Denavit-Hartenberg based transformation matrices accurately captured the kinematic behaviour of the system, validating both joint angle relationships and workspace reach within the limits of the prototype. The full code can be found in appendix G.

The static structural analysis of the robotic arm was run in ANSYS workbench and gave the performance of the robotic arm under loading conditions. The analysis modelled a worst-case scenario, where the robotic arm was fully extended and subjected to a load of 1KG at the gripper tip. Fixed supports were applied to the base of the robotic arm to simulate the mounting condition on the rover chassis, and material properties for PETG were assigned, based on the engineering data within ANSYS. The simulation output revealed that the maximum stress occurred at the joint interface between the shoulder and the elbow, where the load transfer was at its highest. The peak Von-Mises stress was recorded as approximately 7.6 MPa, which remained below the yielding strength of PETG around 50MPa, confirming the structural integrity under loading conditions. Maximum deformation was observed at the gripper end of the arm and was measured to be 7.32 mm, but this displacement did not interfere with joint alignment or affect overall gripping accuracy.

Stress distribution was generally well contained across load paths, and areas of localised stress were observed around bolt holes, support brackets and joiner arm rod. These results validated the design decisions made during modelling and informed small adjustments such as increased wall thickness and increase in infill at high stress regions. The FEA confirmed that the arm could safely support the target load without risk of failure, reinforcing suitability for a lightweight yet high strength robotic arm. Images of the FEA analysis can be found in appendix H.

4.3 CIRCUITRY AND CODING

The control circuitry for the robotic arm was designed to manage multiple servos and sensor inputs through a central Arduino mega 2560. A schematic representation created in cirkit designer, outlining the layout of the key components such as the 5 servos for the actuation, the HC-SR04 ultrasonic sensor, and power distribution of the entire system routed on a breadboard. The circuit was configured to have clean pathways for the digital input/output (I/O) pins for each servo, with each wire having a corresponding colour to each section, green for base, orange for shoulder, purple for wrist, grey for open/close, on pins 2-6 respectively, while power and ground lines were shared across a common rail. The ultrasonic was connected to two digital pins, in this case pins 32 and 33, supporting distance measurement functionality to assist in autonomous functionality. A dedicated bench power supply was used to independently power the system, were voltage set to 7.4 Volts, the power at which the servos were operational as well as a suitable voltage level for an Arduino to function, with use of a DC power connector. The circuitry shown in Figure 30, note it shows a connection.

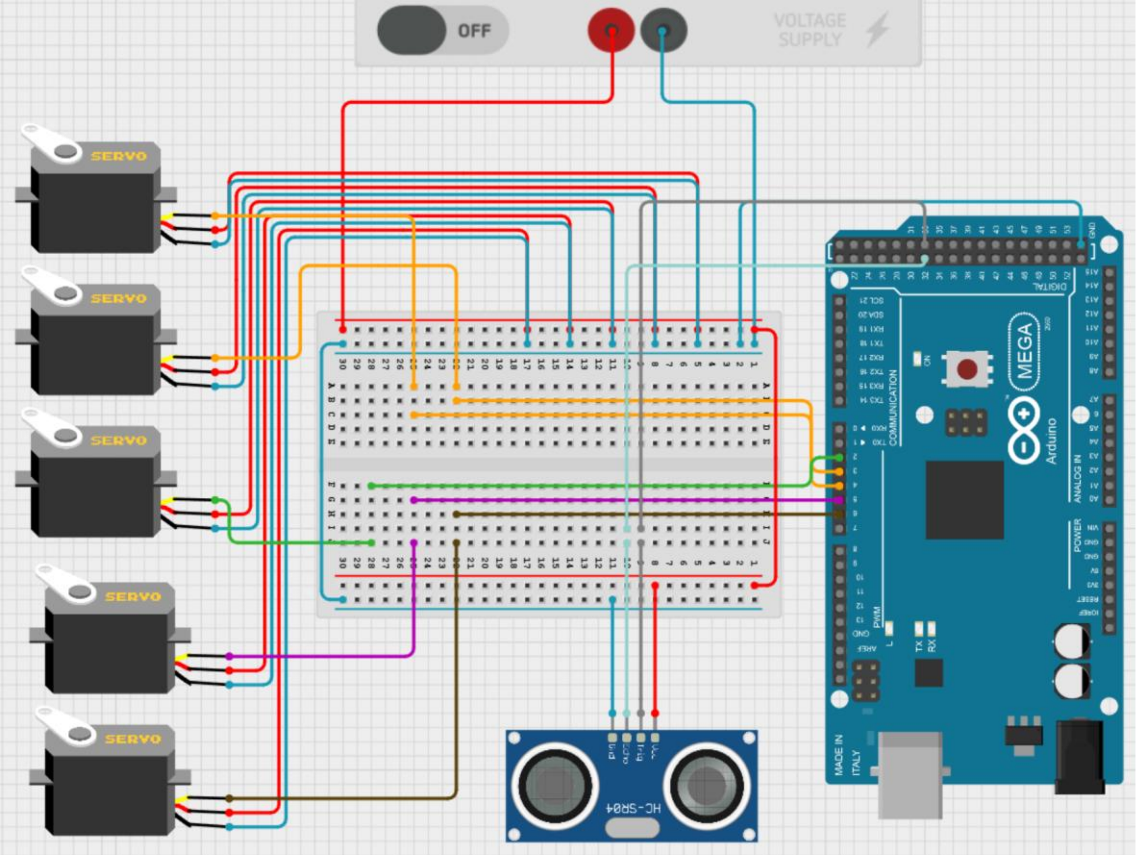

Figure 30 - Circuitry of robotic arm

The digital schematic served as a reference for the physical construction of the wiring, which was assembled using jumper wires on a breadboard, which acted as a makeshift PCB for the prototype. While the layout remained consistent with the digital plan. Practical considerations such as wire length, port accessibility, and cable management influenced the final wiring layout. With headers being soldered onto the jumper wires, for a secure connection for the signal contact when mounted to the breadboard. The final circuit shown in Figure 31.

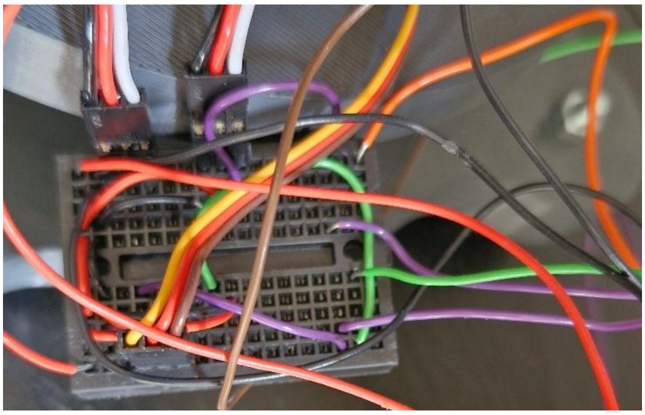

Figure 31- Physical circuit with 3/5 headers connected

The final control program for the robotic arm was developed using Arduino IDE and uploaded to the Arduino mega 2560, with the full code available in appendix I. The code was written in C++ and utilised both the servo.h and NewPing.h libraries, which were imported in lines 1 and 2, to manage servo control and ultrasonic sensor detection. Each major degree of freedom was assigned to a dedicated PWM pin, which were initialised in lines 5 to 9, with servo instances were created accordingly, shown in line 17. A mirrored configuration was implemented for one of the shoulder joints, as the two servos would be rotating in opposite directions to produce a lifting force, this was done in lines 24 to 29. The ultrasonic sensor was wired using trigger and echo pins, shown in lines 10 and 11, with its distance reading averaged over 3 pings, lines 31 to 34. The setup function initialised all the servo connections and positioned the arm into a predefined home pose, to ensure a known starting position, making it easier to control, shown in lines 42 to 45. A continuous loop then followed this which checked for nearby objects using the ultrasonic sensor. If an object were detected within the specified area and distance threshold, which was defined in line 13, the program would send signals to make the arm move incrementally and close the gripper once within the range of the sample. This sequence created a semi-basic autonomous interaction loop, allowing for the robotic arm to respond to environmental sample acquisition without real-time user input.

4.4 TESTING

Testing the robotic arm was split into two separate conditions, testing the overall payload capacity of the robotic arm and testing the autonomous capabilities of the robotic arm.

4.4.1 Carrying capacity

Testing the carrying capacity of the robotic arm was done through controlled weightlifting tests, both static and dynamic. The arm was positioned horizontally and weighed down with sandbags (since it would be mounted to a rover with mass this would not affect the test) and incrementally, the masses were applied the gripper head until the gripper could no longer hold onto the object. This was to determine the maximum amount of mass that the gripper head can hold onto without any form of structural deformation or failure. Throughout the testing, particular attention was given to the gripping properties, servo power and gear arm torque under load. The first test was directly after construction, making use of objects nearby, shown in figure 19, where the cap of a water bottle was used to quickly check the initial gripping power, the mass of this was around 60g. Once tested to see if it were working, the gripper head would hold onto a container with water being poured into it until the gripper failed, the mass of the liquid was then weighed to give the overall mass, including container.

4.4.2 Autonomy

In order to test the semi-autonomous operation, an ultrasonic distance sensor was integrated into the robotic arm, at the cross piece, to assist with object detection. The sensor was mounted roughly 190mm behind the gripper tips, with is "cone of vision" aligned in downward trajectory, following the gripper arm. The data was then fed to the Arduino Mega used to process the data. During operation the sensor enabled the robotic arm to detect objects placed within reach of the arm, however it had to have been directly below it, giving a partial autonomous grip sequence, removing the need for manual control. This proved effective in detecting objects directly below the arm, however due to the narrow field of view, the robotic arm would require more sensors to gain full autonomy. One benefit of this was due to the mounting of the sensor because no matter the orientation of the gripper, it could still detect objects that were in front of the gripper fingers, as there were no obstructions.

This semi-autonomous setup served as a great beginning for a proof-of-concept for proximity detection gripping and demonstrated the potential for increased autonomy with relatively cheap and low hardware complexity.

4.5 MODIFICATION

The servo spindles would be reprinted multiple times due to design changes, with around 4 total iterations with each iteration either making it easier to mount to the servo or to fix dimensioning issues involving swapping servos. The Spacers also had to be redesigned at one point due to them not creating a tight enough friction fit, causing the shaft to slip when the servos would rotate.

Upon completion of the initial construction, the robotic arm was found to be capable of lifting approximately 60 grams, as shown in Figure 19. This result highlighted the need for further investigation into potential performance limitations. One possible factor was the limited torque capacity of the servo used in the initial build. The original servo, rated at 2 kg/cm, was unable to provide adequate lifting force. To address this, it was replaced with a higher-torque 15 kg/cm servo to improve joint actuation under load. Another area of concern was the friction present in the gear arm pivot, which was influenced by the tolerance of the custom-printed shoulder bolts. The original bolts were found to be too loose, allowing unwanted movement at the joint under low force. To resolve this, the bolts were reprinted with an increased shaft diameter of approximately 0.3 mm, achieving a tighter press fit without introducing excessive friction or joint lockup. These modifications collectively contributed to an improvement in overall lifting capability to around 850g and eventually the 1kg mark, supporting the intended operational function of the robotic arm.

The first design had acrylic be the main material for the arm supports, due to the higher strength properties, however once cut using the laser cutter, it was found that some holes were misplaced on the model, this mistake allowed the opportunity to change to PETG, as the mass of the acrylic was 243g each, whilst the mass of the PETG support was 89g each which is a 63.37% reduction, a considerable difference in terms of weight. Once the holes were moved and, it was reprinted using the MK4 for its high speed and accurate printing.

One modification that had to be made was the friction fit between the shaft and lower arm was not tight enough, causing the robotic arm to slip, the same was also true for the shaft and the spacers. Rather than reprinting the whole shaft, taking up excess materials and creating waste, a technique use by machinists was used. A hammer and scribe were used to create indentations where the spacers and the lower arm sits, lifting some material creating a tighter fit once slotted in. Due to this being a prototype, there were no issues with doing this, however if it were final design, reprinting would be the optimal situation.

CHAPTER 5 – DISCUSSION

This chapter presents a reflective analysis of the project, evaluating how the final design was communicated, identifying technical and logistical limitations, and outlining potential improvements for future workings of the project.

5.1 PRESENTATION OF IDEAS

The design and development of the robotic arm was presented through visual explanations of both the CAD models were annotated and supported by MATLAB visualisations, as well as the prototype that was constructed. The forward kinematics of the MATLAB simulations helped communicate how the robotic arm's joints functioned relative to one another. The use of exploded views, joint schematics, and servo layouts provided clear insights into the physical layout of the overall system. This approach is consistent with how similar studies have communicated robotic arm development, such as that by Szczęsny and Rećko [18], who used joint-space modelling and transformation matrices to map arm motion in Martian rover analogues. Additionally, key limitations such as joint reach and material constraints were highlighted through simulation and experimental testing, reinforcing practical design considerations behind each decision. Supporting these references to the Mars surveyor 2001 and Perseverance mission arms offered technical justification for placement and control methodology [2].

5.2 CRITICAL ANALYSIS

This section provides a critical evaluation of the projects limitations and factors that influenced future improvements. Discussing such things as material and hardware constraints, environmental factors, and their impact on the overall mechanical performance and developmental time.

5.2.1 LIMITATIONS

One key limitation of the project was the restricted material selection available for manufacturing. While the use of PETG and ABS provided a reliable and structurally sound foundation for prototyping, more advanced materials such as carbon fibre-reinforced filament, ASA, or other lightweight composite polymers were inaccessible. These materials offer superior strength to weight ratios, thermal resistance, and UV stability, all of which are crucial properties for a robotic arm operating in a Martian environment. Their absence limited both the weight optimisation and over all structural integrity of the final design. Naturally, another significant constraint was the inability to simulate the Martian surface and environment during testing phases. Factors such as reduced gravity, extreme temperature differences, and atmospheric pressure could not be replicated in the laboratory used. As such, although the robotic arm demonstrated functional performance under Earth-based conditions, it is performance under Martian loads, material degradation, or overall interference from Martian factors, such as dust or other weather anomalies, remains speculative. This limits the ability to fully validate the system's reliability in its intended application.

5.2.2 FUTURE WORK

Looking ahead, several opportunities exist to expand and enhance the current design of the robotic arm. A key area for development is the refinement of the current autonomy system to make it into a fully autonomous robotic arm, enabling it to perform sample acquisition tasks without manual control. Increasing the degrees of freedom from 4 to 6 would further improve the manipulation, flexibility, and range, increasing the performance for more complex sample retrieval tasks. Although the current system achieved the lifting capacity of 1kg, future iterations should aim to maintaining the weight more effectively by revisiting mechanical leverages, torque outputs, and amendments in the gripper structure. More extensive testing, including both hardware endurance and software validation, would be critical in evaluating performance over time. Additional refinements could involve more detailed simulations, including precise forward kinematics, implementation of inverse kinematics, and more defined meshing for the FEA, to optimise both movement, accuracy, and structural integrity. Improvements in component tolerance and the development of a single material selection would contribute to a more consistent understanding of the behaviours of the material alongside weight distribution. Environmental factors such as Martian gravity could have also been included into the simulations and testing, particularly if the arm is to be adapted for real-world interplanetary exploration. Hardware enhancements such as replacing the 3D printed ball bearing elements with steel bearings and the design of a PCB could also improve robustness and integration. Due to time constraints, many of these ideas remain unrealised, but they could form the foundation for continued development and refinement of the system.

CHAPTER 6 – CONCLUSION

The objective of this project was to design, simulate and manufacture a lightweight robotic arm suitable for integration onto a mini-Mars rover platform. The arm was intended to support sample acquisition tasks while maintaining mass efficiency, mechanical reliability, and basic semi-autonomous function. Through a combination of CAD modelling, mechanical analysis additive manufacturing, and microcontroller-based control system, a fully functional prototype was developed and evaluated under laboratory conditions.

Key components were modelled using Onshape and fabricated primarily using PETG and ABS, via 3D printing. Material selection and print parameters were adjusted based on each component's structural requirements, balancing weight with durability. MATLAB was then used to simulate forward kinematics through Denavit-Hartenberg parameters, with simulation results confirming agreement between theoretical and physical setups. Structural performance was further validated using FEA conducted in Ansys workbench, ensuring that the robotic arm could support its own weight and lift up to 1Kg without exceeding material yield limits.

Partial autonomy was achieved by integrating an ultrasonic sensor with an Arduino mega, allowing for proximity-based detection near the gripper. While this offered limited feedback and interaction, it demonstrated the feasibility of using lightweight, sensor driven feedback in a compact system. Limitations such as restricted material access, servo torque constraints, and the inability to simulate Martian environment were acknowledged, but did not stray from the project's core achievements, but instead enhance them.

Overall, the project successfully met its primary design objectives and established a robust foundation for further development. The outcomes demonstrate the accessible tools and materials can be used to prototype interplanetary robotic arms in use of exploration. Opportunities for future improvement include producing MATALB code for inverse kinematics, greater autonomy, expanded sensor capabilities, and further mechanical refinement.

References

[1] "NASA Confirms Evidence That Liquid Water Flows on Today's Mars," NASA, 26 July 2023. [Online]. Available: https://www.nasa.gov/news-release/nasa-confirms-evidence-that-liquid-water-flows-on-todays-mars/. [Accessed 31 March 2025].

[2] R. G. Bonitz, T. T. Nguyen and W. S. Kim, "The Mars Surveyor '01 Rover and Robotic Arm," Jet Propulsion Labratory - NASA, [Online]. Available: https://www-robotics.jpl.nasa.gov/media/documents/roverArm01.pdf. [Accessed 30 November 2024].

[3] "How long does it take to get to mars," space.com, 20 January 2025. [Online]. Available: https://www.space.com/24701-how-long-does-it-take-to-get-to-mars.html. [Accessed 9 April 2025].

[4] M. Bajracharya, M. W. Maimon and D. Helmick, Autonomy for Mars Rovers: Past, Present, and Future, IEEE, 2008.

[5] P. Czaplicki, M. Rećko and J. Tołstoj-Sienkiewicz, "Robotic arm control system for mars rover analogue," IEEE, 2016.

[6] K. Kruthika, B. K. Kumar and S. Lakshminarayanan, "Design and development of a robotic arm," IEEE, 2016.

[7] k. R. Bollineni, S. S. Menon and G. Udupa, "Materials Today Proceedings," *Design of Rover and Robotic Arms,* vol. volume 24, pp. 1340-1347, 2020.

[8] NASA, "Mars 2020: Perseverance Rover," 2020. [Online]. Available: https://science.nasa.gov/mission/mars-2020-perseverance/rover-components/. [Accessed 17 October 2024].

[9] NASA, "Mars Rock Samples," NASA, 2021. [Online]. Available: https://science.nasa.gov/mission/mars-2020-perseverance/mars-rock-samples/. [Accessed 17 October 2024].

[10] R. Volpe, J. Balaram, T. Ohm and R. Ivlev, "Rocky 7: a next generation Mars rover prototype," *Advanced Robotics,* vol. 11, no. 4, pp. 341-358, 1996.

[11] D. Gaines, R. Anderson, G. Doran, W. Huffman, H. Justice, R. Mackey, G. Rabideau, A. Vasavada, V. Verma, T. Estlin, L. Fesq, M. Ingham, M. Maimone and I. Nesnas, "Productivity Challenges for mars rover operations," 2016.

[12] "Mars missions," Airbus, [Online]. Available: https://www.airbus.com/en/products-services/space/space-exploration/mars-missions. [Accessed 24 April 2025].

[13] "Europe's Mars exploration," The European Space Agency, 13 March 2023. [Online]. Available:

https://www.esa.int/Science_Exploration/Human_and_Robotic_Exploration/Exploration/ExoMars/Europe_s_Mars_exploration. [Accessed 24 April 2025].

[14] M. MAURETTE, “Mars Rover Autonomous Navigation,” *Autonomous Robots,* vol. volume 14, pp. 199-208, 2003.

[15] “Every mission to Mars ever,” The Planetary Society, [Online]. Available: https://www.planetary.org/space-missions/every-mars-mission. [Accessed 17 October 2024].

[16] M. S. Systems, “Mars 2020 Perseverance Rover,” 2023. [Online]. Available: https://motivss.com/space-flight-missions/mars-2020-perseverance-rover/. [Accessed 17 October 2024].

[17] N. J. P. Laboratory, “NASA’s Perseverance Rover Shows Off Collection of Mars Samples,” NASA, 14 02 2023. [Online]. Available: https://www.jpl.nasa.gov/news/nasas-perseverance-rover-shows-off-collection-of-mars-samples/. [Accessed 17 October 2024].

[18] T. Szczęsny and M. Rećko, Control of robotic arm for Mars rover analogue, Bialystok: IEEE, 2018.

[19] M. E. Moran, “Evolution of robotic arms,” *Journal of Robotic Surgery,* vol. Volume 1, pp. 103-111, 2007.

[20] K. Jahnavi and P. Sivraj, “Teaching and learning robotic arm model,” IEEE, 2017.

[21] D. McKenzie, N. D. Barnett and D.-N. Yuan, “The relationship between Martian gravity and topography,” in *Earth and Planetary Science Letters*, ScienceDirect, 2002, pp. 1-16.

[22] V. Belleguic, L. P and M. Wieczorek, “Constraints on the Martian lithosphere from gravity and topography data,” *Journal of Geophysical Research: Planets,* vol. 110, no. E11, 2005.

[23] P. G. Moustris, C. S. Hiridis, M. K. Deliparaschos and M. K. Konstantinidis, “Evolution of autonomous and semi-autonomous robotic surgical systems: a review of the literature,” 03 August 2011. [Online]. Available: https://onlinelibrary.wiley.com/doi/full/10.1002/rcs.408?casa_token=dElF89RWU8oAAAAA%3AOYlLilMUUCHlVZ0KEvn_i_FQWovYobJgLOJ_U9R8YsN1-BdSEZ4xCpRnf7ozTNHgSbDUylk-IsOmLg. [Accessed 6 February 2025].

[24] D. Hackett, J. Pippine, A. Watson, C. Sullivan and G. Pratt, “An Overview of the DARPA Autonomous Robotic Manipulation (ARM) Program,” 13 April 2013. [Online]. Available: https://www.jstage.jst.go.jp/article/jrsj/31/4/31_31_326/_article/-char/ja/. [Accessed 6 February 2025].

[25] H. Zeng, Y. Shen, X. Hu, A. Song, B. Xu, H. Li, Y. Wang and P. Wen, “Semi-Autonomous Robotic Arm Reaching With Hybrid Gaze–Brain Machine

Interface," 24 January 2020. [Online]. Available: https://www.frontiersin.org/journals/neurorobotics/articles/10.3389/fnbot.2019.00111/full. [Accessed 6 February 2025].

[26] R. Siemasz, K. Tomczuk and Z. Malecha, "3D printed robotic arm with elements of artificial intelligence," in *Procedia Computer Science*, ScienceDirect, 2020, pp. 3741-3750.

[27] A. Cañizares, J. Pazos and D. Benítez, "On the use of 3D printing technology towards the development of a low-cost robotic prosthetic arm," IEEE xplore, 18 January 2018. [Online]. Available: https://ieeexplore.ieee.org/abstract/document/8261579. [Accessed 12 March 2025].

[28] "Filament Properties table," Simplify3D, 2025. [Online]. Available: https://www.simplify3d.com/resources/materials-guide/properties-table/?filas=abs,petg. [Accessed 16 01 2025].

[29] Arduino, "Arduino Mega 2560 Rev3," Arduino store, [Online]. Available: https://store.arduino.cc/products/arduino-mega-2560-rev3?srsltid=AfmBOooaOHjsj0sVirmWvWG0zKcX4PqvmTvldCG9_GRSRbeoNHwHEJw_. [Accessed 12 03 2025].

[30] Dejan, "Ultrasonic Sensor HC-SR04 and Arduino – Complete Guide," How to Mechatronics, 24 November 2015. [Online]. Available: https://howtomechatronics.com/tutorials/arduino/ultrasonic-sensor-hc-sr04/. [Accessed 12 March 2025].

[31] M. McHenry, N. Abcouwer, J. Biesiadecki, J. Chang, T. D. Sesto, A. Johnson, T. Litwin, M. Maimone, J. Morrison, R. Rieber, O. Toupet and P. Twu, "MARS 2020 AUTONOMOUS ROVER NAVIGATION," California Institute of Technology, California, 2020.

APPENDICES

APPENDIX A – ADDITIONAL 3D MODELS

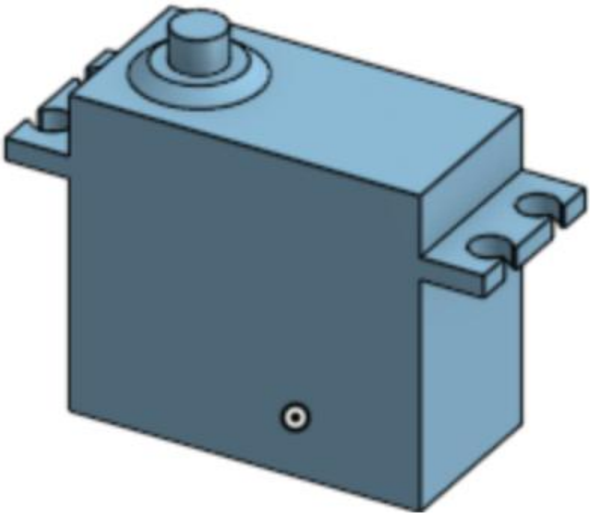

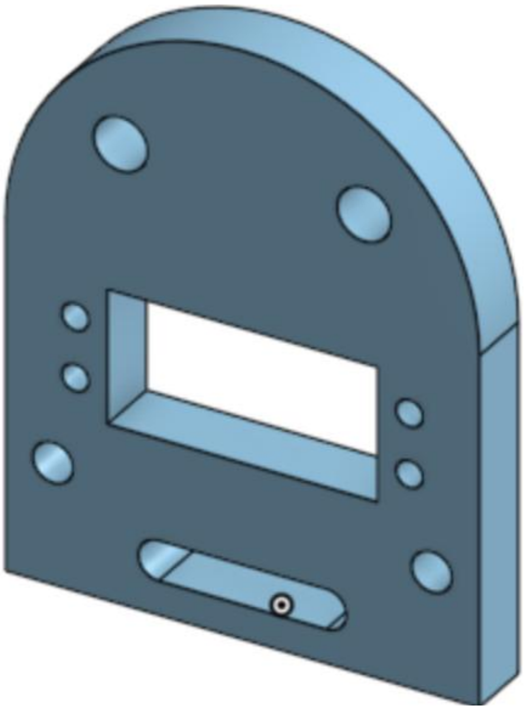

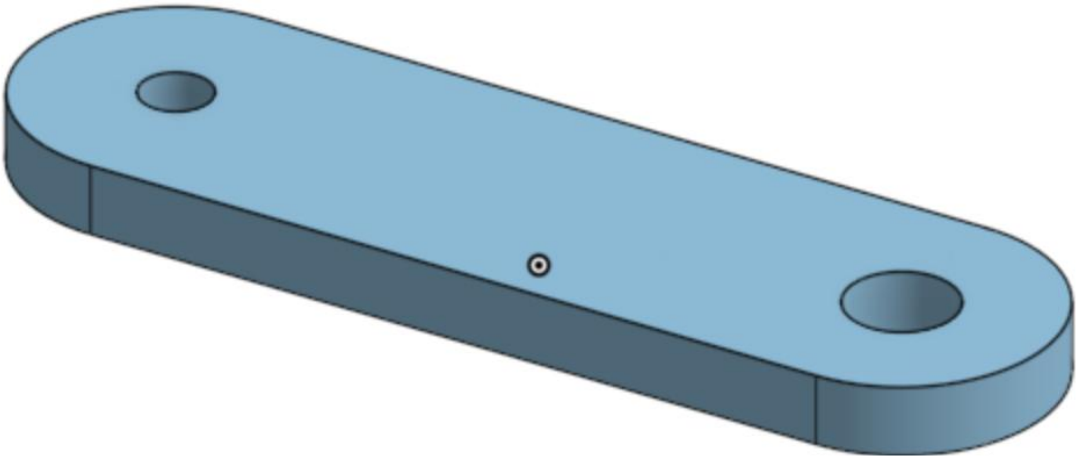

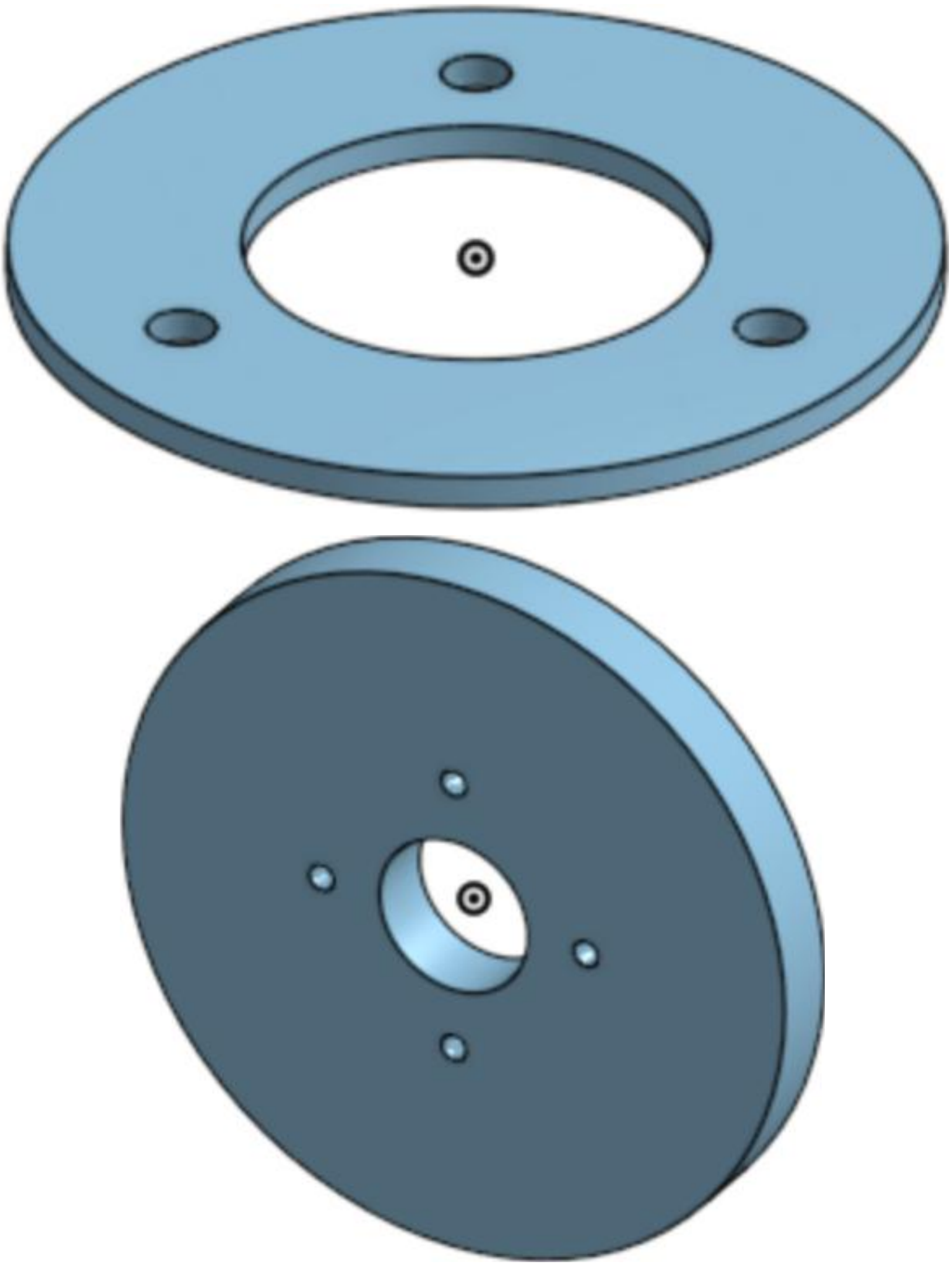

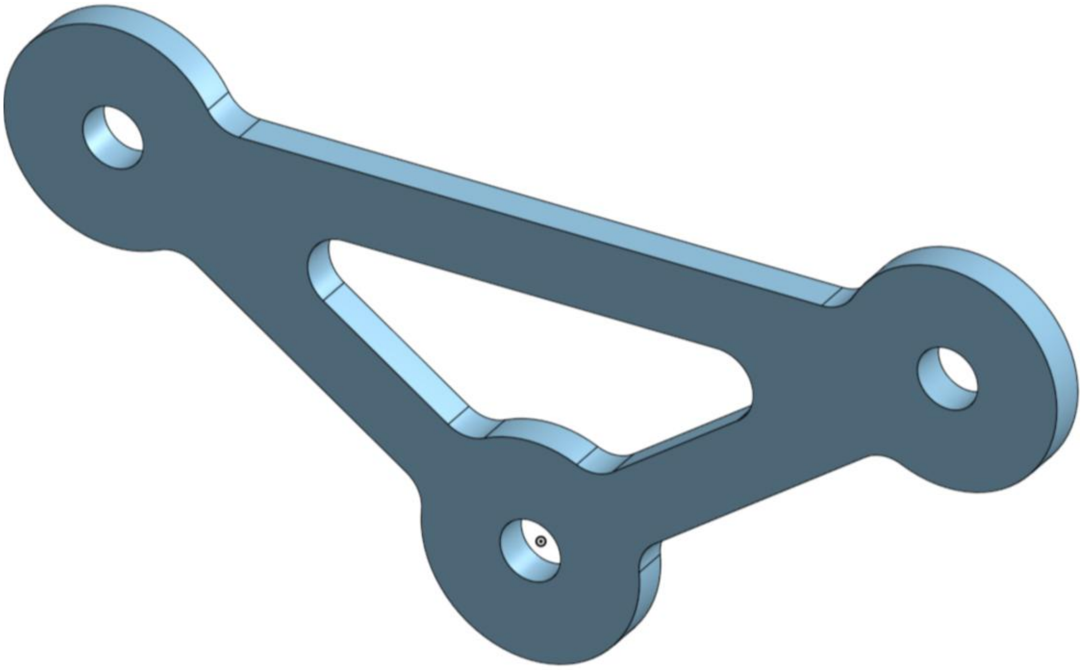

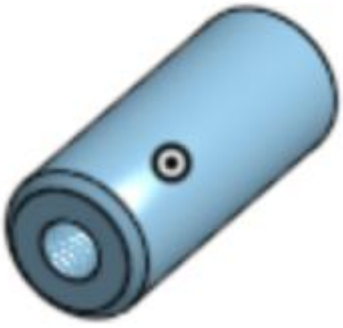

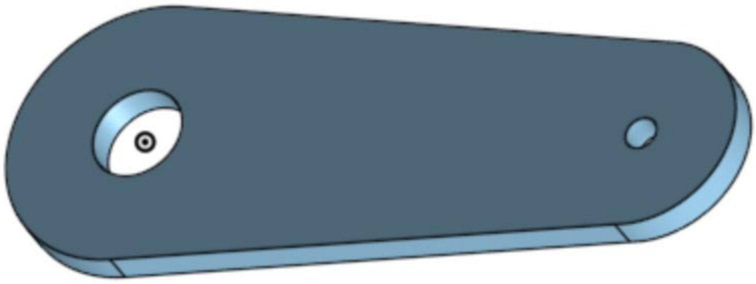

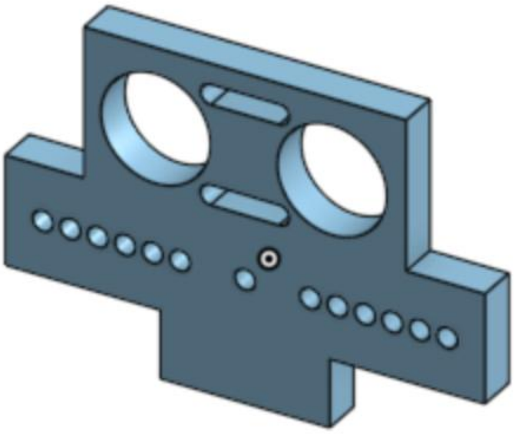

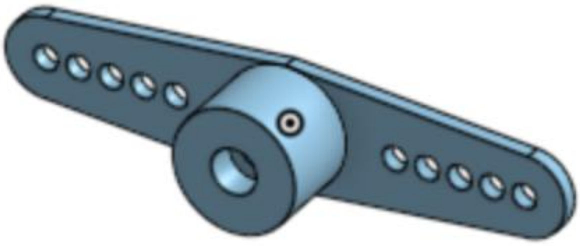

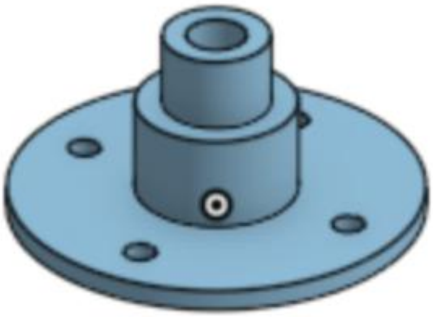

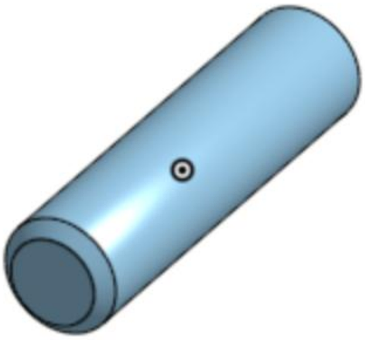

APPENDIX B – EXPLODED DIAGRAMS

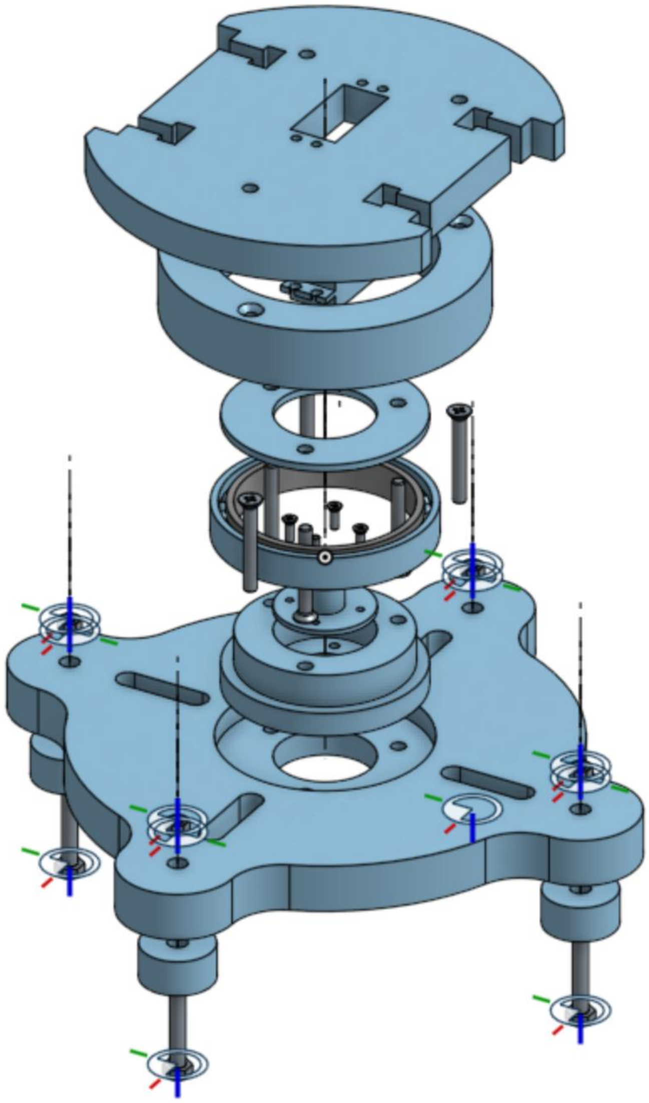

APPENDIX C – WEIGHT REDUCTION

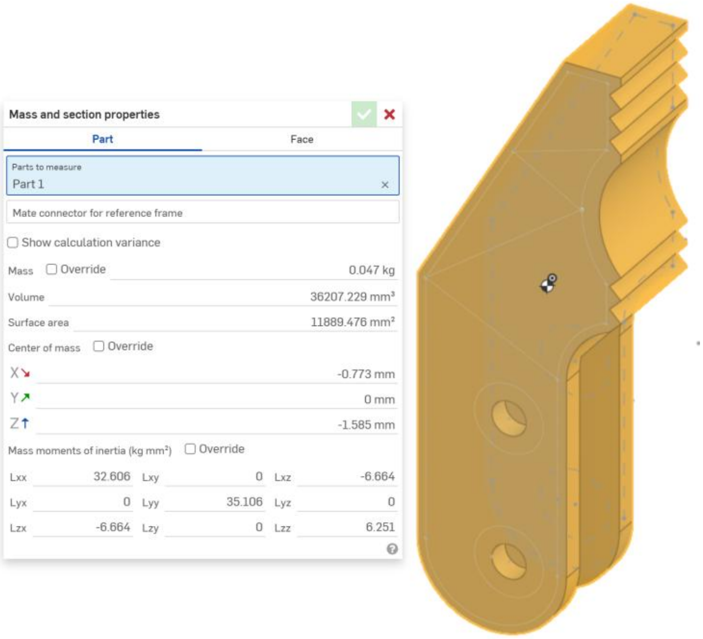

Mass and section properties

Part | Face

Parts to measure
Part 1

Mate connector for reference frame

☐ Show calculation variance

Mass ☐ Override 0.047 kg

Volume 36207.229 mm³

Surface area 11889.476 mm²

Center of mass ☐ Override

X -0.773 mm

Y 0 mm

Z -1.585 mm

Mass moments of inertia (kg mm²) ☐ Override

Lxx	32.606	Lxy	0	Lxz	-6.664
Lyx	0	Lyy	35.106	Lyz	0
Lzx	-6.664	Lzy	0	Lzz	6.251

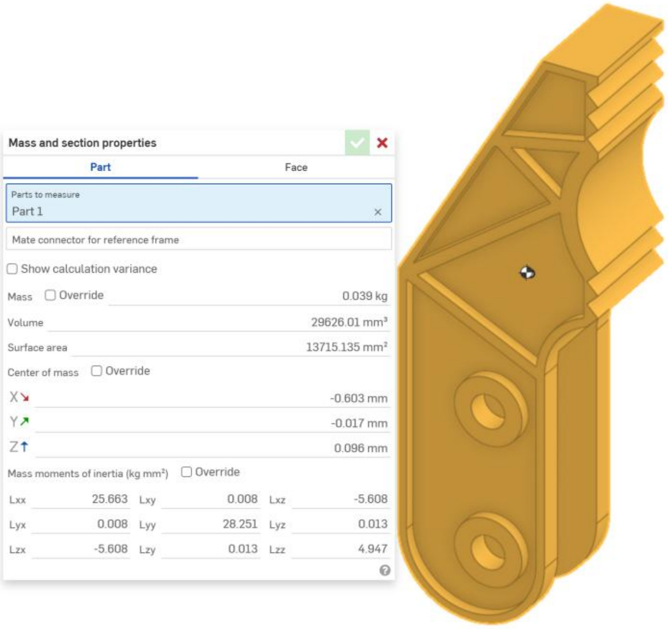

Mass and section properties

Part | Face

Parts to measure
Part 1

Mate connector for reference frame

☐ Show calculation variance

Mass ☐ Override 0.039 kg

Volume 29626.01 mm³

Surface area 13715.135 mm²

Center of mass ☐ Override

X -0.603 mm

Y -0.017 mm

Z 0.096 mm

Mass moments of inertia (kg mm²) ☐ Override

Lxx	25.663	Lxy	0.008	Lxz	-5.608
Lyx	0.008	Lyy	28.251	Lyz	0.013
Lzx	-5.608	Lzy	0.013	Lzz	4.947

APPENDIX D – MATLAB COMPARISON

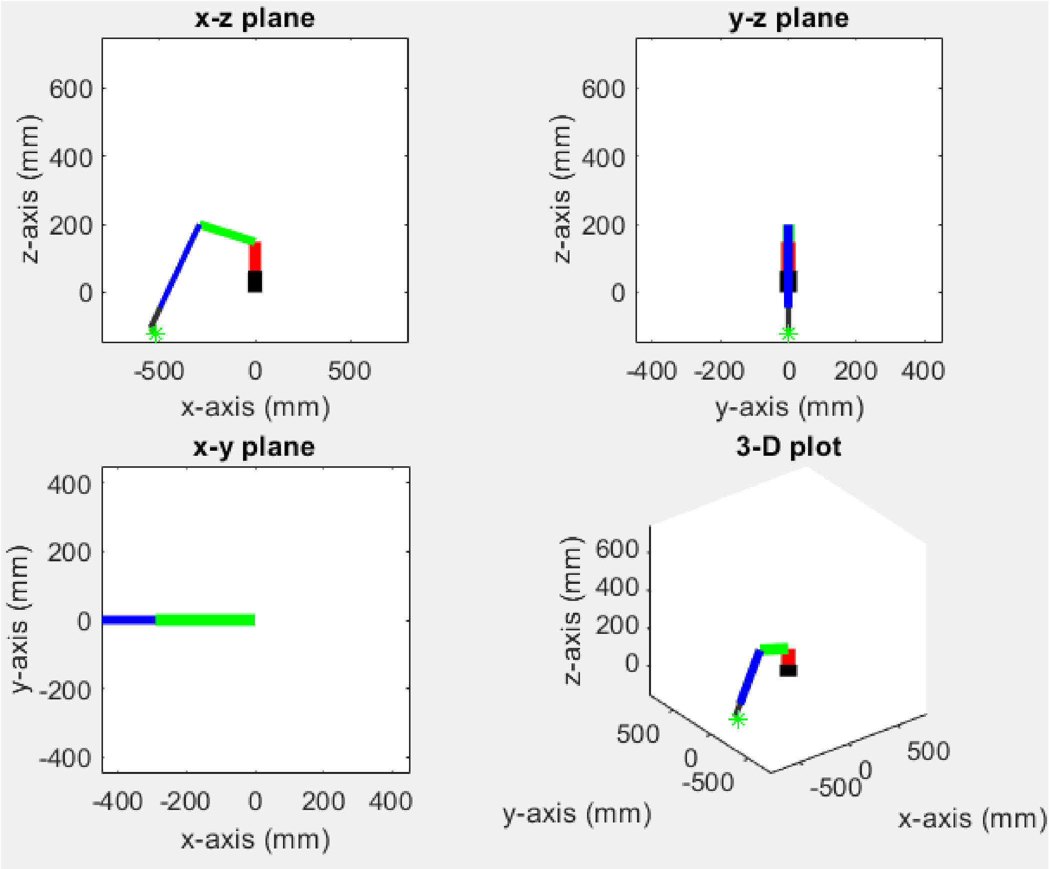

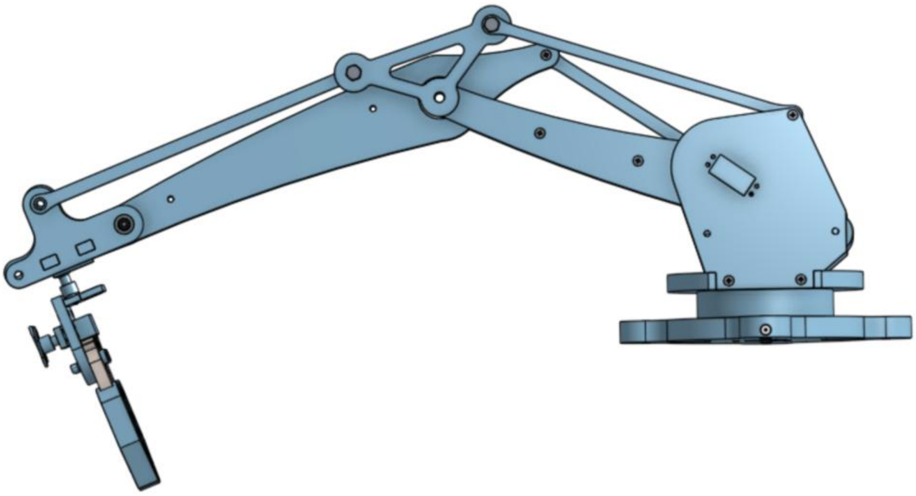

APPENDIX E - CAD DRAWINGS

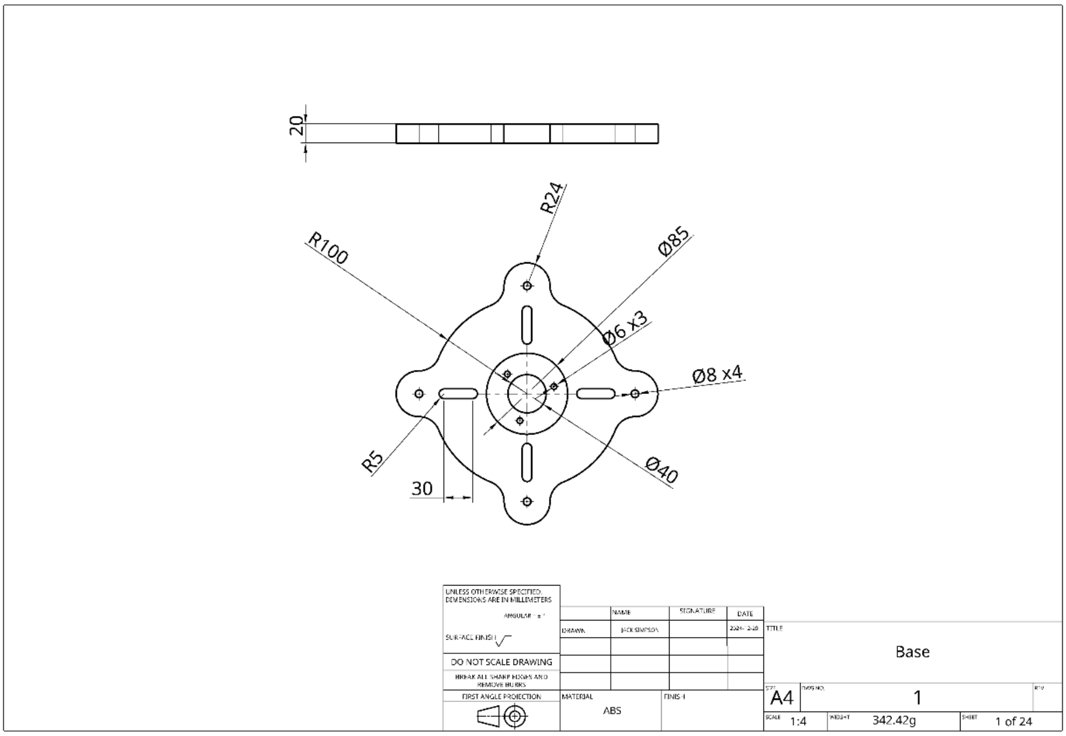

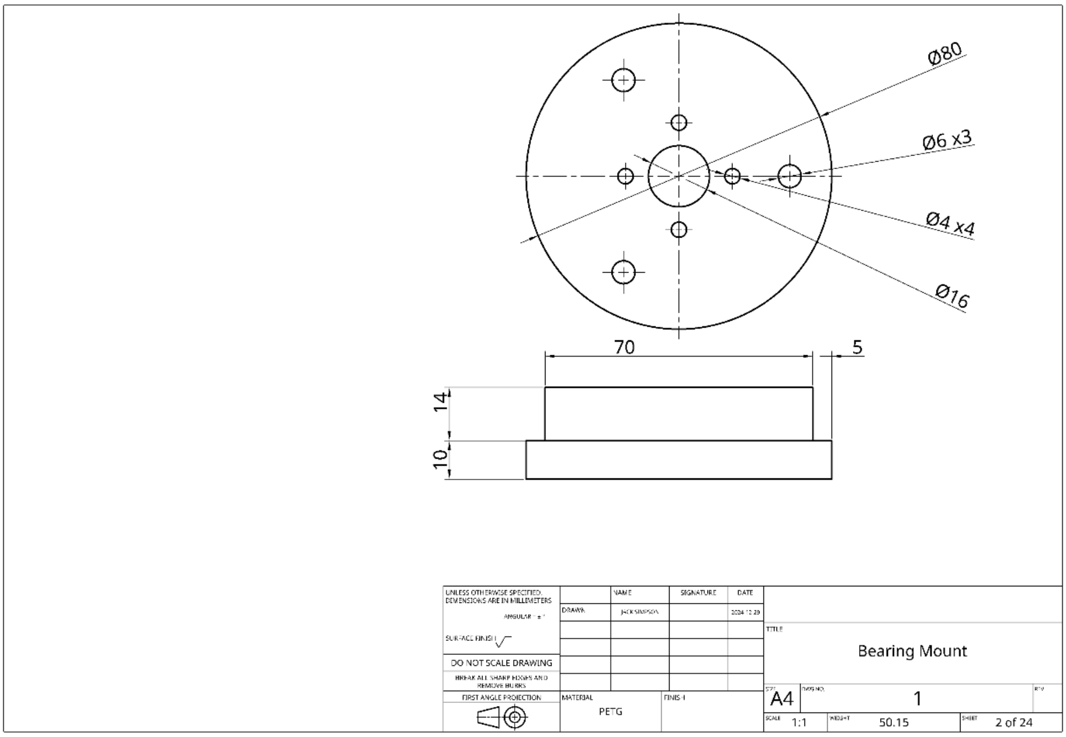

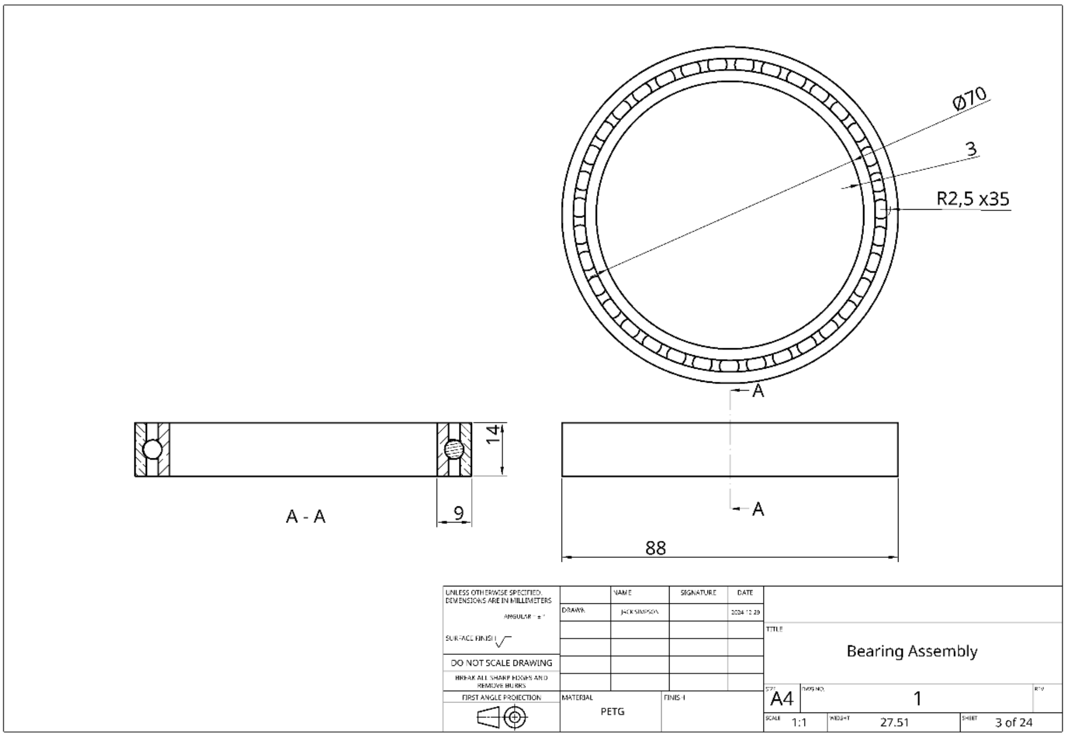

UNLESS OTHERWISE SPECIFIED.
DIMENSIONS ARE IN MILLIMETERS
ANGULAR ±1°
SURFACE FINISH √

DO NOT SCALE DRAWING

BREAK ALL SHARP EDGES AND REMOVE BURRS

FIRST ANGLE PROJECTION

	NAME	SIGNATURE	DATE
DRAWN	JACK SIMPSON		2024-12-29

MATERIAL PETG

FINISH

TITLE Bearing Assembly

SIZE A4 DWG NO. 1 REV

SCALE 1:1 WEIGHT 27.51 SHEET 3 of 24

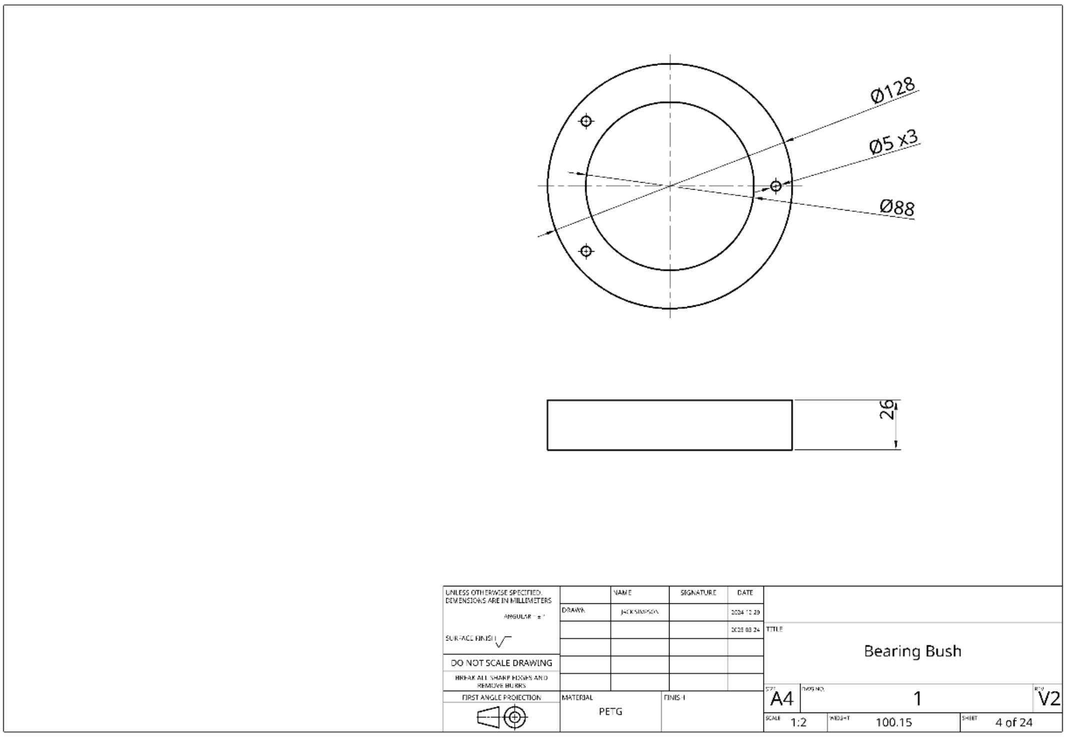

UNLESS OTHERWISE SPECIFIED.
DIMENSIONS ARE IN MILLIMETERS
ANGULAR ±1°
SURFACE FINISH √

DO NOT SCALE DRAWING

BREAK ALL SHARP EDGES AND REMOVE BURRS

FIRST ANGLE PROJECTION

	NAME	SIGNATURE	DATE
DRAWN	JACK SIMPSON		2024-12-29
			2025-03-24

MATERIAL PETG

FINISH

TITLE Bearing Bush

SIZE A4 DWG NO. 1 REV V2

SCALE 1:2 WEIGHT 100.15 SHEET 4 of 24

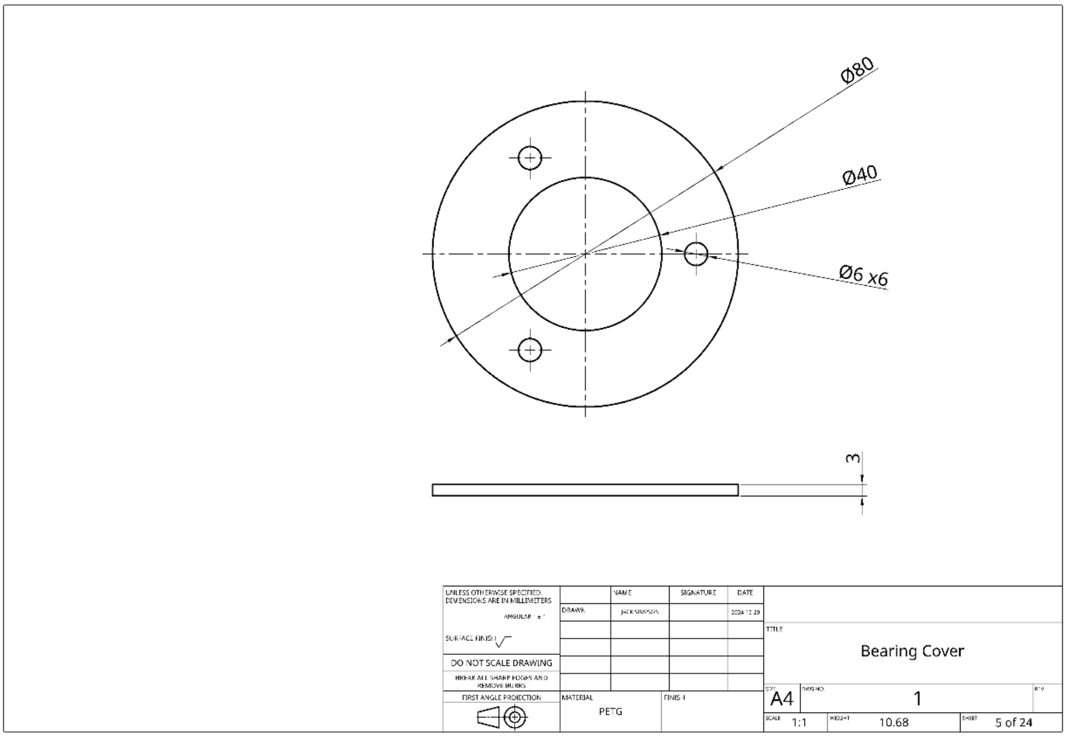
Ø80
Ø40
Ø6 x6
3
UNLESS OTHERWISE SPECIFIED,
DIMENSIONS ARE IN MILLIMETERS
ANGULAR = ±1°
SURFACE FINISH
DO NOT SCALE DRAWING
BREAK ALL SHARP EDGES AND REMOVE BURRS
FIRST ANGLE PROJECTION
NAME
SIGNATURE
DATE
DRAWN
JACK SIMPSON
2024 12 29
MATERIAL
PETG
FINISH
TITLE
Bearing Cover
SIZE
A4
DWG NO.
1
REV
SCALE
1:1
WEIGHT
10.68
SHEET
5 of 24

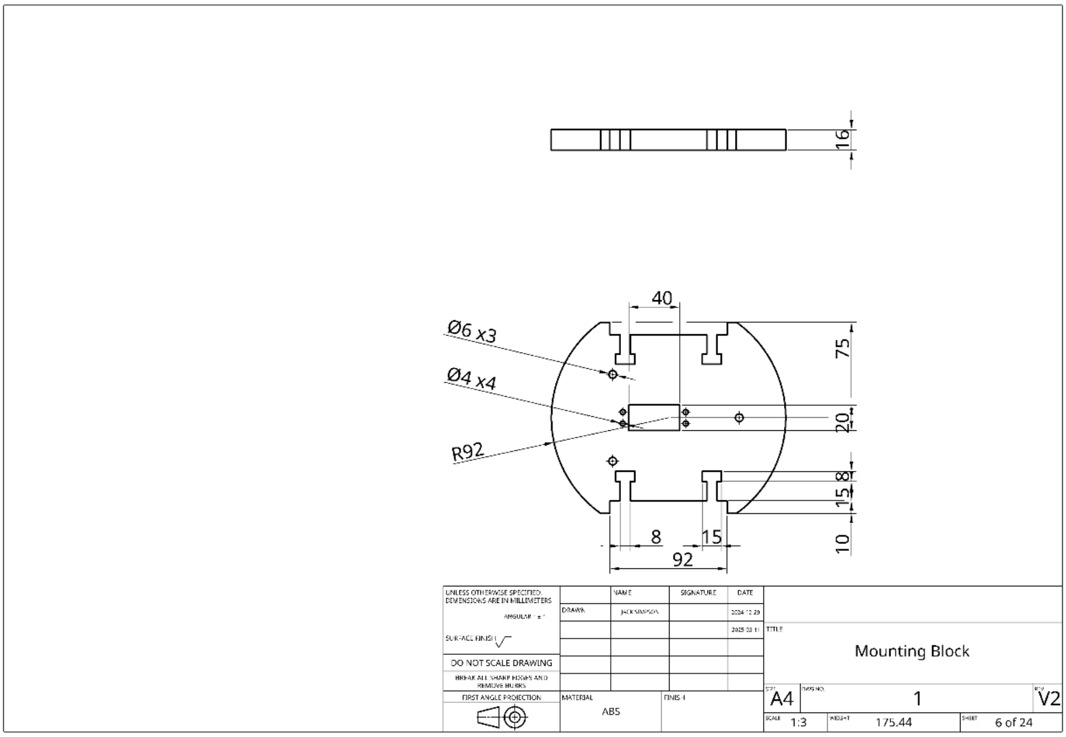
16
40
Ø6 x3
Ø4 x4
R92
75
20
8
15
10
8
15
92
UNLESS OTHERWISE SPECIFIED,
DIMENSIONS ARE IN MILLIMETERS
ANGULAR = ±1°
SURFACE FINISH
DO NOT SCALE DRAWING
BREAK ALL SHARP EDGES AND REMOVE BURRS
FIRST ANGLE PROJECTION
NAME
SIGNATURE
DATE
DRAWN
JACK SIMPSON
2024 12 29
2025 03 11
MATERIAL
ABS
FINISH
TITLE
Mounting Block
SIZE
A4
DWG NO.
1
REV
V2
SCALE
1:3
WEIGHT
175.44
SHEET
6 of 24

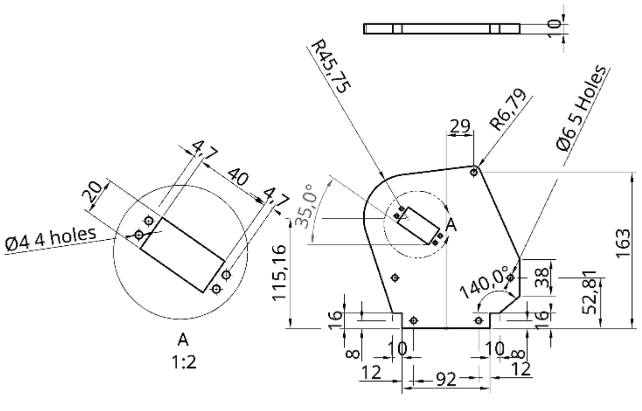

UNLESS OTHERWISE SPECIFIED. DIMENSIONS ARE IN MILLIMETERS		NAME	SIGNATURE	DATE
ANGULAR: ±°	DRAWN	JACK SIMPSON		2025 01 13
SURFACE FINISH √				2025 03 10
DO NOT SCALE DRAWING				
BREAK ALL SHARP EDGES AND REMOVE BURRS				
FIRST ANGLE PROJECTION	MATERIAL PETG		FINISH	

TITLE	Arm Support	
SIZE A4	DWG NO. 1	REV
SCALE 1:4	WEIGHT 98.3	SHEET 7 of 24

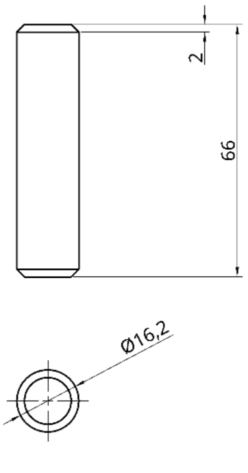

UNLESS OTHERWISE SPECIFIED. DIMENSIONS ARE IN MILLIMETERS		NAME	SIGNATURE	DATE
ANGULAR: ±°	DRAWN	JACK SIMPSON		2025 01 13
SURFACE FINISH √				
DO NOT SCALE DRAWING				
BREAK ALL SHARP EDGES AND REMOVE BURRS				
FIRST ANGLE PROJECTION	MATERIAL PETG		FINISH	

TITLE	Shaft	
SIZE A4	DWG NO. 1	REV
SCALE 1:1	WEIGHT 7.04	SHEET 8 of 24

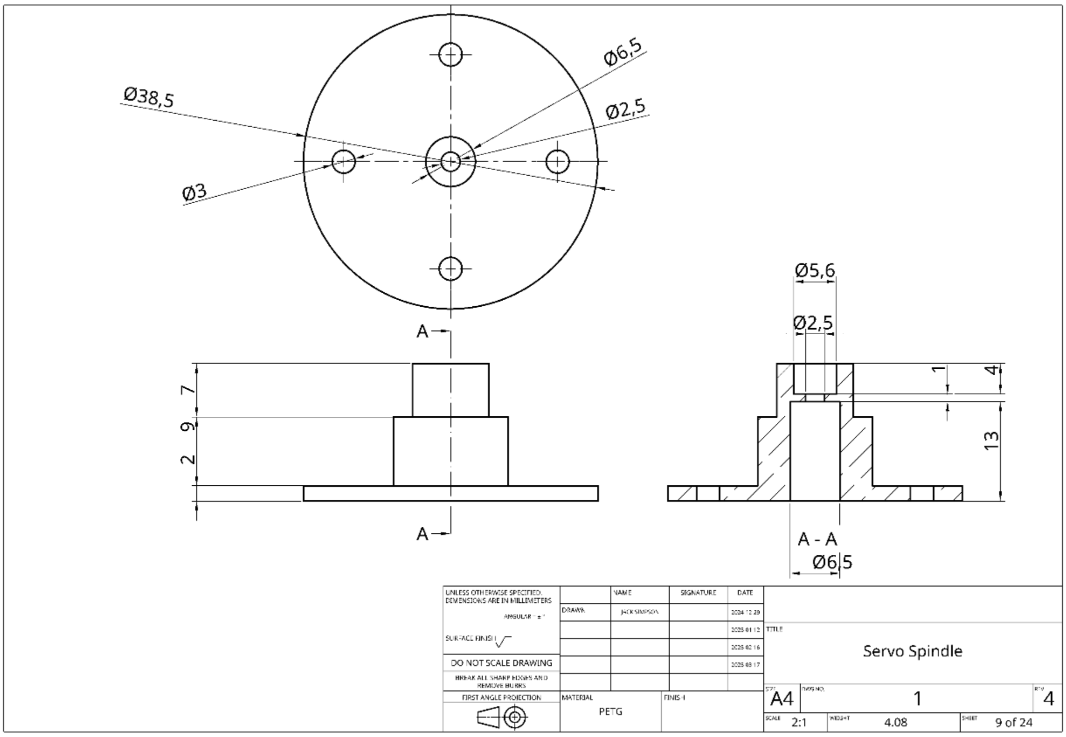

UNLESS OTHERWISE SPECIFIED, DIMENSIONS ARE IN MILLIMETERS
ANGULAR : ±1°
SURFACE FINISH √
DO NOT SCALE DRAWING
BREAK ALL SHARP EDGES AND REMOVE BURRS
FIRST ANGLE PROJECTION

	NAME	SIGNATURE	DATE
DRAWN	JACK SIMPSON		2024 12 29
			2025 01 12
			2025 02 16
			2025 03 17

MATERIAL PETG
FINISH

TITLE Servo Spindle

SIZE A4 DWG NO. 1 REV 4
SCALE 2:1 WEIGHT 4.08 SHEET 9 of 24

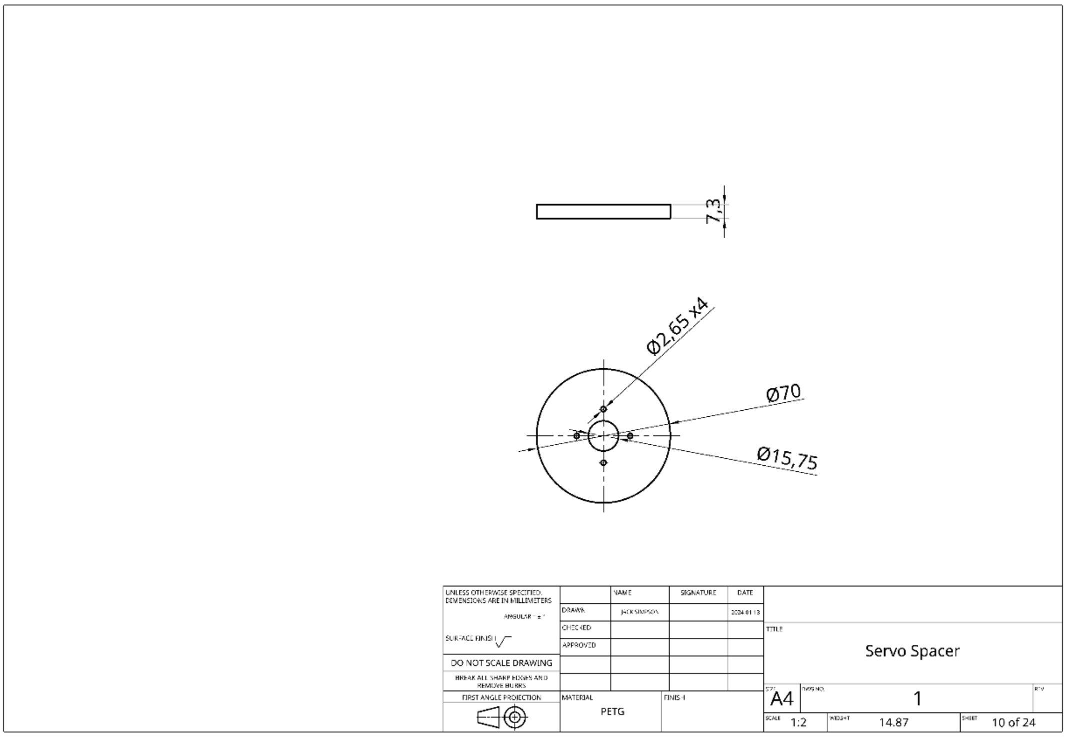

UNLESS OTHERWISE SPECIFIED, DIMENSIONS ARE IN MILLIMETERS
ANGULAR : ±1°
SURFACE FINISH √
DO NOT SCALE DRAWING
BREAK ALL SHARP EDGES AND REMOVE BURRS
FIRST ANGLE PROJECTION

	NAME	SIGNATURE	DATE
DRAWN	JACK SIMPSON		2024 01 13
CHECKED			
APPROVED			

MATERIAL PETG
FINISH

TITLE Servo Spacer

SIZE A4 DWG NO. 1 REV
SCALE 1:2 WEIGHT 14.87 SHEET 10 of 24

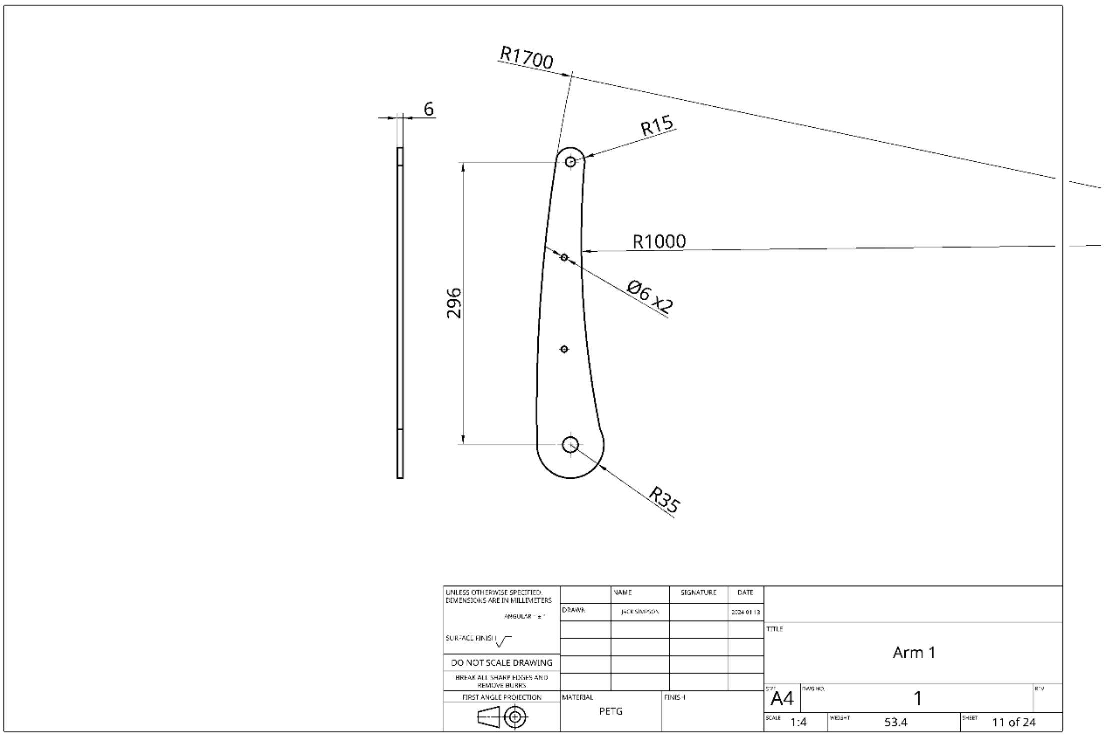
R1700
6
R15
R1000
296
Ø6 x2
R35
UNLESS OTHERWISE SPECIFIED. DIMENSIONS ARE IN MILLIMETERS
ANGULAR ± °
SURFACE FINISH
DO NOT SCALE DRAWING
BREAK ALL SHARP EDGES AND REMOVE BURRS
FIRST ANGLE PROJECTION
NAME
SIGNATURE
DATE
DRAWN
JACK SIMPSON
2024 01 13
MATERIAL
PETG
FINISH
TITLE
Arm 1
SIZE
A4
DWG NO.
1
REV
SCALE
1:4
WEIGHT
53.4
SHEET
11 of 24

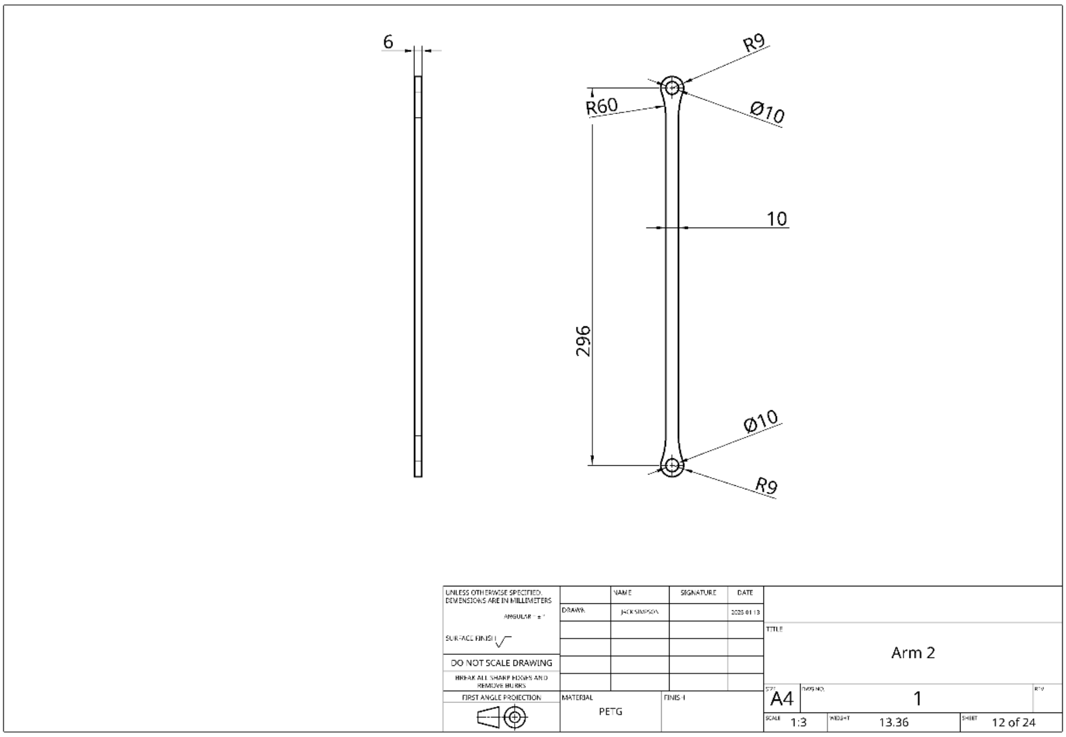
6
R9
R60
Ø10
10
296
Ø10
R9
UNLESS OTHERWISE SPECIFIED. DIMENSIONS ARE IN MILLIMETERS
ANGULAR ± °
SURFACE FINISH
DO NOT SCALE DRAWING
BREAK ALL SHARP EDGES AND REMOVE BURRS
FIRST ANGLE PROJECTION
NAME
SIGNATURE
DATE
DRAWN
JACK SIMPSON
2025 01 13
MATERIAL
PETG
FINISH
TITLE
Arm 2
SIZE
A4
DWG NO.
1
REV
SCALE
1:3
WEIGHT
13.36
SHEET
12 of 24

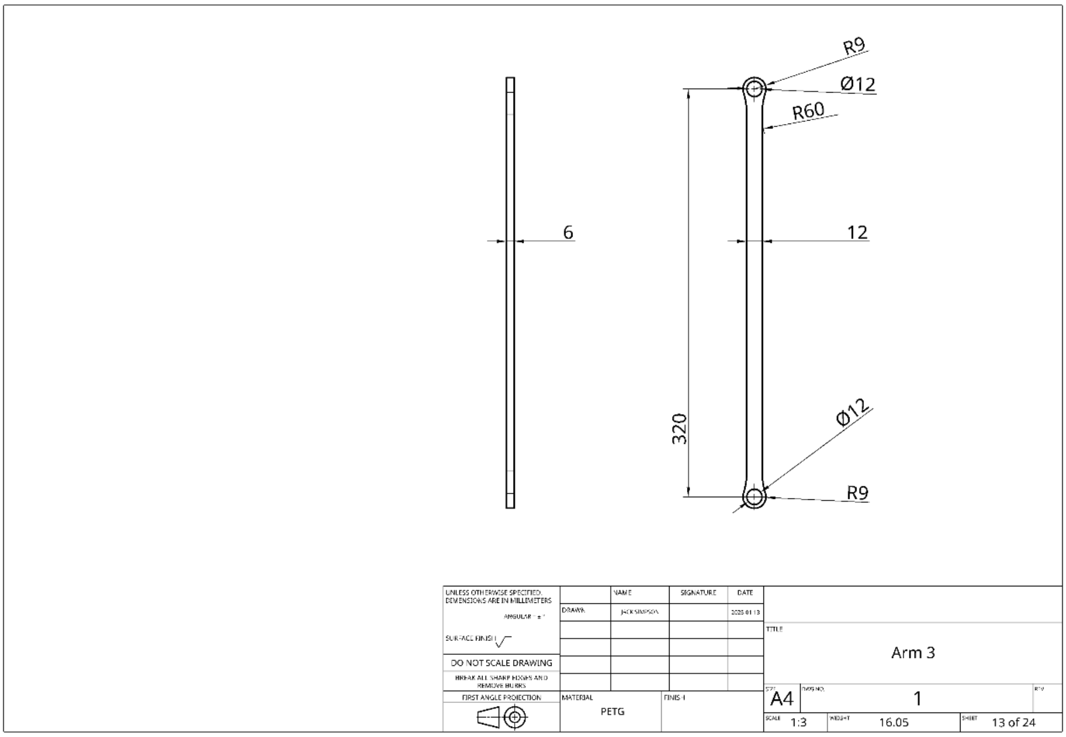

UNLESS OTHERWISE SPECIFIED, DIMENSIONS ARE IN MILLIMETERS

ANGULAR: ± °

SURFACE FINISH

DO NOT SCALE DRAWING

BREAK ALL SHARP EDGES AND REMOVE BURRS

FIRST ANGLE PROJECTION

	NAME	SIGNATURE	DATE
DRAWN	JACK SIMPSON		2025 01 13

MATERIAL: PETG

FINISH

TITLE: Arm 3

SIZE: A4 DWG NO.: 1 REV

SCALE: 1:3 WEIGHT: 16.05 SHEET: 13 of 24

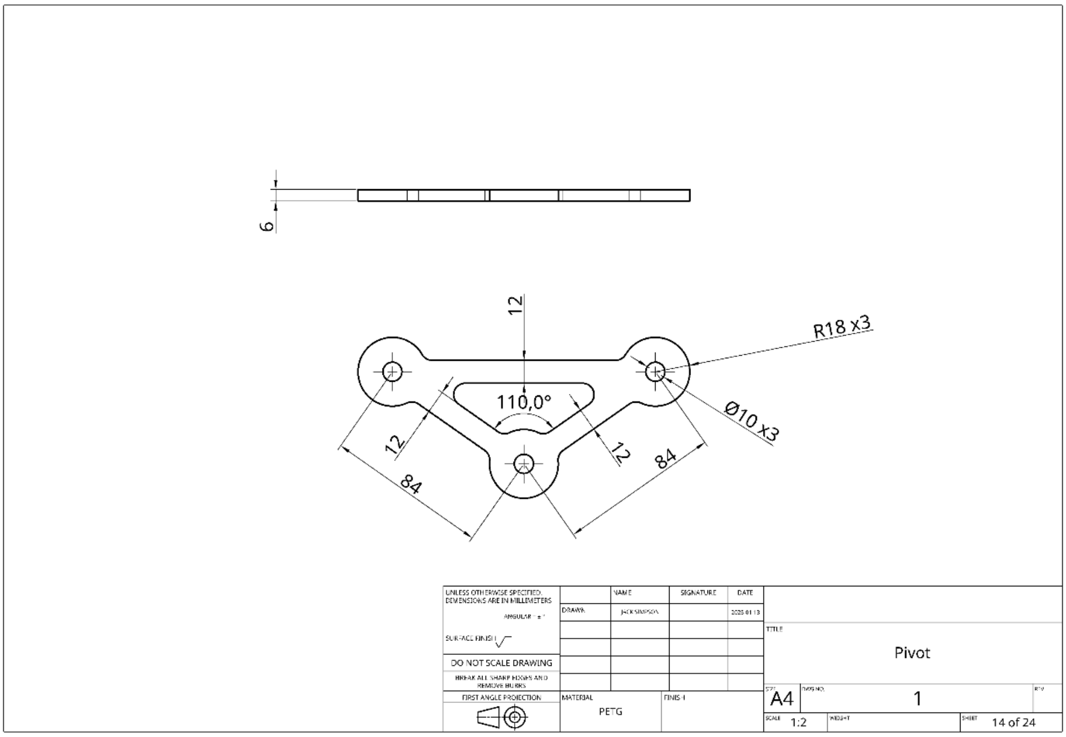

UNLESS OTHERWISE SPECIFIED, DIMENSIONS ARE IN MILLIMETERS

ANGULAR: ± °

SURFACE FINISH

DO NOT SCALE DRAWING

BREAK ALL SHARP EDGES AND REMOVE BURRS

FIRST ANGLE PROJECTION

	NAME	SIGNATURE	DATE
DRAWN	JACK SIMPSON		2025 01 13

MATERIAL: PETG

FINISH

TITLE: Pivot

SIZE: A4 DWG NO.: 1 REV

SCALE: 1:2 WEIGHT SHEET: 14 of 24

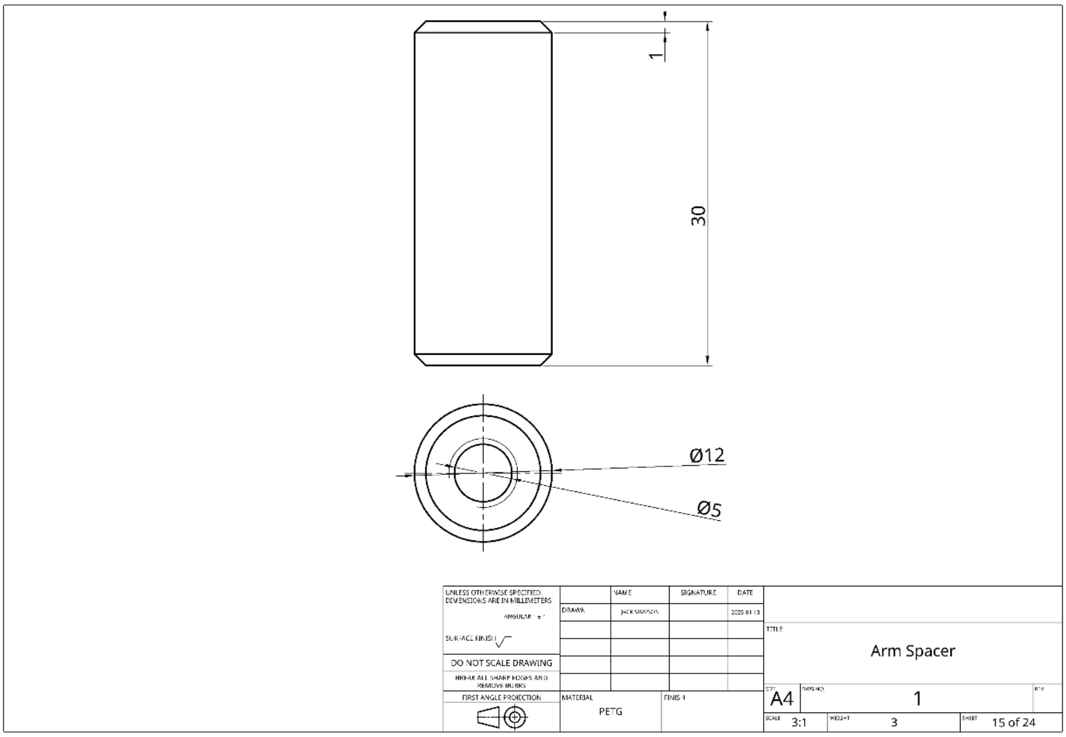

UNLESS OTHERWISE SPECIFIED. DIMENSIONS ARE IN MILLIMETERS

ANGULAR : ± °

SURFACE FINISH √

DO NOT SCALE DRAWING

BREAK ALL SHARP EDGES AND REMOVE BURRS

FIRST ANGLE PROJECTION

	NAME	SIGNATURE	DATE
DRAWN	JACK SIMPSON		2025 01 13

MATERIAL PETG

FINISH

TITLE Arm Spacer

SIZE A4 DWG NO. 1 REV

SCALE 3:1 WEIGHT 3 SHEET 15 of 24

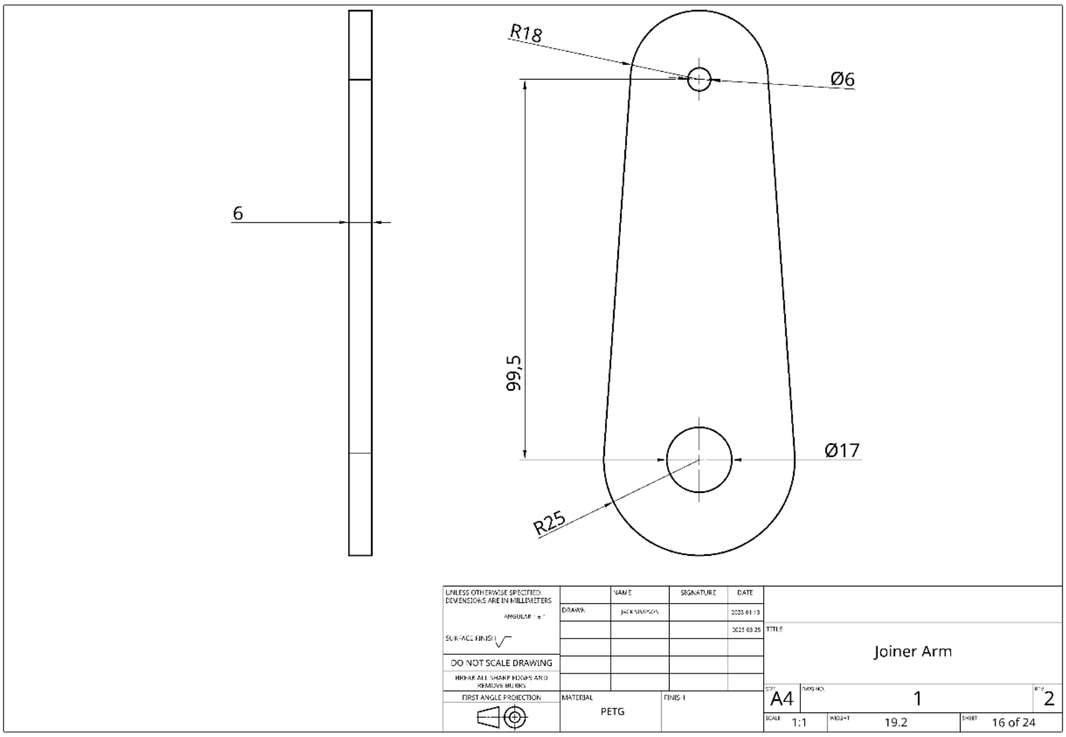

UNLESS OTHERWISE SPECIFIED. DIMENSIONS ARE IN MILLIMETERS

ANGULAR : ± °

SURFACE FINISH √

DO NOT SCALE DRAWING

BREAK ALL SHARP EDGES AND REMOVE BURRS

FIRST ANGLE PROJECTION

	NAME	SIGNATURE	DATE
DRAWN	JACK SIMPSON		2025 01 13
			2025 03 25

MATERIAL PETG

FINISH

TITLE Joiner Arm

SIZE A4 DWG NO. 1 REV 2

SCALE 1:1 WEIGHT 19.2 SHEET 16 of 24

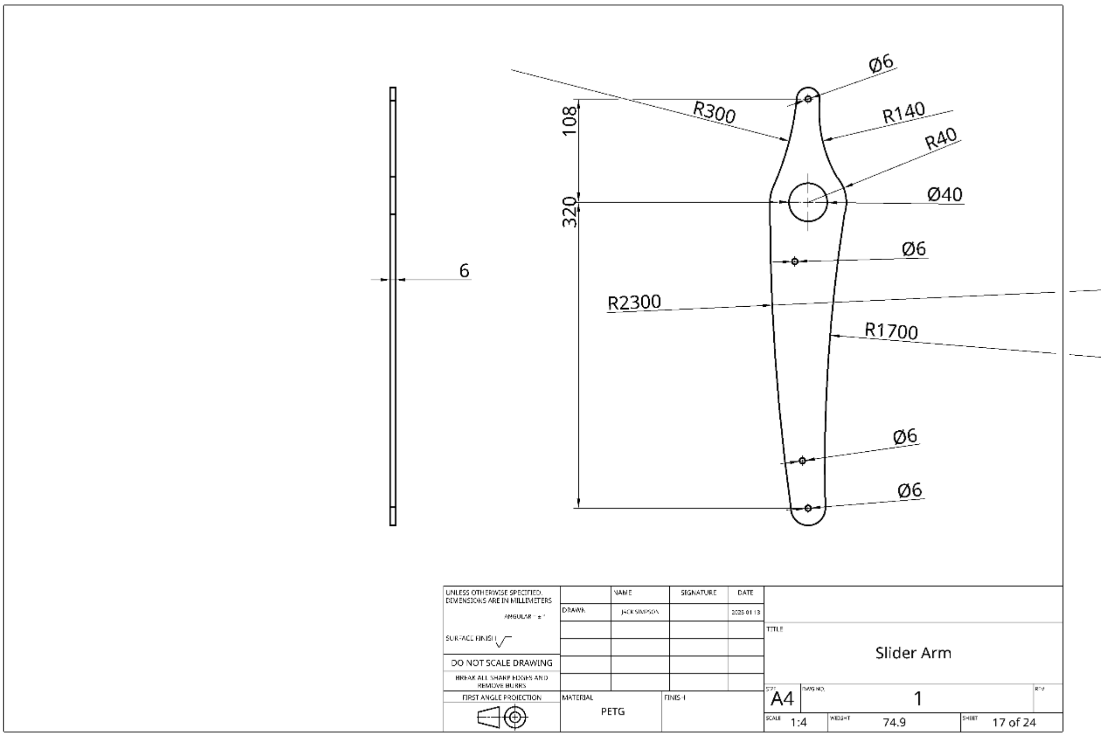
Ø6
108
R300
R140
R40
Ø40
320
Ø6
6
R2300
R1700
Ø6
Ø6
UNLESS OTHERWISE SPECIFIED, DIMENSIONS ARE IN MILLIMETERS
ANGULAR ± °
SURFACE FINISH
DO NOT SCALE DRAWING
BREAK ALL SHARP EDGES AND REMOVE BURRS
FIRST ANGLE PROJECTION
NAME
SIGNATURE
DATE
DRAWN
JACK SIMPSON
2025 01 13
MATERIAL
PETG
FINISH
TITLE
Slider Arm
SIZE
A4
DWG NO.
1
REV
SCALE
1:4
WEIGHT
74.9
SHEET
17 of 24

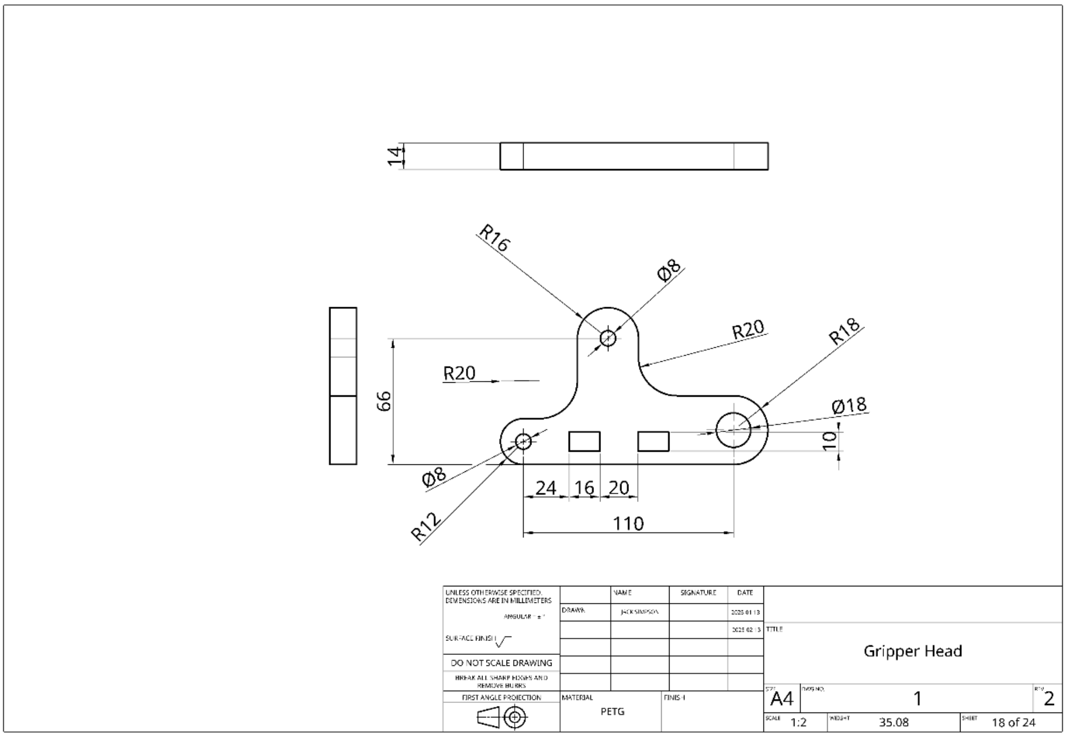
14
R16
Ø8
R20
R18
R20
66
Ø18
10
Ø8
R12
24
16
20
110
UNLESS OTHERWISE SPECIFIED, DIMENSIONS ARE IN MILLIMETERS
ANGULAR ± °
SURFACE FINISH
DO NOT SCALE DRAWING
BREAK ALL SHARP EDGES AND REMOVE BURRS
FIRST ANGLE PROJECTION
NAME
SIGNATURE
DATE
DRAWN
JACK SIMPSON
2025 01 13
2025 02 13
MATERIAL
PETG
FINISH
TITLE
Gripper Head
SIZE
A4
DWG NO.
1
REV
2
SCALE
1:2
WEIGHT
35.08
SHEET
18 of 24

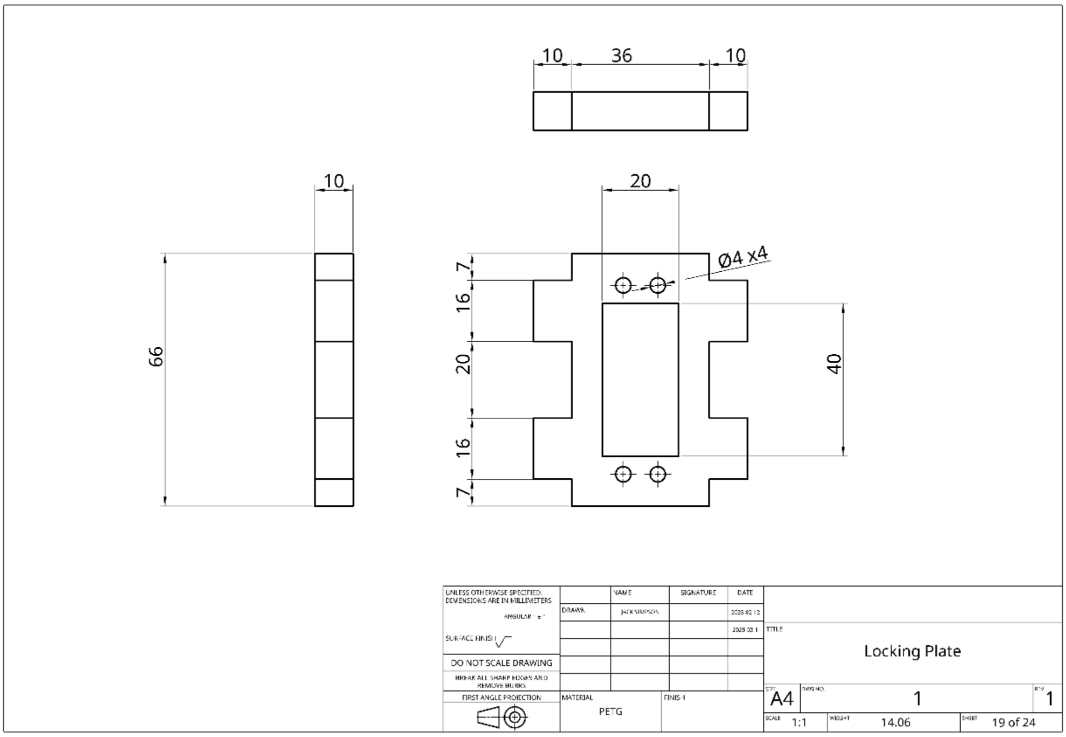
10
36
10
10
20
Ø4 x4
66
7
16
20
16
7
40
UNLESS OTHERWISE SPECIFIED.
DIMENSIONS ARE IN MILLIMETERS
ANGULAR ± °
SURFACE FINISH
DO NOT SCALE DRAWING
BREAK ALL SHARP EDGES AND REMOVE BURRS
FIRST ANGLE PROJECTION
NAME
SIGNATURE
DATE
DRAWN
JACK SIMPSON
2025.02.12
2025.03.1
TITLE
Locking Plate
MATERIAL
PETG
FINISH
SIZE
A4
DWG NO.
1
REV
1
SCALE
1:1
WEIGHT
14.06
SHEET
19 of 24

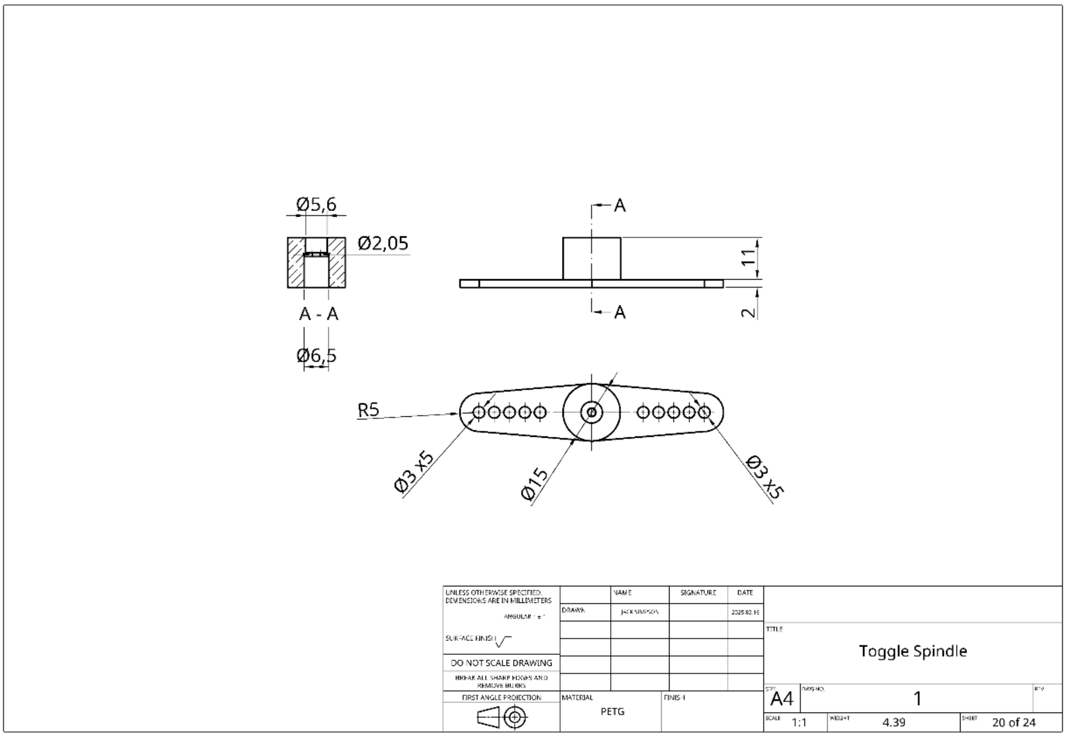
Ø5,6
Ø2,05
A - A
Ø6,5
A
A
11
2
R5
Ø3 x5
Ø15
Ø3 x5
UNLESS OTHERWISE SPECIFIED.
DIMENSIONS ARE IN MILLIMETERS
ANGULAR ± °
SURFACE FINISH
DO NOT SCALE DRAWING
BREAK ALL SHARP EDGES AND REMOVE BURRS
FIRST ANGLE PROJECTION
NAME
SIGNATURE
DATE
DRAWN
JACK SIMPSON
2025.02.16
TITLE
Toggle Spindle
MATERIAL
PETG
FINISH
SIZE
A4
DWG NO.
1
REV
SCALE
1:1
WEIGHT
4.39
SHEET
20 of 24

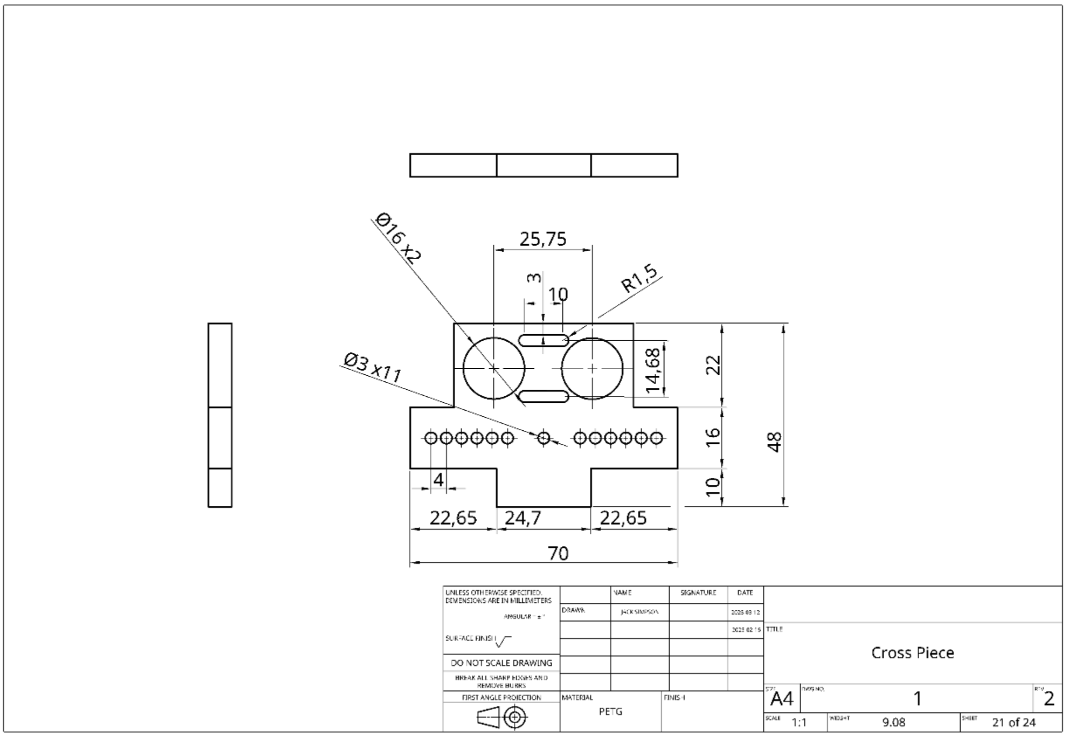
Ø16 x2
25,75
3
10
R1,5
Ø3 x11
14,68
22
16
48
10
4
22,65
24,7
22,65
70
UNLESS OTHERWISE SPECIFIED, DIMENSIONS ARE IN MILLIMETERS
ANGULAR ± °
SURFACE FINISH
DO NOT SCALE DRAWING
BREAK ALL SHARP EDGES AND REMOVE BURRS
FIRST ANGLE PROJECTION
NAME
SIGNATURE
DATE
DRAWN
JACK SIMPSON
2025 03 12
2025 02 16
TITLE
Cross Piece
MATERIAL
PETG
FINISH
SIZE
A4
DWG NO.
1
REV
2
SCALE
1:1
WEIGHT
9.08
SHEET
21 of 24

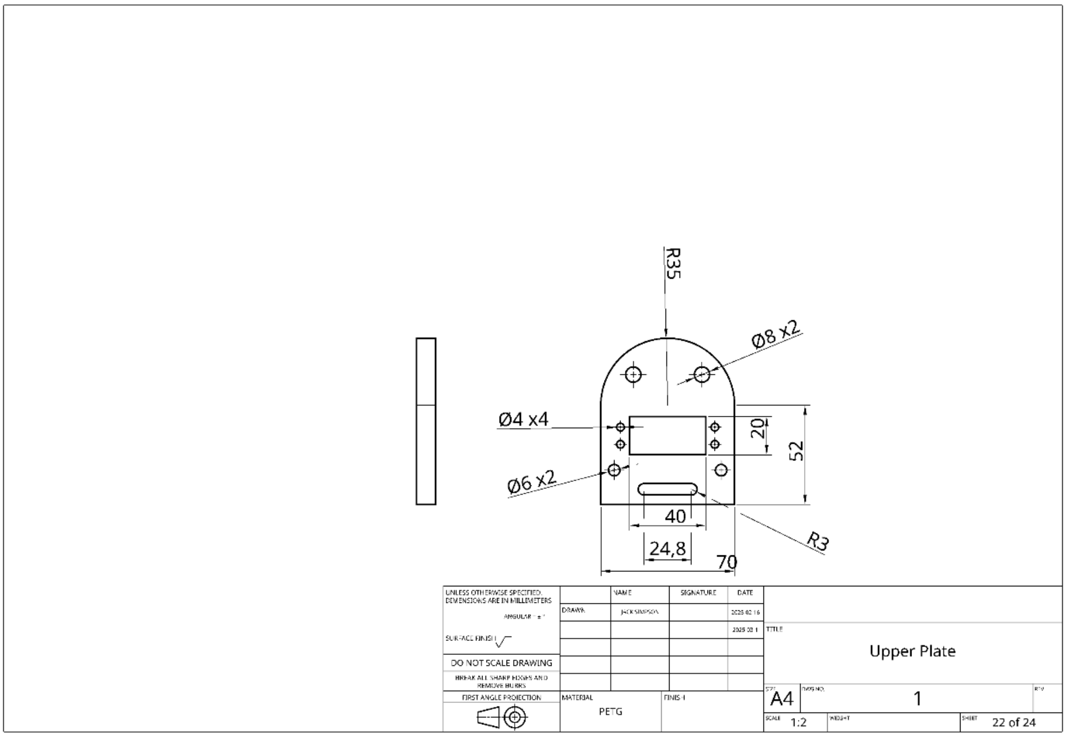
R35
Ø8 x2
Ø4 x4
20
52
Ø6 x2
40
24,8
70
R3
UNLESS OTHERWISE SPECIFIED, DIMENSIONS ARE IN MILLIMETERS
ANGULAR ± °
SURFACE FINISH
DO NOT SCALE DRAWING
BREAK ALL SHARP EDGES AND REMOVE BURRS
FIRST ANGLE PROJECTION
NAME
SIGNATURE
DATE
DRAWN
JACK SIMPSON
2025 02 16
2025 03 1
TITLE
Upper Plate
MATERIAL
PETG
FINISH
SIZE
A4
DWG NO.
1
REV
SCALE
1:2
WEIGHT
SHEET
22 of 24

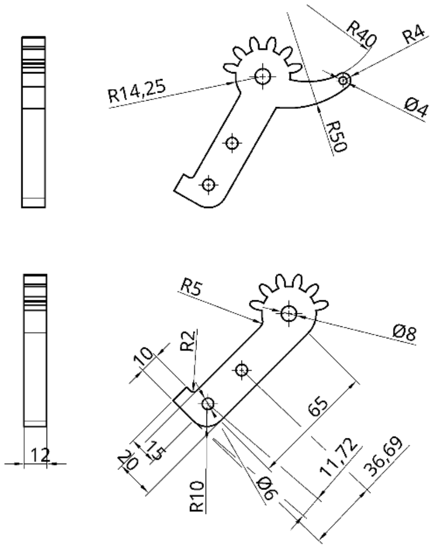

UNLESS OTHERWISE SPECIFIED. DIMENSIONS ARE IN MILLIMETERS

ANGULAR ± °

SURFACE FINISH √

DO NOT SCALE DRAWING

BREAK ALL SHARP EDGES AND REMOVE BURRS

FIRST ANGLE PROJECTION

	NAME	SIGNATURE	DATE
DRAWN	JACK SIMPSON		2024 03 24

MATERIAL PETG

FINISH

TITLE

Gear Arms

SIZE A4 DWG NO. 1 REV 3

SCALE 1:2 WEIGHT 31.9 SHEET 23 of 24

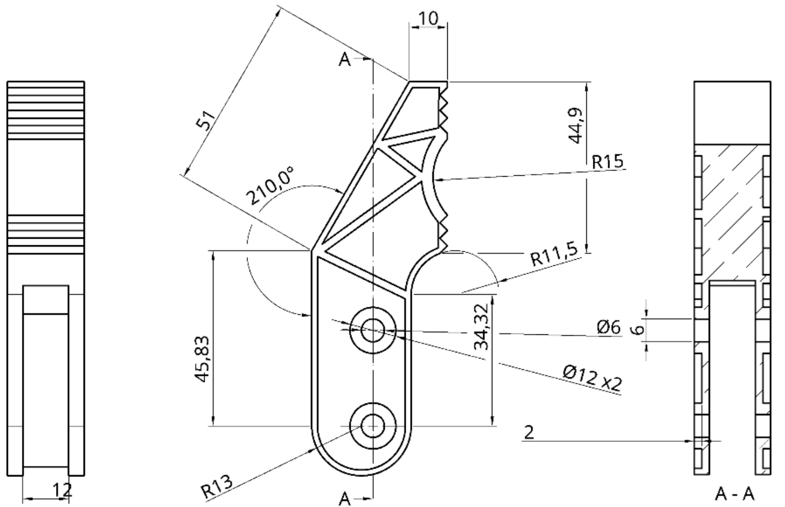

UNLESS OTHERWISE SPECIFIED. DIMENSIONS ARE IN MILLIMETERS

ANGULAR ± °

SURFACE FINISH √

DO NOT SCALE DRAWING

BREAK ALL SHARP EDGES AND REMOVE BURRS

FIRST ANGLE PROJECTION

	NAME	SIGNATURE	DATE
DRAWN	JACK SIMPSON		2025 02 16
			2025 03 3

MATERIAL PETG

FINISH

TITLE

Gripper Arm

SIZE A4 DWG NO. 1 REV

SCALE 1:1 WEIGHT 20.5 SHEET 24 of 24

APPENDIX F – MASS OF ROBOTIC ARM

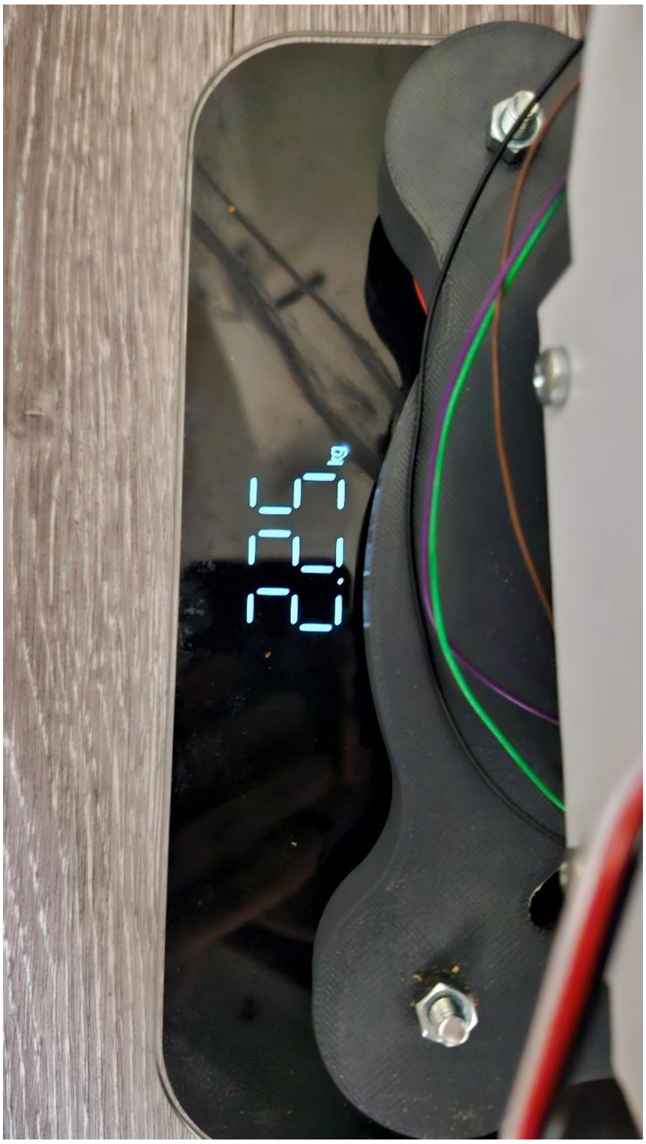

APPENDIX G - MATLAB CODE

```
% Input parameters:
%   joints        1x4 array for joint position values (angle or displacement) [J1,J2,J3,J4]
%                  rotational joints must have values -180 - +180 degrees
%   tool          1x2 array for gripper configuration values [gripper width, distance from finger tips to grip]
%                   note: this gripper has a width range of 0 - 70 mm and a
%                         maximum gripping distance of 128mm
%   disp          flag value to determine if the robot arm figure is generated
%                   0 --> do not display the plot
%                   1 --> display the plot (default)
%
% Output parameters:
%   end_effector   1x3 array for end effector coordinates [x,y,z]mm
%   target_pos     1x3 array for end effector coordinates of object interaction position [x,y,z]mm
%   link_pos      12x3 array for link coordinates [[  0 ,  0 ,  0 ]
%                                                  [L0_x,L0_y,L0_z]
%                                                  [L1_x,L1_y,L1_z]
%                                                  [L2_x,L2_y,L2_z]
%                                                  [L3_x,L3_y,L3_z]
%                                                  [Gs_x,Gs_y,Gs_z]    gripper stem
%                                                  [Gl1_x,Gl1_y,Gl1_z] gripper left finger base
%                                                  [Gl2_x,Gl2_y,Gl2_z] gripper left finger grip location
%                                                  [Gl3_x,Gl3_y,Gl3_z] gripper left finger tip
%                                                  [Gr1_x,Gr1_y,Gr1_z] gripper right finger base
%                                                  [Gr2_x,Gr2_y,Gr2_z]]  gripper right finger grip location
%                                                  [Gr3_x,Gr3_y,Gr3_z]]  gripper right finger tip
%                 note: gripper position between the finger tips will be
%                       considered the end effector location

function [end_effector,target_pos,link_pos] = Robo_Arm(joints,tool,disp)

% ensure input arguments are specified, of the correct format, and are
% within acceptable ranges
arguments
% default joint values: joint=[0,0,0,0] --> J1 = 0; J2 = 0; J3 = 0; J4 = 0
joints(1,4) {mustBeNumeric} = [0,0,0,0];
% default tool values: joint=[0,0] --> gripper width = 0; distance from tip to grip location = 0
tool(1,2) {mustBeNumeric} = [0,0];
% default disp value: 1 (plot the figure)
disp(1,1) {mustBeNumeric,mustBeInteger,mustBeInRange(disp,0,1)} = 1;
end
% test for acceptable ranges
% this needs to be a set of special checks since there is a mix of
% rotational and prismatic joints, each have their own allowed ranges
if any(joints([1,4])<-180) || any(joints([1,4])>180)
disp("Joint J1 and/or J4 is out of bounds (-180 - +180)");
exit
end
if joints(2)<-90 || joints(2)>90
disp("Joint J2 is out of bounds (-90 - +90)");
exit
end
if joints(3)<-90 || joints(3)>90
disp("Joint J3 is out of bounds (-90 - +90)");
exit
end
if tool(1)<0 || tool(1)>70
disp("Gripper width is out of bounds (0 - 70)");
exit
end
if tool(2)<0 || tool(2)>128
disp("Distance from finger tips to grip is out of bounds (0 - 128)");
exit
end

% declare an array to hold link length values
%   units: mm
%            L0  L1  L2  L3  gripper(stem) gripper(finger half width) gripper(finger length to grip position)
link_lens = [63,85,296, 320, 76, tool(1)/2, 30-tool(2)];

% declare an array to hold the origin and link segment end coordinates
link_pos = zeros(12,3);

% create a new array to hold joint values in radian format
joints_r = deg2rad(joints);



% Origin -> Link L0
TO0 = [[   1       0       0       0      ]
[   0       1       0       0      ]
[   0       0       1   link_lens(1)]
[   0       0       0       1      ]];

% Link L0 -> Link L1
c1 = cos(joints_r(1));
s1 = sin(joints_r(1));
T01 = [[   c1      s1      0       0      ]
[  -s1      c1      0       0      ]
[   0       0       1   link_lens(2)]
[   0       0       0       1      ]];

% Link L1 -> Link L2
c2 = cos(joints_r(2));
s2 = sin(joints_r(2));
T12 = [[   c2      0       s2      0      ]
[   0       1       0       0      ]
[  -s2      0       c2  link_lens(3)]
[   0       0       0       1      ]];

% Link L2 -> Link L3
c3 = cos(joints_r(3));
```

```
s3 = sin(joints_r(3));
T23 = [[   c3      0       s3 -link_lens(4)]
[   0       1       0        0      ]
[  -s3      0       c3       0      ]
[   0       0       0        1      ]];

% Link L3 -> gripper stem
c4 = cos(joints_r(4));
s4 = sin(joints_r(4));
T3Gs = [[   c4      s4      0  -link_lens(5)]
[  -s4      c4      0        0      ]
[   0       0       1        0      ]
[   0       0       0        1      ]];



% gripper stem -> left gripper finger start
TGl1 = [[   1       0       0       0      ]
[   0       1       0  -link_lens(6)]
[   0       0       1       0      ]
[   0       0       0       1      ]];

% left gripper finger start -> left gripper finger grip location
TGl2 = [[   1       0       0       0      ]
[   0       1       0       0      ]
[   0       0       1  -link_lens(7)]
[   0       0       0       1      ]];

% left gripper finger grip location -> left gripper finger tip
TGl3 = [[   1       0       0       0      ]
[   0       1       0       0      ]
[   0       0       1    -tool(2)   ]
[   0       0       0       1      ]];

% gripper stem -> right gripper finger start
TGr1 = [[   1       0       0       0      ]
[   0       1       0 -link_lens(6)]
[   0       0       1       0      ]
[   0       0       0       1      ]];

% right gripper finger start -> right gripper finger grip location
TGr2 = [[   1       0       0       0      ]
[   0       1       0       0      ]
[   0       0       1  -link_lens(7)]
[   0       0       0       1      ]];

% right gripper finger grip location -> right gripper finger tip
TGr3 = [[   1       0       0       0      ]
[   0       1       0       0      ]
[   0       0       1    -tool(2)   ]
[   0       0       0       1      ]];

% perform the Forward Kinematics matrix multiplications
L0 = TO0;
L1 = TO0'*(T01'*T01)*TO0;
L2 = TO0'*T01'*(T12'*T12)*T01*TO0;
L3 = TO0'*T01'*T12'*(T23'*T23)*T12*T01*TO0;
Gs = TO0'*T01'*T12'*T23'*(T3Gs'*T3Gs)*T23*T12*T01*TO0;
% the left gripper finger continues from the end of the gripper stem (ignoring the right finger)
```

```
    Gl1 = T00'*T01'*T12'*T23'*T3Gs'*(TGl1'*TGl1)*T3Gs*T23*T12*T01*T00;
    Gl2 = T00'*T01'*T12'*T23'*T3Gs'*TGl1'*(TGl2'*TGl2)*TGl1*T3Gs*T23*T12*T01*T00;
    Gl3 = T00'*T01'*T12'*T23'*T3Gs'*TGl1'*TGl2'*(TGl3'*TGl3)*TGl2*TGl1*T3Gs*T23*T12*T01*T00;
    % the right gripper finger continues from the end of the gripper stem (ignoring the left finger)
    Gr1 = T00'*T01'*T12'*T23'*T3Gs'*(TGr1'*TGr1)*T3Gs*T23*T12*T01*T00;
    Gr2 = T00'*T01'*T12'*T23'*T3Gs'*TGr1'*(TGr2'*TGr2)*TGr1*T3Gs*T23*T12*T01*T00;
    Gr3 = T00'*T01'*T12'*T23'*T3Gs'*TGr1'*TGr2'*(TGr3'*TGr3)*TGr2*TGr1*T3Gs*T23*T12*T01*T00;

    % extract the link segment positions from the resulting matrices
    link_pos( 2,:) = L0(1:3,4)';
    link_pos( 3,:) = L1(1:3,4)';
    link_pos( 4,:) = L2(1:3,4)';
    link_pos( 5,:) = L3(1:3,4)';
    link_pos( 6,:) = Gs(1:3,4)';
    link_pos( 7,:) = Gl1(1:3,4)';
    link_pos( 8,:) = Gl2(1:3,4)';
    link_pos( 9,:) = Gl3(1:3,4)';
    link_pos(10,:) = Gr1(1:3,4)';
    link_pos(11,:) = Gr2(1:3,4)';
    link_pos(12,:) = Gr3(1:3,4)';

    % the end effector location is the same as the midpoint between the gripper
    % fingers
    end_effector = mean([link_pos(9,:);link_pos(12,:)],1);

    % the target position is the same as the midpoint between the gripper
    % fingers at the specified distance from the finger tips
    target_pos = mean([link_pos(8,:);link_pos(11,:)],1);

    % if the display flag is set (disp = 1), create a figure and show the
    % various plots for the robot arm
    if disp==1

    % define a set of RGB values for the link segment colours
    l_colours = [[0.0,0.0,0.0]   % L0
    [1.0,0.0,0.0]   % L1
    [0.0,1.0,0.0]   % L2
    [0.0,0.0,1.0]   % L3
    [0.2,0.2,0.2]   % gripper stem
    [0.8,0.0,0.0]   % gripper left finger
    [0.0,0.8,0.0]   % gripper right finger
    [0.0,1.0,0.0]]; % target position

    % spawn a figure window with index label 1
    % show a 2x2 grid of subplots within the figure
    figure(1);


    % plot the x-z plane
    subplot(2,2,1)
    plot(link_pos(1:2,1),link_pos(1:2,3),'LineWidth',5,'Color',l_colours(1,:))    % plot origin->L0
    hold on
    plot(link_pos(2:3,1),link_pos(2:3,3),'LineWidth',4,'Color',l_colours(2,:))  % plot L0->L1
    plot(link_pos(3:4,1),link_pos(3:4,3),'LineWidth',3,'Color',l_colours(3,:))  % plot L1->L2
    plot(link_pos(4:5,1),link_pos(4:5,3),'LineWidth',2,'Color',l_colours(4,:))  % plot L2->L3
    plot(link_pos(5:6,1),link_pos(5:6,3),'LineWidth',2,'Color',l_colours(5,:))  % plot L3->gripper stem
    plot(link_pos(6:9,1),link_pos(6:9,3),'LineWidth',2,'Color',l_colours(6,:))  % plot gripper stem->left finger
    plot(link_pos([6,10:12],1),link_pos([6,10:12],3),'LineWidth',2,'Color',l_colours(7,:))  % plot gripper stem->right finger
    plot(target_pos(1),target_pos(3),'*','Color',l_colours(8,:))  % plot target position
    hold off
    axis([-800 800 -150 750])  % set the plot area as: -450 < x < 450; -150 < z < 750
    axis square
    title('x-z plane')
    xlabel('x-axis (mm)')
    ylabel('z-axis (mm)')


    % plot the y-z plane
    subplot(2,2,2)
    plot(link_pos(1:2,2),link_pos(1:2,3),'LineWidth',6,'Color',l_colours(1,:))    % plot origin->L0
    hold on
    plot(link_pos(2:3,2),link_pos(2:3,3),'LineWidth',5,'Color',l_colours(2,:))  % plot L0->L1
    plot(link_pos(3:4,2),link_pos(3:4,3),'LineWidth',4,'Color',l_colours(3,:))  % plot L1->L2
    plot(link_pos(4:5,2),link_pos(4:5,3),'LineWidth',3,'Color',l_colours(4,:))  % plot L2->L3
    plot(link_pos(5:6,2),link_pos(5:6,3),'LineWidth',2,'Color',l_colours(5,:))  % plot L3->gripper stem
    plot(link_pos(6:9,2),link_pos(6:9,3),'LineWidth',2,'Color',l_colours(6,:))  % plot gripper stem->left finger
    plot(link_pos([6,10:12],2),link_pos([6,10:12],3),'LineWidth',2,'Color',l_colours(7,:))  % plot gripper stem->right finger
    plot(target_pos(2),target_pos(3),'*','Color',l_colours(8,:))  % plot target position
    hold off
    axis([-450 450 -150 750])  % set the plot area as: -450 < y < 450; -150 < z < 750
    axis square
    title('y-z plane')
    xlabel('y-axis (mm)')
    ylabel('z-axis (mm)')

    % plot the x-y plane
    subplot(2,2,3)
    plot(link_pos(1:2,1),link_pos(1:2,2),'LineWidth',6,'Color',l_colours(1,:))    % plot origin->L0
    hold on
    plot(link_pos(2:3,1),link_pos(2:3,2),'LineWidth',5,'Color',l_colours(2,:))  % plot L0->L1
    plot(link_pos(3:4,1),link_pos(3:4,2),'LineWidth',4,'Color',l_colours(3,:))  % plot L1->L2
    plot(link_pos(4:5,1),link_pos(4:5,2),'LineWidth',3,'Color',l_colours(4,:))  % plot L2->L3
    plot(link_pos(5:6,1),link_pos(5:6,2),'LineWidth',2,'Color',l_colours(5,:))  % plot L3->gripper stem
    plot(link_pos(6:9,1),link_pos(6:9,2),'LineWidth',2,'Color',l_colours(6,:))  % plot gripper stem->left finger
    plot(link_pos([6,10:12],1),link_pos([6,10:12],2),'LineWidth',2,'Color',l_colours(7,:))  % plot gripper stem->right finger
    plot(target_pos(1),target_pos(2),'*','Color',l_colours(8,:))  % plot target position
    hold off
    axis([-450 450 -450 450])  % set the plot area as: -450 < x < 450; -450 < y < 450
    axis square
    title('x-y plane')
    xlabel('x-axis (mm)')
    ylabel('y-axis (mm)')

    % plot the 3-D view
    subplot(2,2,4)
    plot3(link_pos(1:2,1),link_pos(1:2,2),link_pos(1:2,3),'LineWidth',6,'Color',l_colours(1,:))    % plot origin->L0
    hold on
    plot3(link_pos(2:3,1),link_pos(2:3,2),link_pos(2:3,3),'LineWidth',5,'Color',l_colours(2,:))  % plot L0->L1
    plot3(link_pos(3:4,1),link_pos(3:4,2),link_pos(3:4,3),'LineWidth',4,'Color',l_colours(3,:))  % plot L1->L2
    plot3(link_pos(4:5,1),link_pos(4:5,2),link_pos(4:5,3),'LineWidth',3,'Color',l_colours(4,:))  % plot L2->L3
    plot3(link_pos(5:6,1),link_pos(5:6,2),link_pos(5:6,3),'LineWidth',2,'Color',l_colours(5,:))  % plot L3->gripper stem
    plot3(link_pos(6:9,1),link_pos(6:9,2),link_pos(6:9,3),'LineWidth',2,'Color',l_colours(6,:))  % plot gripper stem->left finger
    plot3(link_pos([6,10:12],1),link_pos([6,10:12],2),link_pos([6,10:12],3),'LineWidth',2,'Color',l_colours(7,:))  % plot gripper stem->right finger
    plot3(target_pos(1),target_pos(2),target_pos(3),'*','Color',l_colours(8,:))                  % plot target position
    hold off
    axis([-800 800 -800 800 -150 750])  % set the plot area as: -450 < x < 450; -450 < y < 450; -150 < z < 750
    axis square
    title('3-D plot')
    xlabel('x-axis (mm)')
    ylabel('y-axis (mm)')
    zlabel('z-axis (mm)')

    end  % if disp==1
```

APPENDIX H – FEA

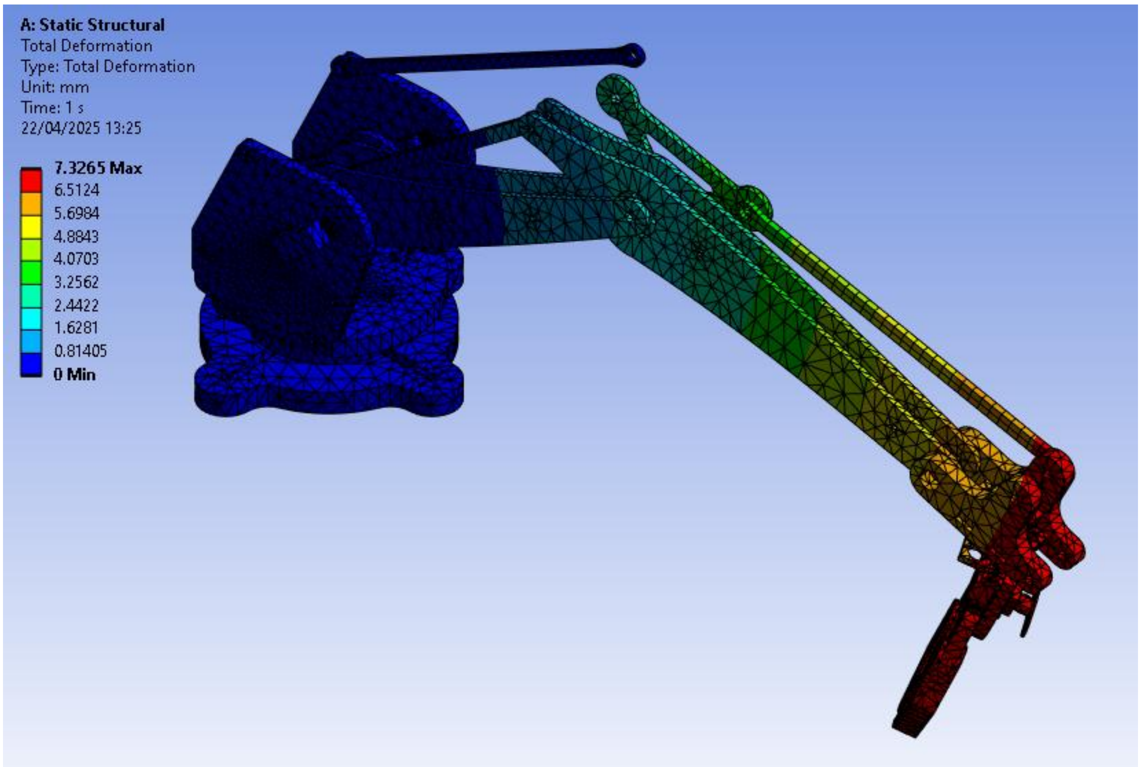

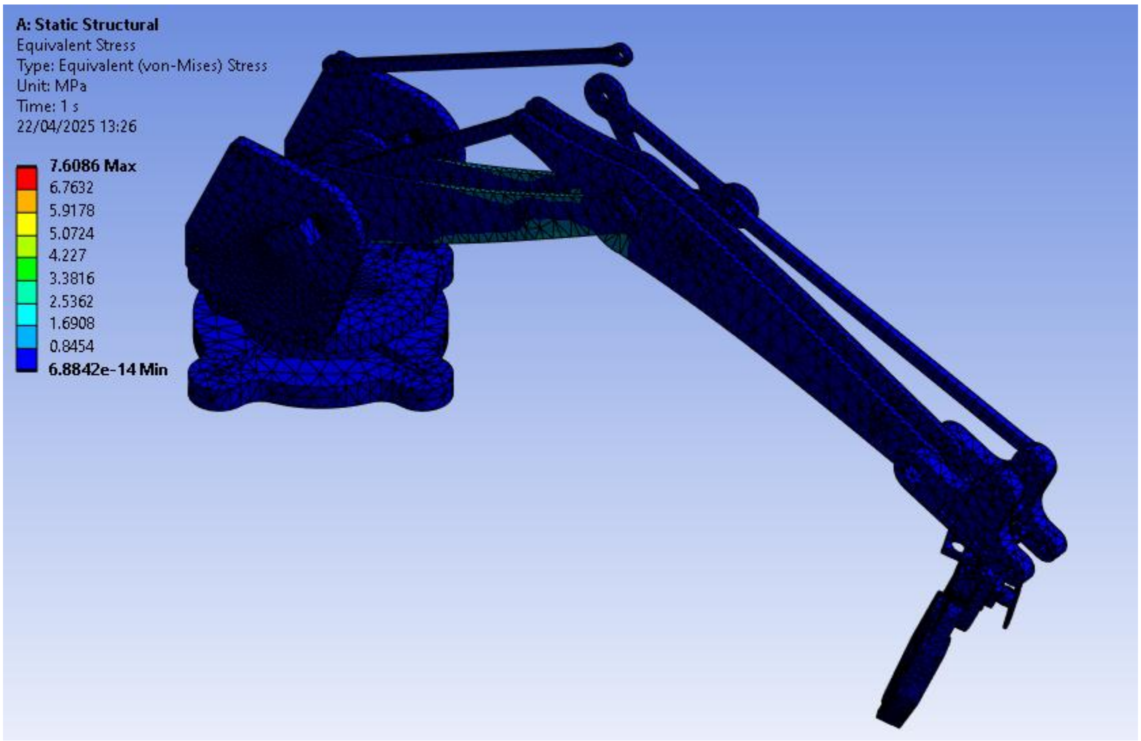
A: Static Structural
Equivalent Stress
Type: Equivalent (von-Mises) Stress
Unit: MPa
Time: 1 s
22/04/2025 13:26
7.6086 Max
6.7632
5.9178
5.0724
4.227
3.3816
2.5362
1.6908
0.8454
6.8842e-14 Min

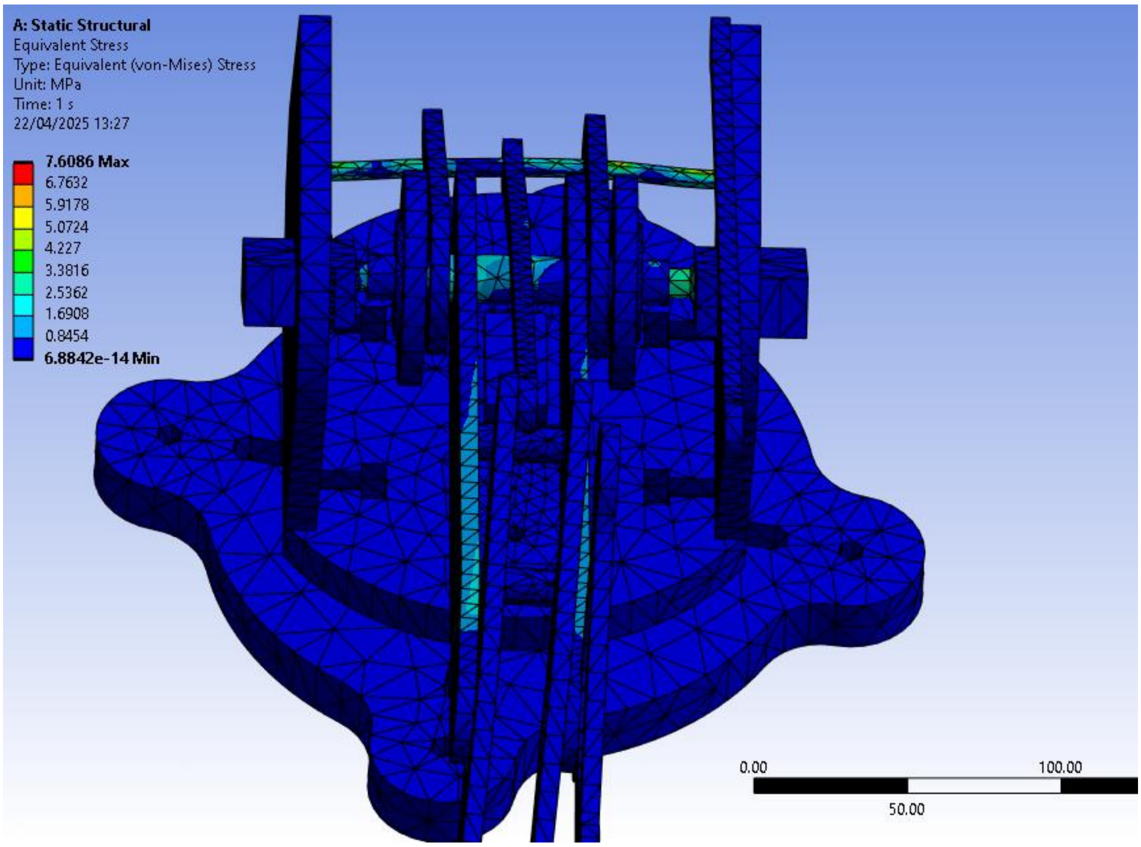
A: Static Structural
Equivalent Stress
Type: Equivalent (von-Mises) Stress
Unit: MPa
Time: 1 s
22/04/2025 13:27
7.6086 Max
6.7632
5.9178
5.0724
4.227
3.3816
2.5362
1.6908
0.8454
6.8842e-14 Min
0.00
100.00
50.00

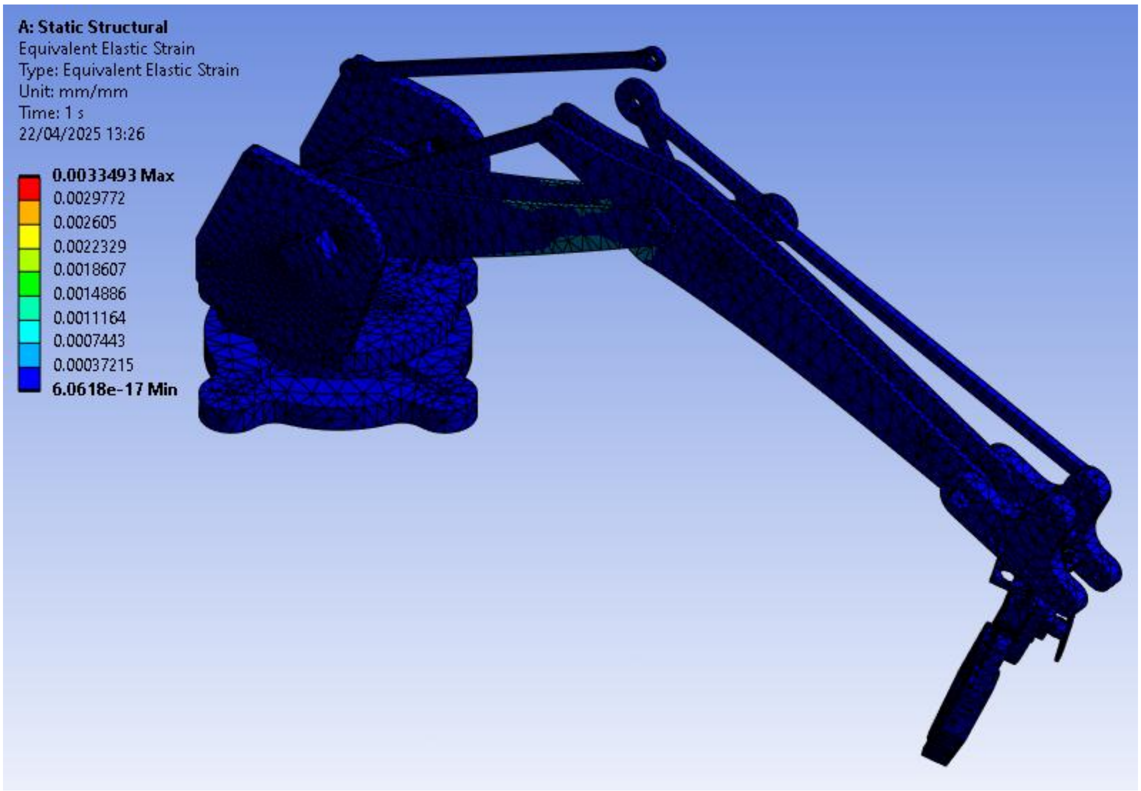
A: Static Structural
Equivalent Elastic Strain
Type: Equivalent Elastic Strain
Unit: mm/mm
Time: 1 s
22/04/2025 13:26
0.0033493 Max
0.0029772
0.002605
0.0022329
0.0018607
0.0014886
0.0011164
0.0007443
0.00037215
6.0618e-17 Min

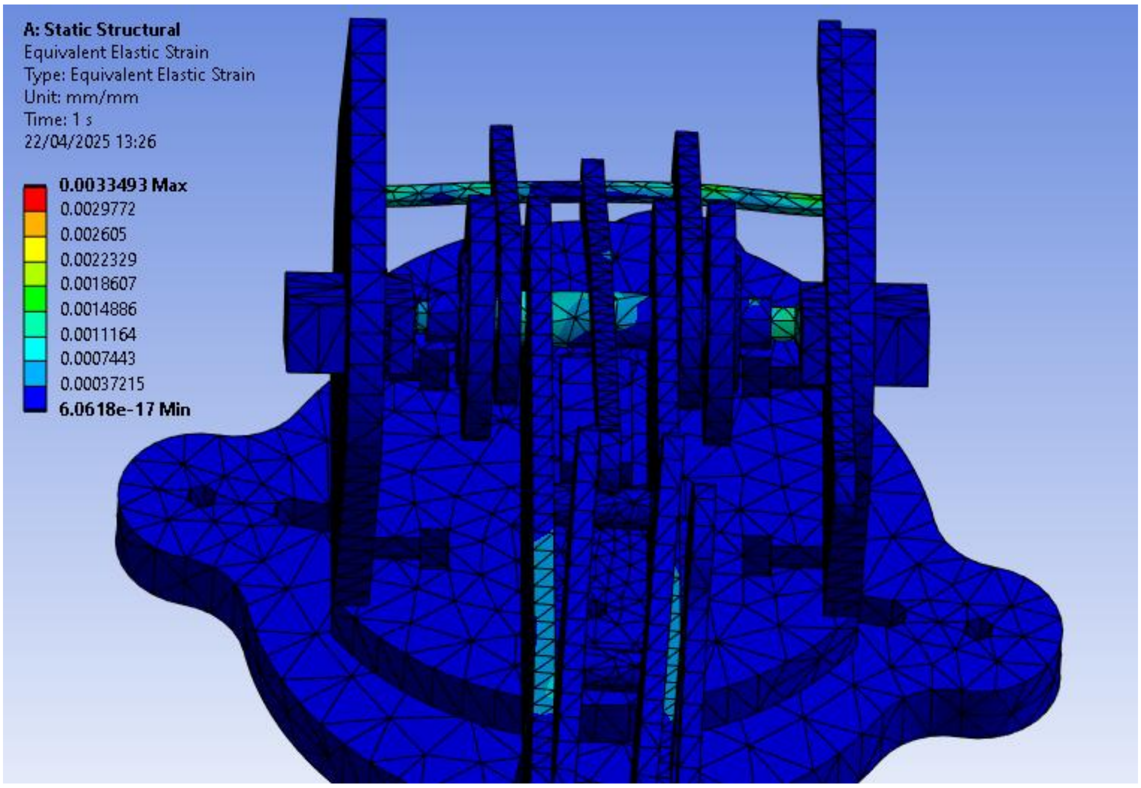
A: Static Structural
Equivalent Elastic Strain
Type: Equivalent Elastic Strain
Unit: mm/mm
Time: 1 s
22/04/2025 13:26
0.0033493 Max
0.0029772
0.002605
0.0022329
0.0018607
0.0014886
0.0011164
0.0007443
0.00037215
6.0618e-17 Min

APPENDIX I- ARDUINO CODE

```
#include <Servo.h>
#include <NewPing.h>

/* ---- Pin assignments ---- */
const uint8_t PIN_BASE   = 2;
const uint8_t PIN_SHL_A  = 3;   // shoulder servo A
const uint8_t PIN_SHL_B  = 4;   // shoulder servo B (mirrored)
const uint8_t PIN_WRIST  = 5;
const uint8_t PIN_GRIP   = 6;

const uint8_t PIN_TRIG   = 32;
const uint8_t PIN_ECHO   = 33;

/* ---- Geometry / behaviour ---- */
const float  SENSOR_OFFSET_MM = 184.0;  // sensor → finger-tip
const float  pickupDistance   = 60.0;   // mm ahead of gripper
const int    extendSteps      = 40;
const int    stepDelay        = 60;

/* ---- Objects ---- */
Servo sBase, sShlA, sShlB, sWrist, sGrip;
NewPing sonar(PIN_TRIG, PIN_ECHO, 600);

/* ---- Helpers ---- */
void setBase(int a)  { sBase .write(constrain(a,0,180));          }
void setWrist(int a) { sWrist.write(constrain(a,0,180));          }
void setGrip(int a)  { sGrip .write(constrain(a,0,180));          }

void setShoulder(int angle)
{
    angle = constrain(angle, 0, 180);
    sShlA.write(angle);           // Servo A
    sShlB.write(180 - angle);     // Servo B (invert mounted opposite)
}

float senseMM()
{
    float d=0;
    for(int i=0;i<3;i++) d += sonar.ping_cm();
    return (d/3.0)*10.0;          // to millimetres
}

void setup()
{
    Serial.begin(115200);

    sBase .attach(PIN_BASE);
    sShlA .attach(PIN_SHL_A);
    sShlB .attach(PIN_SHL_B);
    sWrist.attach(PIN_WRIST);
    sGrip .attach(PIN_GRIP);

    /* Home pose */
    setBase(90);
    setShoulder(60);
    setWrist(90);
    setGrip(45);   // open
    delay(1500);
}

void loop()
{
    Serial.println(F("\n--- new cycle ---"));
    setBase(60);                          // turn to workspace
    delay(500);

    for(int i=0;i<extendSteps;i++)
    {
        setShoulder(60 + i);                  // extend
        delay(stepDelay);

        float d = senseMM() - SENSOR_OFFSET_MM;
        Serial.print(F("Δ mm=")); Serial.println(d);

        if(d>0 && d<=pickupDistance)
    {
        setGrip(10);                          // close
        delay(400);

        setShoulder(60);                      // lift
       delay(600);

       setBase(90);                           // return
       delay(600);

       setGrip(45);                           // release
       delay(600);
       return;                                // restart main loop
    }
}

// nothing found, reset
setShoulder(60);
setBase(90);
delay(1500);
}
```

TIME-MANAGEMENT CHART

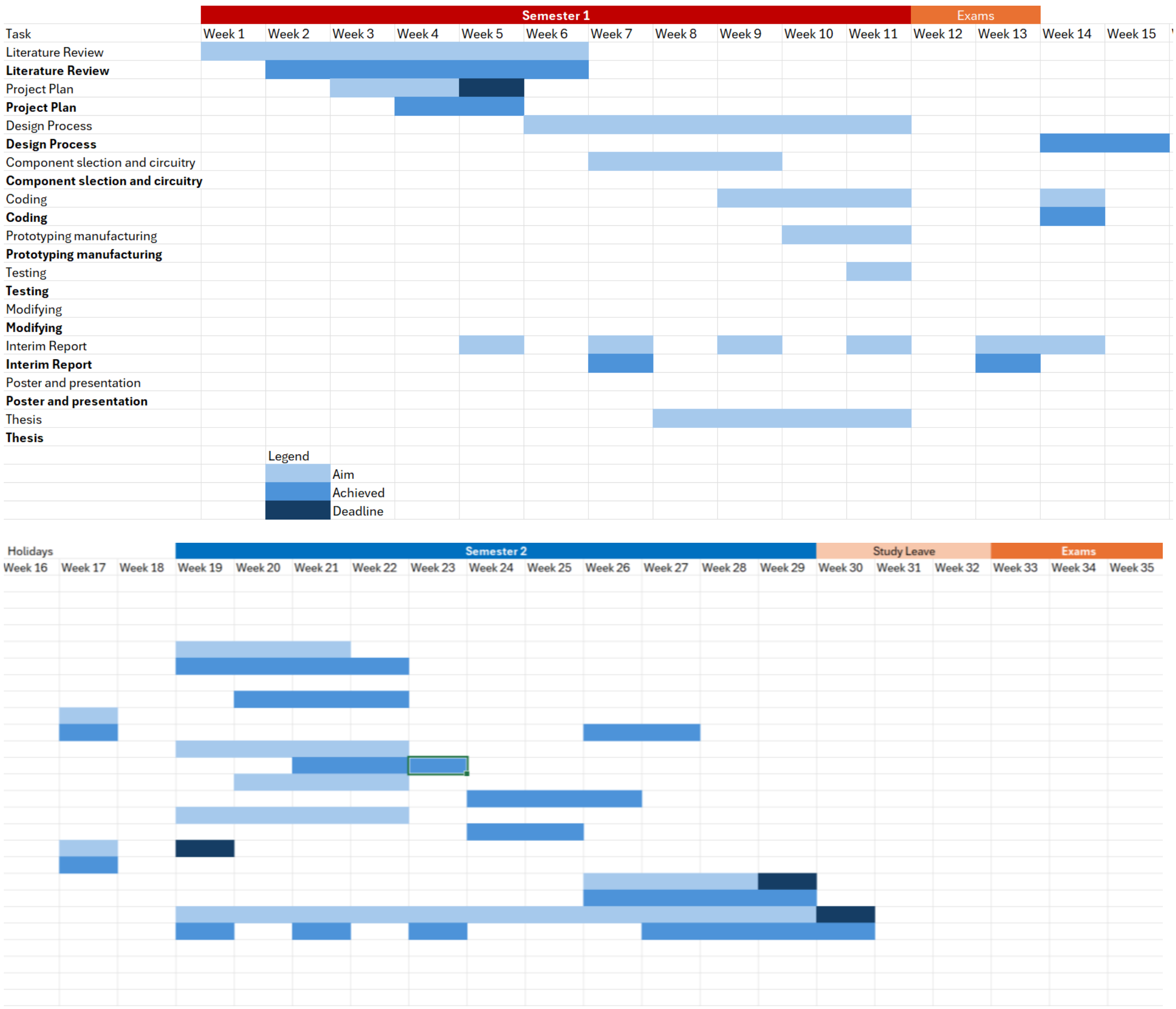

	Semester 1											Exams			
Task	Week 1	Week 2	Week 3	Week 4	Week 5	Week 6	Week 7	Week 8	Week 9	Week 10	Week 11	Week 12	Week 13	Week 14	Week 15
Literature Review	░	░	░	░	░	░									
Literature Review		▓	▓	▓	▓	▓									
Project Plan			░	░	█										
Project Plan				▓	▓										
Design Process						░	░	░	░	░	░				
Design Process														▓	▓
Component slection and circuitry							░	░	░						
Component slection and circuitry															
Coding									░	░	░			░	
Coding														▓	
Prototyping manufacturing										░	░				
Prototyping manufacturing															
Testing											░				
Testing															
Modifying															
Modifying															
Interim Report					░		░		░		░		░	░	
Interim Report							▓						▓		
Poster and presentation															
Poster and presentation															
Thesis								░	░	░	░				
Thesis															

Legend

░ Aim

▓ Achieved

█ Deadline

	Holidays			Semester 2											Study Leave			Exams		
Task	Week 16	Week 17	Week 18	Week 19	Week 20	Week 21	Week 22	Week 23	Week 24	Week 25	Week 26	Week 27	Week 28	Week 29	Week 30	Week 31	Week 32	Week 33	Week 34	Week 35
Literature Review																				
Literature Review																				
Project Plan																				
Project Plan																				
Design Process				░	░	░														
Design Process				▓	▓	▓	▓													
Component slection and circuitry																				
Component slection and circuitry					▓	▓	▓													
Coding		░																		
Coding		▓									▓	▓								
Prototyping manufacturing				░	░	░	░													
Prototyping manufacturing						▓	▓	▓												
Testing					░	░	░													
Testing									▓	▓	▓									
Modifying				░	░	░	░													
Modifying									▓	▓										
Interim Report		░		█																
Interim Report		▓																		
Poster and presentation											░	░	░	█						
Poster and presentation											▓	▓	▓	▓						
Thesis				░	░	░	░	░	░	░	░	░	░	░	█					
Thesis				▓		▓		▓				▓	▓	▓	▓					

RISK ASSESSMENT

University of Dundee

REASEARCH PROJECT RISK ASSESSMENT FORM

SCHOOL OF SCIENCE AND ENGINEERING

1.1 OUTLINE THE PROJECT (complete well in advance of the project)

Title of the project: Building a lightweight robotic arm for a mini-mars river with the use of 3D printing
Department: Mechanical Engineering
Location(s) of work (including fieldwork): Heathfield Lab
Description of the project including methods, fieldwork locations & duration: 3D printing and construction of the robotic arm will be performed at the Heathfield Lab, for approximately 12 weeks. This would involve the use of hand tools and 3D printing applications to manufacture and fabricate the lightweight robotic arm.

1.2 SUPERVISOR FOR THIS PROJECT

Name: Dr Jan Bernd Vorstius	Position: Supervisor
Department: Mechanical Engineering	Date: 14/01/2025

1.3 PERSON UNDERTAKING THIS PROJECT

Name: Jack Simpson	Signature: J Simpson
Date assessment undertaken: 14/01/2025	Position: Project lead

1.5 PERSONS AT RISK

Identify all categories of individuals who may be affected either directly or indirectly through the work activity and status.

Who is at risk?		**Status**
Staff	☐	Trained ☐ Competent ☐ Inexperienced ☐ Disability ☐ Supervision required ☐ Lone working ☐
Students	☒	Trained ☐ Competent ☒ Inexperienced ☐ Disability ☐ Supervision required ☐ Lone working ☒
Visitors	☐	Trained ☐ Competent ☐ Inexperienced ☐ Disability ☐ Supervision required ☐ Lone working ☐
Contractors	☐	Trained ☐ Competent ☐ Inexperienced ☐ Disability ☐ Supervision required ☐ Lone working ☐
Public	☐	Trained ☐ Competent ☐ Inexperienced ☐ Disability ☐ Supervision required ☐ Lone working ☐

1.6 PROTECTIVE EQUIPMENT REQUIRED

PPE is a last resort and engineering controls (fume cupboard or Local Exhaust Ventilation) should always be used in preference. Consult with the SSEN health and safety advisor regarding Personal Protective Equipment required. Insert any EN standard or details such as FFP2, Versaflo RPE, steel toe capped boots to be worn at all times below:

Engineering control/s	**3D printer enclosure with fume filtration and extraction, fixed pillar drill, low-voltage DC supplies**
PPE required (head, eye, ear, mask type, glove etc. Training requirements?	**Steel toe capped boots, basic tool training, safety goggles, secured clothing**

1.7 ENVIRONMENTAL RISKS

Possible risks to the environment either from the project or as an accidental release to the environment

Microplastics from the use of abrasive materials (sand paper, files, hacksaws, drill) becoming airborne, metal shavings from cut materials

1.8 WASTE

Is waste generated in this project: Yes ☒ No ☐	Type of waste and correct disposal: Plastic & metal waste, disposed of in appropriate receptacles

1.9 PROJECT IDENTIFICATION HAZARDS & EVALUATION OF RISKS

Likelihood harm will occur (Probability)
5. Almost certain (Occurs several times a day /daily)
4. Likely (could happen/once a week)
3. Possible (could easily happen/Once a month)
2. Unlikely (could happen/known to happen/once a year)
1. Rare (hasn't happened but could/once every 10 years
Severity of harm (Likely consequences)
5. Fatality
4. Major injury, resulting in permanent damage
3. Injury require doctor or hospital attendance/absence
2. Minor injury, first aid required
1. No injury, damage

		RISK LEVEL				
5	Likelihood	5	10	15	20	25
4		4	8	12	16	20
3		3	6	9	12	16
2		2	4	6	8	10
1		1	2	3	4	5
		1	2	3	4	5
		Severity				

RISK LEVEL	RISK EVALUATION
1 to 5	**LOW** - No Further action necessary, but if something can easily be done to reduce further then do. Monitor all existing controls.
6 to 8	**MEDIUM** – Further controls must be considered, and situation must be monitored.
10 to 25	**HIGH** – STOP Activity then make immediate improvements- Contact Safety Advisor.

From your proposal above consider main hazards below: (including chemicals)	**From your persons at risk (1.5) what actions might cause harm? Think about HOW harm might occur. (Not injury)**	**List any existing controls in place now.**	**Risk level L x S = R**	**Identify any additional controls required (including supervision and training).** Cross reference with action register below	**New risk level L x S =R**
Use of Hand tools(Sharp tools such as hacksaws, drill bits, wire cutters)	Slippage through improper tool handling, poor clamping, distraction during use	Basic PPE (gloves, boots, goggles)	3 * 2 = 6	Up to date training on tool usage, ensure component is secured, decrease amount of distractions	2 * 2 = 4
Isopropyl alcohol 99.9%, WD	Vapour buildup in poorly ventilated areas or contact with eyes/skin during wiping	small quantities used, well-ventilated room, either wipes or directly with cloth	2 * 2 = 4	Only use with gloves, avoid ignition sources, add eye protection	1 * 2 = 2
Fumes and hot surfaces from 3D printer	Poor ventilation during printing, accidental contact with printer nozzle or print bed	Printers in ventilated enclosure with filter, labeled hot zones, minimal handling	2 * 2 = 4	Optional FFP mask potentially FFP2, usage signs on printer	1 * 2 = 2
Connecting servos and sensors to Arduino	Incorrect wiring or power mismatch, resulting in shorting and heating elements	Low voltage circuits using 7.2V, USB isolation and ensured proper grounding	2 * 1 = 2	Colour coded wires, with potential of adding a fuse	1 * 1 = 1
WD-40 and White lithium grease	Aerosol spray near face, skin contact, slippery surfaces formed	Targeted application (use straw nozzle) workspace wiped down after every use	2 * 2 = 4	Only use with gloves, use in dedicated zone, apply with COSHH standards	1 * 2 = 2
Bench supply	Incorrect wiring, loose connections, short circuits releasing sparks	Operated at low voltage, usually the rated voltage of servos, terminals secured before use	2 * 2 = 4	Fuse protection, voltage readings from multimeter, have a qualified technician check the setup	1 * 2 = 2

2.0 Action Register

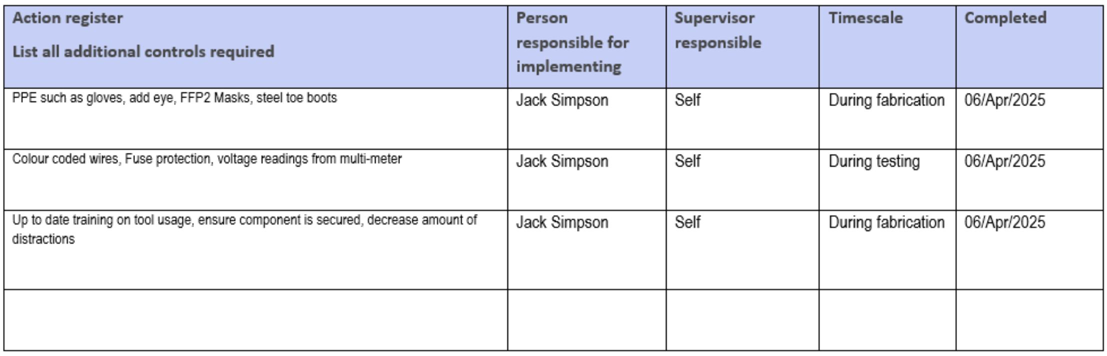

Action register List all additional controls required	Person responsible for implementing	Supervisor responsible	Timescale	Completed
PPE such as gloves, add eye, FFP2 Masks, steel toe boots	Jack Simpson	Self	During fabrication	06/Apr/2025
Colour coded wires, Fuse protection, voltage readings from multi-meter	Jack Simpson	Self	During testing	06/Apr/2025
Up to date training on tool usage, ensure component is secured, decrease amount of distractions	Jack Simpson	Self	During fabrication	06/Apr/2025

2.1 LINKS TO OTHER ASSESSMENTS & SOPS

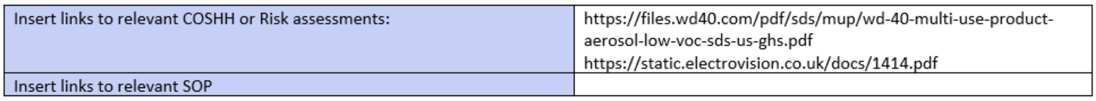

Insert links to relevant COSHH or Risk assessments:	https://files.wd40.com/pdf/sds/mup/wd-40-multi-use-product-aerosol-low-voc-sds-us-ghs.pdf https://static.electrovision.co.uk/docs/1414.pdf
Insert links to relevant SOP	